Title
Order and disorder in metal-organic frameworks

Author
Lee, Seungkyu

Publication Date
2018

Peer reviewed|Thesis/dissertation

Order and disorder in metal-organic frameworks

by

Seungkyu Lee

A dissertation submitted in partial satisfaction of the

requirements for the degree of

Doctor of Philosophy

in

Chemistry

in the

Graduate Division

of the

University of California, Berkeley

Committee in charge:

Professor Omar M. Yaghi, Chair

Professor Kenneth N. Raymond

Professor Bryan D. McCloskey

Spring 2018

Abstract

Order and disorder in metal-organic frameworks

by

Seungkyu Lee

Doctor of Philosophy in Chemistry

University of California, Berkeley

Professor Omar M. Yaghi, Chair

Metal-organic frameworks (MOFs) are crystalline porous materials, in which the pores represent most of the materials' volume. Characterization of guest molecules within the pores and the interactions between MOFs and the guests are important research topics in this field for various industrial applications and for deepening our fundamental understanding of the bonding nature that takes place within MOFs. Although the crystalline nature of MOFs allows for atomic level characterization by x-ray diffraction techniques, heavily disordered guest molecules often limit the full characterization of the framework materials. In this dissertation, I present a strategy to make the guests ordered across the unit cells of MOFs in order to determine their structures, including absolute configurations. A chiral metal-organic framework (MOF-520) was used to covalently bond and align disordered molecules. The reduced motional degrees of freedom obtained with this covalent alignment method allowed the structures of molecules to be determined by single-crystal x-ray diffraction techniques. The chirality of the MOF backbone also served as a reference in the structure solution for an unambiguous assignment of the absolute configuration of bound molecules.

An additional problem that the disordered guests cause is a reduction of MOFs' diffraction intensities, which prevents atomic resolution characterization. The disordered guests interact with the frameworks making them disordered, thus reducing the scattering power of MOFs at high angles. Although there are many reports concerned with guest induced phase transitions - such as breathing effects, unusual thermal expansions, and symmetry changes, where the interactions and changes of the structures are ordered across the unit cells - the disordered interactions have not been the main focus of study in this field. To emphasize the significance of the disordered interactions, UiO-66, which is known for its architecturally robust induced mechanical stability, was chosen and its diffraction qualities with and without guests were compared. UiO-66 without guests exhibited considerably increased mean I/σ values around the resolution limit when compared with UiO-66 with guests. This finding indicated that the disordered interactions significantly impacted the diffraction intensity of UiO-66. To glean additional insight into the nature of the interaction, the unusual phase transition and twinning of MOF-5 was also studied as a function of temperature variation. A single crystal of MOF-5 with guests displayed merohedral twinning accompanied by a phase transition upon temperature decrease, whereas the evacuated MOF-5 did not show such a transition nor twinning.

To my parents, Heesu Lee and Jeongrea Kim

Table of Contents

Acknowledgments

Chapter 1. Introduction

Chapter 2.

Chapter 3.

Chapter 4.

Chapter 5. Perspective

Acknowledgements

I would like to thank Prof. Omar M. Yaghi, a special PI. I appreciate his support for me to focus on projects that I'm interested in and his invaluable mentorship. We have invented a net, **sky** named after SeungKyu and Yaghi, which is the topology of a new MOF-1004.

I would like to thank;

Prof. Hans-Beat Bürgi. Although we have been together only for a short time, I have learned most of my crystallographic knowledge from him. He is really one of the best crystallographer in the world. He has also invented an angle with his PI, Bürgi-Dunitz angle.

Prof. Osamu Terasaki. I have two words in my mind that I was told by him, and these are still important directions in my scientific career.

Prof. Kenneth N. Raymond for the great teaching in the x-ray crystallography class and giving me inspirations.

Prof. Sir. Fraser J. Stoddart. Prof. Jeongyoung Park and Prof. Jaheon Kim for helping me to get the admission from Berkeley.

Dr. Simon J. Teat, Dr. Kevin Gagnon, and Dr. Laura J. McCormick for wonderful supporting for the data acquisitions at ALS.

Prof. Bryan D. McCloskey for being one of my dissertation committee members in spite of my short notice and his advice about this dissertation.

All my group members, especially, Dr. Felipe Gandara, Dr. Hiroyasu Furukawa, Kyle Cordova, Dr. Christian Diercks, Dr. Eugene Kapustin, Dr. Bunyarat Runtaweevoranit, Xiang Gao, Philjun Kang, Bing Zhang and Karen Wong for their mentorships, professional collaborations, helpful discussions, and supports

My Sisters, Eunsook Lee, Eunjeong Lee, Eunna Lee and my precious friends, Eunsook Kim, Geunhong Jeong for being with me all the time.

Specially, I like to thank my God for giving me the opportunity to study at Berkeley and meet these wonderful people.

Chapter 1. Introduction

Metal-organic frameworks and guest molecules as seen by x-ray crystallography

Imagine you are building a house with Lego kits. First, you would grab nodes and struts, and then connect them together to make a cube. Synthesizing a metal-organic framework (MOF) is something like that. If you are creative, you would build other shapes, such as a hexagon, using other types of building blocks. However, actually, a MOF is an apartment complex. There are other units next to yours, upstairs and downstairs. The units repeat three dimensionally and the interiors are decorated until the kits are used up. Now, you have a framework that supports the building and has furnished spaces inside. You might want to invite guests to make chemistry or store precious things that can fit. The uses of MOFs are similar in this regard. When you are bored, you might want to make your apartment bigger, more stable, or, even, install electricity. That is how MOFs are developing nowadays.

From a scientific perspective, MOFs are typically crystalline porous materials synthesized through chemical reactions (*1*-*3*). The structures can be illustrated by connecting metal-based inorganic nodes with organic linkers into three dimensional extended frameworks, where nanometer sized spaces, called pores, are generated as a result of connecting the nodes and linkers. There are roughly 3000 types of reported or hypothesized crystalline nets that MOFs can bear and these are registered in the Reticular Chemistry Structure Resource database (*4*). However, this does not mean that there are only 3000 types of MOF that can exist. Each net can be modified by simply choosing different types of nodes and linkers, the options of which can be found in cluster chemistry and organic chemistry, respectively (*5*-*7*). Theoretically, an infinite number of MOFs can be designed, which are, in practice, limited by the synthesis.

The structures of MOFs are repeated in two or three dimensions, which defines them as crystalline. In general, MOFs are periodic crystals and the symmetries belong to one of the 230 space groups (*8*). The crystalline nature makes the characterization of MOFs possible on the atomic level by x-ray diffraction techniques. X-rays scattered by a crystal are the Fourier transformation of the internal structure and create a reciprocal space where constructive x-rays form Bragg reflections. The inverse Fourier transformation of the Bragg reflections with phase information provides averaged atomic positions in the unit cell of the crystal in direct space (*9*).

The pores are more important part of MOFs than the backbone of the frameworks. The pore can be considered the same as the space in your room, which would be considered more precious than the walls that enclose the room. Size, shape, and the functionality of MOF's pore primarily decide the uses of a MOF since these determine the types of molecules, called guests, allowed within (*9*). There are a number of applications that are fundamentally based on inclusion or exclusion of molecules within MOFs by carefully designing the interiors of the pores. These include gas storage, separation, catalysis, drug delivery, protein inclusion, and energy storage (*10*-*23*).

In this dissertation, the main focus is placed on the ordered or disordered guest molecules within the pores of MOFs and how disordered guests affect the diffraction properties as characterized by single crystal x-ray diffraction (SXRD). Structure determination is a starting point

for understanding these materials. However, for in-depth studies of MOFs and development of their applications, the structures and guest molecules need to be characterized precisely. This means the relative atomic positions of all elements found in the material (elements from both the guest molecules as well as those in the frameworks) are of the utmost priority.

Order and disorder are crystallographic terms. If a crystal is perfect without vibrations, the atomic positions in each unit cell are identical across the crystal (*i.e*. perfectly ordered). It is hard to imagine a perfectly disordered state of a material, which would have infinite entropy value. In reality, MOFs are somewhere in between perfectly ordered and disordered states. Qualitatively, the frameworks are well ordered and crystalline. The averaged atomic positions obtained from structure refinements are, in fact, well defined. However, the guest molecules within the pores are disordered as compared to the frameworks. In general, this is due to a lack of strong bonds, such as covalent and ionic bonds, and/or multiple interactions with the backbone of the framework. As a consequence, the averaged electron densities of the guests are ill-defined and, from a chemistry standpoint, do not make sense (*24*.*25*)

The atomic positions and occupancies of guest molecules are important since they provide clues for identifying the type and strength of interactions with frameworks. Weakly bound and thus, disordered, guests are desired for many applications of MOFs since strongly bound guests require more energy for regeneration processes. Depending on the purpose of the targeted application, different levels of information about the guests is required. The averaged locations and orientations of the guests are enough if the structures of the guests are known. The atomic positions can reasonably be modeled and refined. From successful experiments, information about the nature of the interactions can be deduced. In these cases, it is important to understand the level of their disorder and characterize them appropriately as seen by x-ray diffraction.

When considering the order/disorder issue in MOFs, there is one particular application, called the crystalline sponge method, that deserves attention. This method seeks to target structure determination of guest molecules within MOFs including their absolute configuration (*26*,*27*). The demand for this method arises from pharmaceutical, molecular biology, and synthesis of organic molecules in chemistry labs, where chemical products or intermediates of compounds need to be characterized on the atomic level. For this method to be viable, the guests must be ordered enough to extract full structure information. This is possible since the pores of MOFs provide different degrees of translation symmetries. In the circumstances that the guests are chiral, the intensities of Bijvoet pairs, originating from anomalous scattering effects, are examined in the last part of structure refinement in order to determine the absolute structure of the crystal, from which the absolute configurations of the guests can be deduced (*28*,*29*). The precision of determining the absolute structure depends on the intensity difference of the Bijvoet pairs (*30*).

Although the crystalline sponge method is powerful and has broad impacts on many fields in science, there remain many improvements, as is true of any new field, to be made before it is used as a general approach for structure determination. This method should be further developed as follows: (i) increase the strengths of the interactions, thus pushing the equilibria to the bound states; (ii) precisely determine the absolute configurations; (iii) determine more complex structures of macromolecules, such as proteins; and (iv) determine molecular structures of diverse types. When it comes to (i), previous methods exploited weak interactions such as pi-pi interactions and hydrogen bonding (*27*). A single interaction of these types is not sufficiently strong enough to induce guest ordering throughout the unit cells, which means that multiple interactions are required.

These multiple interactions depend on the specificity of a MOF and its guest, which is also related to (iv). Needless to say, absolute structure determination must be precise. However, obtaining sufficient anomalous scattering is not trivial. Chapter 2 includes my contributions to (i) and (ii). In chapter 5, I will discuss (iii) and (iv).

The topics of chapters 3 and 4 are concerned with the unusual diffraction properties of MOFs induced by the disordered guest molecules within their pores. The conclusion of the research detailed therein focuses on addressing a generally accepted fundamental issue commonly experienced in the MOF field. By this, I mean that in MOFs it is known that the guests play important roles during and after the crystallization process by supporting the pores and retaining their crystallinity. This is based on a common observation that MOF crystals frequently lose their crystallinity after removal of guest molecules. This observation has brought about developments in the optimization of guest molecule removal, including, but not limited to, solvent exchange and supercritical CO_2 drying procedures. The results of my research indicate that the internal structures and diffraction properties of MOFs are significantly affected by disordered guest molecules residing within the pores. Since the structure determination is only a starting point for understanding these materials, it is absolutely essential to gain correct insight into their properties under the appropriate measurement conditions, such that wrong interpretation and analysis does not occur.

References and notes

1. M. Kondo, T. Yoshitomi, H. Matsuzaka, S. Kitagawa, K. Seki, Three-Dimensional Framework with Channeling Cavities for Small Molecules. *Angew. Chem. Int. Ed.* **36**, 1725 (1997).

2. S. S.-Y. Chui, S. M.-F. Lo, J. P. H. Charmant, A. G. Orpen, I. D. Williams, A Chemically Functionalizable Nanoporous Material. *Science* **283**, 1148 (1999).

3. H. Li, M. Eddaoudi, M. O'Keeffe, O. M. Yaghi, Design and synthesis of an exceptionally stable and highly porous metal-organic framework. *Nature* **402**, 276 (1999).

4. M. O'Keeffe, M. A. Peskov, S. J. Ramsden, O. M. Yaghi, The Reticular Chemistry Structure Resource (RCSR) Database of, and Symbols for, Crystal Nets. *Acc. Chem. Res.* **41**, 1782 (2008).

5. M. Eddaoudi *et al.*, Systematic Design of Pore Size and Functionality in Isoreticular MOFs and Their Application in Methane Storage. *Science* **295**, 469(2002).

6. Z. Wang, S. M. Cohen, Postsynthetic modification of metal-organic frameworks. *Chem. Soc. Rev.* **38**, 1315 (2009).

7. K. K. Tanabe, S. M. Cohen, Postsynthetic modification of metal-organic frameworks-a progress report. *Chem. Soc. Rev.* **40**, 498 (2011).

8. T. Hahn, *International Tables for Crystallography, Volume A: Space Group Symmetry*. (Springer Netherlands, 2005).

9. C. Giacovazzo, *Fundamentals of Crystallography*. (Oxford University Press, 2002).

10. Q. Li *et al.*, Docking in Metal-Organic Frameworks. *Science* **325**, 855 (2009).

11. D. Britt, H. Furukawa, B. Wang, T. G. Glover, O. M. Yaghi, Highly efficient separation of carbon dioxide by a metal-organic framework replete with open metal sites. *Proc. Natl. Acad. Sci. U.S.A.* **106**, 20637 (2009).

12. L. J. Murray, M. Dincă, J. R. Long, Hydrogen Storage in Metal–Organic Frameworks. *Chem. Soc. Rev.* **38**, 1294 (2009).

13. D. Farrusseng, S. Aguado, C. Pinel, Metal–Organic Frameworks: Opportunities for Catalysis. *Angew. Chem. Int. Ed.* **48**, 7502 (2009).

14. H. Deng *et al.*, Large-Pore Apertures in a Series of Metal-Organic Frameworks. *Science* **336**, 1018 (2012).

15. M. P. Suh, H. J. Park, T. K. Prasad, D.-W. Lim, Hydrogen Storage in Metal–Organic Frameworks. *Chem. Rev.* **112**, 782 (2012).

16. M. Yoon, R. Srirambalaji, K. Kim, Homochiral Metal–Organic Frameworks for Asymmetric Heterogeneous Catalysis. *Chem. Rev.* **112**, 1196 (2012).

17. Y. Peng *et al.*, Methane Storage in Metal–Organic Frameworks: Current Records, Surprise Findings, and Challenges. *J. Am. Chem. Soc.* **135**, 11887 (2013).

18. H. Furukawa, K. E. Cordova, M. O'Keeffe, O. M. Yaghi, The Chemistry and Applications of Metal-Organic Frameworks. *Science* **341**, 974 (2013).

19. A. A. Talin *et al.*, Tunable Electrical Conductivity in Metal-Organic Framework Thin-Film Devices. *Science* **343**, 66 (2014).

20. T. M. McDonald *et al.*, Cooperative insertion of CO_2 in diamine-appended metal-organic frameworks. *Nature* **519**, 303 (2015).

21. J. A. Mason *et al.*, Methane storage in flexible metal–organic frameworks with intrinsic thermal management. *Nature* **527**, 357 (2015).

22. L. Sun, M. G. Campbell, M. Dincă, Electrically Conductive Porous Metal–Organic Frameworks. *Angew. Chem. Int. Ed.* **55**, 3566 (2016).

23. P. Li *et al.*, Toward Design Rules for Enzyme Immobilization in Hierarchical Mesoporous Metal-Organic Frameworks. *Chem.* **1**, 154 (2016).

24. P. Debye, Interferenz von Röntgenstrahlen und Wärmebewegung. *Annalen der Physik* **348**, 49 (1913).

25. I. Waller, Zur Frage der Einwirkung der Wärmebewegung auf die Interferenz von Röntgenstrahlen. *Zeitschrift für Physik* **17**, 398 (1923).

26. Y. Inokuma *et al.*, X-ray analysis on the nanogram to microgram scale using porous complexes. *Nature* **495**, 461 (2013).

27. M. Hoshino, A. Khutia, H. Xing, Y. Inokuma, M. Fujita, The crystalline sponge method updated. *IUCrJ* **3**, 139 (2016).

28 H. D. Flack, G. Bernardinelli, Absolute structure and absolute configuration. *Acta Crystallogr. A* **55**, 908 (1999).

29 H. D. Flack, U. Shmueli, The mean-square Friedel intensity difference in P1 with a centrosymmetric substructure. *Acta Crystallogr. A* **63**, 257 (2007).

30. J. M. Bijvoet, A. F. Peerdeman, A. J. van Bommel, Determination of the Absolute Configuration of Optically Active Compounds by Means of X-Rays. *Nature* **168**, 271 (1951).

Chapter 2.

Coordinative alignment of molecules in chiral metal-organic frameworks

(This is reprint from *Science*, 2016, **353**, 808: "Coordinative alignment of molecules in chiral metal-organic frameworks." **Seungkyu Lee**, Eugene A. Kapustin, Omar M. Yaghi.)

Abstract

A chiral metal-organic framework (MOF-520) was used to covalently bond and align molecules of varying size, complexity, and functionality. The reduced motional degrees of freedom obtained with this covalent alignment method allowed the structures of molecules to be determined by single-crystal x-ray diffraction techniques. The chirality of the MOF backbone also served as a reference in the structure solution for an unambiguous assignment of the absolute configuration of bound molecules. Sixteen molecules representing four common functional groups (primary alcohol, phenol, vicinal diol, and carboxylic acid) and ranging in complexity from methanol to plant hormones (gibberellins, containing eight stereocenters) were crystallized and had their precise structure determined. We distinguished single and double bonds in gibberellins, and enantioselectively crystallized racemic jasmonic acid, whose absolute configuration had only been inferred from derivatives.

Introduction

Single-crystal x-ray diffraction is a powerful technique for the definitive identification of chemical structures. Although most molecules and molecular complexes can be crystallized, often enthalpic and entropic factors introduce orientational disorder that prevent determination of a high-resolution structure (*1*). Several strategies based on the inclusion of guests in a host framework (*1-3*) that helps maintain molecular orientation have been used to overcome this challenge. However, most of these methods rely primarily on weak interactions to induce crystalline order of the included molecules. Here, we demonstrate a strategy for crystallization of molecules within the pores of chiral metal-organic frameworks (MOFs) (*4*). The advantages that this strategy provides are: (i) the molecules make covalent bonds to well-defined metal sites of the MOF; these bonds anchor them and lower their motional degrees of freedom, thereby promoting their alignment into an ordered pattern across the interior of the crystalline framework; and (ii) the absolute structure of the chiral MOF framework serves as a reference for the direct determination of the absolute configuration of bound chiral molecules (*5*). Indeed, this latter feature forgoes the reported pseudo-symmetry problems that have obscured the absolute structures that specify the enantiomorph in achiral host framework systems (*6-8*).

Specifically, we used this covalent alignment method to crystallize 16 different molecules in the interior of the MOF-520-type structure (*9*). These molecules represent a range of functionality, flexibility, and complexity. The first 12 are relatively simple molecules but the other 4 are large and complex molecules: benzoic acid, **1**, methanol, **2**, ethylene glycol, **3**, 3-nitrophenol, **4**, heptanoic acid, **5**, 3-hydroxybenzoic acid, **6**, 3,5-diaminobenzoic acid, **7**, trimesic acid, **8**, 4-bromophenol, **9**, 2-(2,6-dichloranilino)phenylacetic acid (diclofenac), **10**, 5,7-dihydroxy-3-(4-hydroxyphenyl)chromen-4-one (genistein), **11**, and *tert*-butyloxycarbonyl-(RS)-3-amino-1,2-propanediol, **12**. In addition, this method led us to successfully crystallize two different type of

plant hormones within the MOF: gibberellins (form A_1, **13**, and A_3, **14**) with eight stereocenters, and (±)-jasmonic acid (**15**, **16**). The precision of the crystal structures with only 30 % occupancy of the bound gibberellins permitted the distinction of the single bond in **13** from the double bond in **14**, this being the only difference between the two complex molecules. The crystal structure of (±)-jasmonic acid, whose absolute configuration had only been inferred from derivatives, was obtained enantioselectively with each enantiomorph single crystal of the MOF binding only one enantiomer of jasmonic acid.

Results and discussions

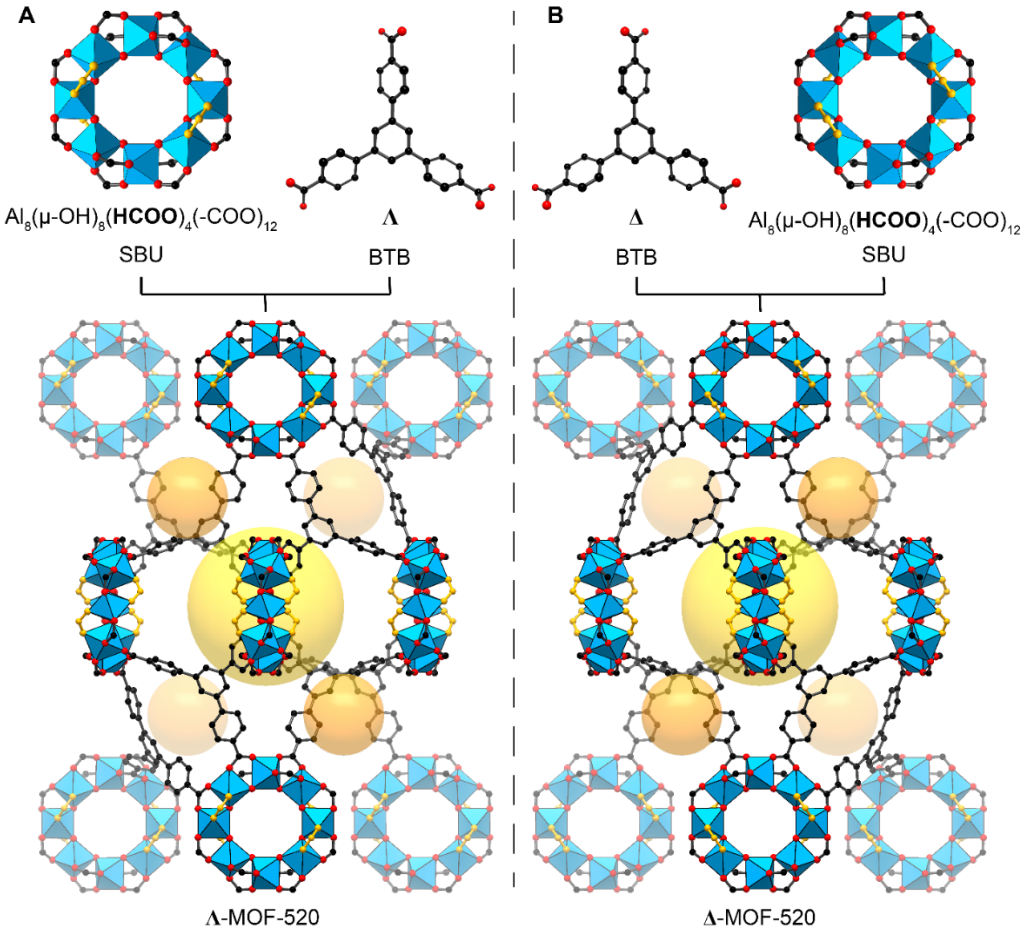

Fig. 1. **Structures of MOF-520 enantiomorphs and their building units.** MOF-520 is comprised of the SBU, $Al_8(\mu\text{-}OH)_8(HCOO)_4(\text{-}COO)_{12}$ and BTB linker. Each SBU is coordinated by sixteen carboxylates, twelve from BTB linkers and four from formate ligands (highlighted in yellow on the SBU). The absolute structure descriptors **Λ**-MOF-520 (**A**) and **Δ**-MOF-520 (**B**) are assigned based on the absolute configuration of the BTB linker. The large yellow and small orange balls represent the octahedral and tetrahedral pores, respectively. Color code: black, C; red, O; blue polyhedra, Al.

We chose MOF-520, $Al_8(\mu\text{-}OH)_8(HCOO)_4(BTB)_4$, (BTB = 1,3,5-benzenetribenzoate), as the framework for implementing the CAL method of crystallization because of its high

crystallinity, robustness, and chirality (Fig. 1). Its secondary building units (SBUs) are rings of eight aluminum octahedra sharing corners through eight μ-OHs and four formate ligands. Each of these SBUs is linked by 12 BTB units, and each BTB is linked to three SBUs to make a three-dimensional, extended porous framework. Two types of ellipsoidal pores form from elongated arrangements of SBUs that octahedral (10.01 Å by 10.01 Å by 23.23 Å) and tetrahedral (5.89 Å by 5.89 Å by 6.21 Å). The framework of MOF-520 crystallizes in the noncentrosymmetric space group $P4_22_12$, with a chiral atomic arrangement. The absolute structure of each enantiomorph is designated as **Λ** or **Δ** according to the chirality of the BTB linker in the respective crystal structure (Fig. 1, A and B). Although each single crystal is nearly enantiomorphically pure, according to the Flack parameters of the refined structures, 0.049(17) for **Λ** and 0.031(11) for **Δ** (*11*), the overall bulk sample is a racemic conglomerate containing both enantiomorphs [table S1 and S2 (*12*)].

The distinctive nature of this MOF lies in each of the aluminum SBUs having four formate ligands in addition to 12 carboxyl units from BTB linkers to complete the octahedral coordination sites of the aluminum centers (Fig. 1). These formate ligands occupy two sites on each face of the SBU in a chiral tetrahedral arrangement with D_2 symmetry. We anticipated that through acid-base chemistry, we could substitute these formates with incoming organic molecules such as carboxylates, alkoxides, and phenolates (Fig. 2A). Given that the interior of the MOF has large octahedral pores, it is reasonable to expect molecules of varying size and complexity to diffuse into this space and covalently bind to the metal sites (Fig. 2B), and as we will show, align themselves within the MOF to be amenable to x-ray structure determination.

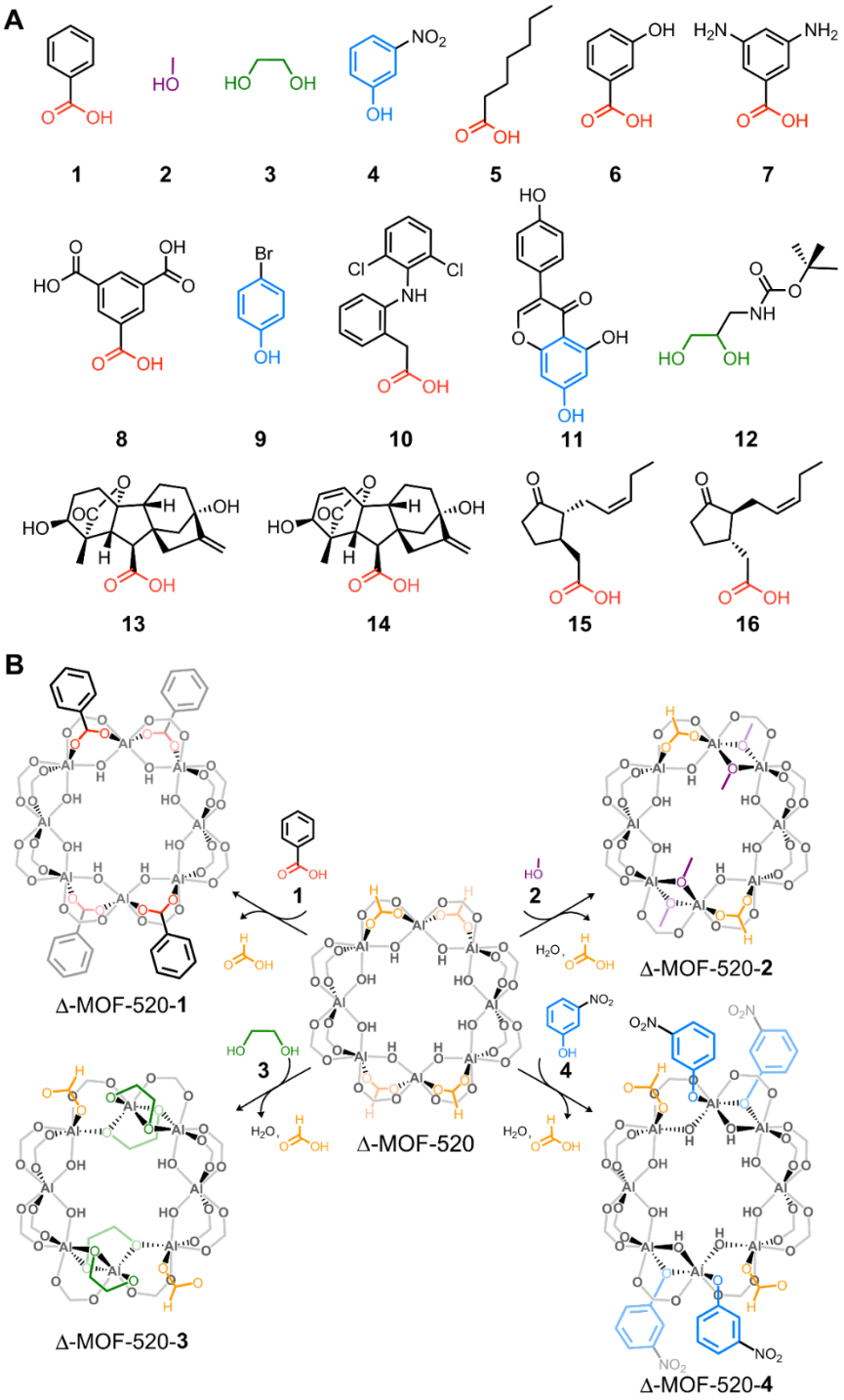

Fig. 2. Structures of incoming molecules (1 to 16) and coordination modes of their deprotonated forms on the SBU of Δ-MOF-520. (**A**) The structures of **1** to **16** represent the molecules binding to the SBU, where their functionalities are highlighted with colors: red for carboxylic acid, purple for primary alcohol, green for vicinal diol, and blue for phenol. (**B**) The SBU of **Δ**-MOF-520 is shown in the center with the four formate ligands (yellow) highlighted. The deprotonated forms of **1** to **4** replace all (**1**) or some (**2**-**4**) of the formate ligands and μ-OH on the SBU; the resulting coordination modes and the functionalities of the molecules are colored. For clarity, the chirality of **Λ**-MOF-520-**2** and -**4** are converted to **Δ** configuration.

Prior to examining the incorporation of molecules into the pores of MOF-520, we ensured that the structure of the MOF is fully characterized using single crystal x-ray diffraction (SXRD) techniques according to our previous report (*10, 12*). We confirmed the chemical composition of the evacuated MOF-520 by ^{1}H NMR of digested samples (calculated formate to BTB ratio: 1 to 1; found: 1 to 0.93) and by elemental analysis, (calculated, wt. %: C 58.81; H 3.14; N 0.0 and found, wt. %: C 59.20; H 3.19; N < 0.2). The porosity of MOF-520 was confirmed by measurement of N_2 type I isotherm at 77 K, which led to a final uptake of 770 $cm^3{}_{STP}\ g^{-1}$ at 1 bar, similar to a calculated uptake, 821 $cm^3{}_{STP}\ g^{-1}$, from SXRD model. The MOF-520 samples were also characterized by infrared spectroscopy to ensure the absence of solvent in the pores, thermal gravimetric analysis to confirm the thermal stability of the MOF, and powder x-ray diffraction to confirm the bulk purity of the crystals (*12*).

The molecules **1** to **16** have the functionalities that include primary alcohol, phenol, vicinal diol, and carboxylic acid (Fig 2A). These molecules were covalently bonded to the MOF by immersion of single crystals of MOF-520 in a concentrated solution of the respective molecule followed by heating (40° to 100°C) for at least 12 hours (*12*). The architectural robustness and high chemical stability of MOF-520 enabled the substitution of the symmetrically equivalent four formates in the SBU with the carboxylates of incoming molecules and their covalent binding to the SBUs with full retention of crystallinity. In addition, alkoxides and phenolates replaced only two formates on the same face of the SBU in addition to μ-OHs, as shown in Fig. 2B. This substitution pattern led to a doubling of the unit cell in the *c*-direction without affecting the connectivity of the MOF backbone. Consecutive SBUs along *c* were substituted strictly on the opposite face of the ring, leading to a change in the space groups, $P4_22_12$ of **Λ** and **Δ**-framework to $P4_32_12$ and $P4_12_12$, respectively.

Relatively small achiral molecules were chosen to describe in detail the four different binding modes in **Δ**-MOF-520 for all incoming molecules: benzoic acid, **1**, as an aromatic carboxylic acid, methanol, **2**, as a primary alcohol, ethylene glycol, **3**, as a vicinal diol, and 3-nitrophenol, **4**, as a phenol. Benzoic acid shared the same binding mode as formate, where for methanol, two methoxides replaced two formates on the same face of the ring and doubly bridged the Al in a μ^2 manner, thus changing the corner sharing Al octahedra to edge sharing. This geometry change induced further substitution of two μ-OHs with the alkoxide molecules. Overall, four alkoxides replaced two formates and two μ-OHs, with two coordinated formates remaining on the C_2 symmetric SBU. The binding mode of **3** is similar to that of **2**, where the formates and μ-OHs were substituted and the same geometry change of the SBU occurred. The main difference is that the remaining two formates are now bonded to the SBU as terminal ligands, which were previously bridging ligands on the SBU of **Δ**-MOF-520. In the case of **4**, two different binding modes were observed with positional disorder: one is similar to that of **2,** and the other is shown in Fig. 2B (two of four phenolic oxygen atoms are bridging).

The resulting substituted frameworks, MOF-520-**2** and -**3**, have a larger pore width compared to the original MOF-520 [the distance between the Al of adjacent SBUs, 14.70(4) and 14.13(5) Å, respectively, compared to the distance, 13.73(4) Å of MOF-520] (fig. S16). Thus, we used MOF-520 for the crystallization of incoming molecules **1** to **10**, **12**, **15**, and **16**, MOF-520-**2** for **11**, and MOF-520-**3** for **13** and **14**.

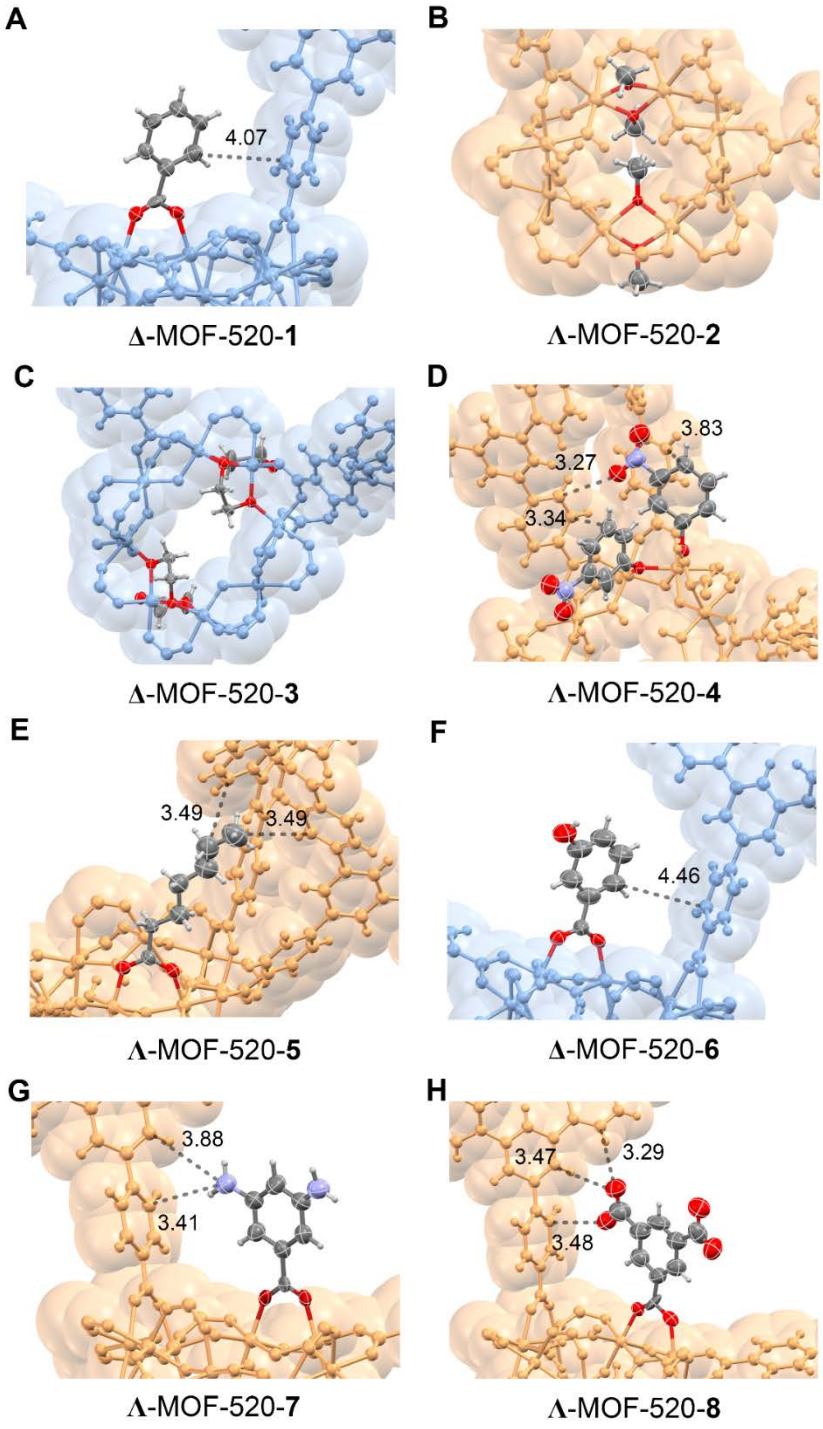
A
4.07
Δ-MOF-520-1
B
Λ-MOF-520-2
C
Δ-MOF-520-3
D
3.83
3.27
3.34
Λ-MOF-520-4
E
3.49
3.49
Λ-MOF-520-5
F
4.46
Δ-MOF-520-6
G
3.88
3.41
Λ-MOF-520-7
H
3.47
3.29
3.48
Λ-MOF-520-8

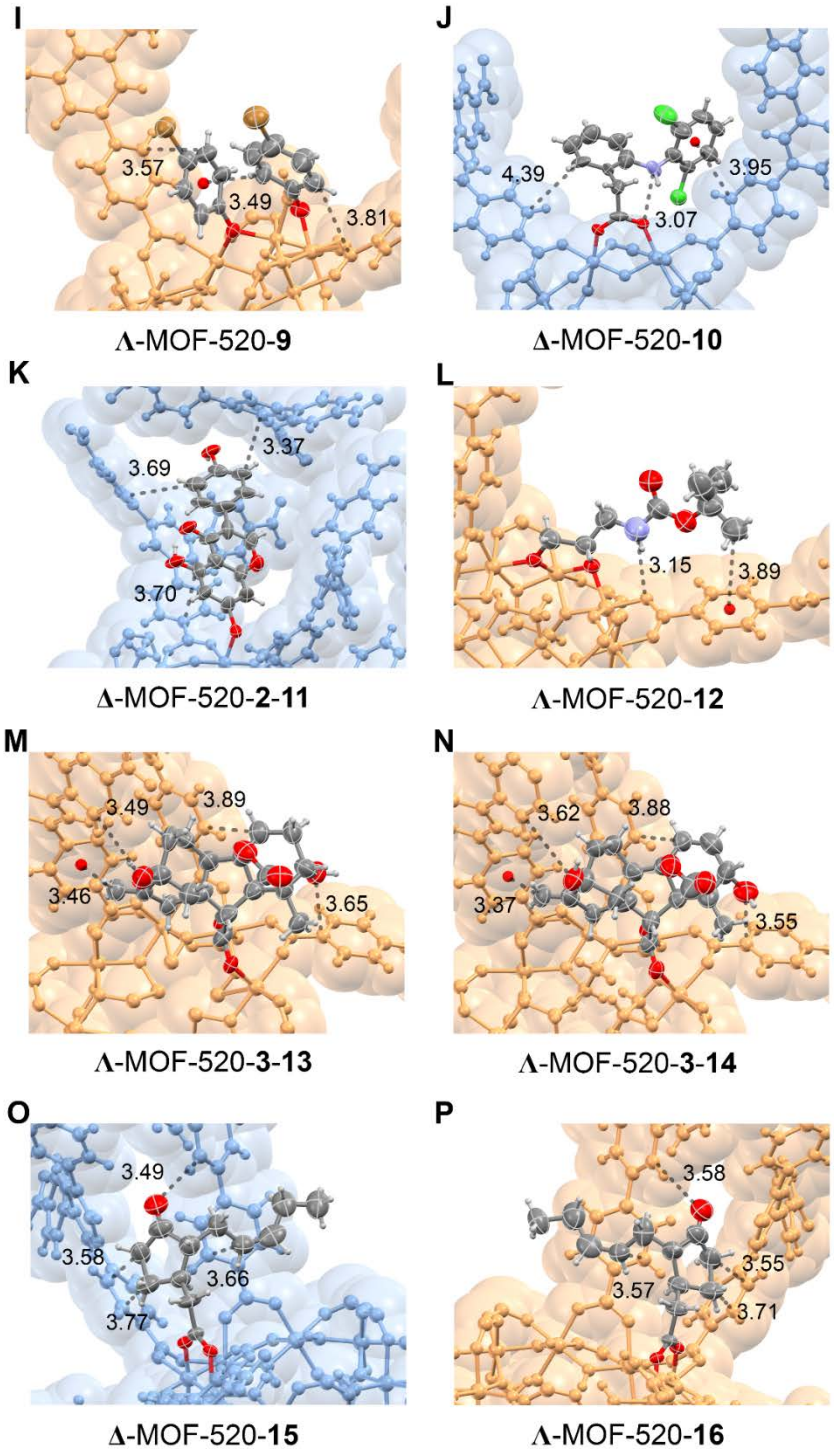

Fig. 3. Refined structures of 1 to 16 crystallized in Λ or Δ-MOF-520. (**A** to **P**) The refined structures of the molecules obtained from SXRD data are indicated with 50 % probability thermal ellipsoids. The surroundings of the coordination sites of **Λ**- and **Δ**-MOF-520 are shown with orange and blue space filling models, respectively. Intramolecular interactions between the moieties of the molecules and the surroundings of the coordination sites are indicated with dotted lines and distances (Å). In the case of positional disorder, only one conformation of bound molecules is shown for clarity. Color code: gray, C; red, O; white, H; pale violet, N; green, Cl; brown, Br.

The crystal structures of all molecules bound to the MOF have been determined by SXRD and show the binding modes outlined above. All of the structures were refined anisotropically (Fig. 3). In general, the value of anisotropic displacement parameters of the incorporated molecules increased with their distance from the binding sites; as expected because the orientation of the bound molecules are mainly governed by a single site of covalent attachment. Those parts of the bound molecules that are far from the binding sites are stabilized by noncovalent interactions such as π-π interactions and weak hydrogen bonds with the aromatic rings and carboxylates of the framework (Fig. 3 and table S3).

The bound molecules **1** to **3** and **6** are simple and small in their structure; their ordering within the MOF is sustained only by covalent bonds to aluminum with no weak interactions with the framework observed (Fig. 3, A to C, and F). The covalent binding is sufficient to anchor these molecules and lower their degrees of freedom, an aspect that is present in all crystal structures of **1** to **16**; weak interactions play a role for some molecules but not all. For example, in **Δ**-MOF-520-**6**, the closest distance apart the covalent bond **6** makes to the framework is 4.46 Å, which corresponds to the distance between the *ortho*-carbon of **6** and the adjacent phenyl ring of the MOF, indicating that there are no contributing secondary interactions with the framework (Fig. 3F). However, the entire structure of **6** was solved without ambiguity. The OH group of **6** is pointing away from the framework, suggesting a possible repulsive interaction with the adjacent phenyl ring of the linker. No detectable residual electron density was observed in the structure refinement for the second OH group at the other *meta* position.

Within the MOF, molecules **10** and **11** were also ordered by anchoring through covalent bonding to aluminum, but their order was further enhanced by the presence of π-π (T-shaped for **10** and parallel-displaced for **11**) and hydrogen bonding (N–H···O for **10** and O–H···π for **11**) interactions to the framework (Fig. 3, J and K). Similar interactions are also observed for the molecules **4**, **5, 7** to **9**, and **12** to **16**. Details of the structural information including the covalent bond distances, the types of closest noncovalent interactions between the bound molecules and the framework, and refinement parameters are tabulated (table S3).

Because the coordinative alignment method yields highly ordered arrangements for molecules within the MOF, their structure can be determined even with low occupancy of the binding sites. This feature makes it possible to obtain structures of larger and more complex molecules with high accuracy and to determine the absolute configuration of chiral molecules with high certainty. The structures of gibberellins **13** and **14**, two derivatives of a natural plant hormone, illustrate the advantages of the coordinative alignment method (Fig. 3, M and N, and Fig. 4). All non-hydrogen atoms of these complex molecules with eight stereocenters could be assigned from an occupancy of only 30 %. The structures were refined without applying any geometrical constraints and restraints on the gibberellin molecules. The accuracy of the method is documented by the characterization of the subtle structure difference between **13** and **14**, where we find C_1–C_2 to be a single bond [1.57(2) Å] in **13** and a double bond [1.30(3) Å] in **14**. The C–C–C bond angles at C_1 and C_2 are 105.0(15)° and 113.3(14)° in **13** and 121.6(17)° and 117.6(18)° in **14**, indicative of sp^3 and sp^2 hybridization, respectively. Ball-and-stick representations of the structures are superimposed for direct comparison in Fig. 4.

The absolute structures of **Λ**-MOF-520-**2**-**13** and -**14** were assigned on the basis of their Flack parameters, 0.063(9) and 0.05(2), respectively, in spite of the low occupancies of the molecules. In previous reports, the absolute configurations of the guests were determined in achiral host frameworks (*7-9, 13*). In those methods, pseudo-centrosymmetry problems were reported and

the absolute structure determinations were obscured, even though the structures of the guests were identified in the structure solution. This problem may be caused by several factors, such as low guest occupancy (*7, 9*), lack of high angle reflections because of disorder of the guest (*9, 14*), and the nearly centrosymmetric nature of the guest (8, *9*, *15*). The chiral MOFs show anomalous scattering from the framework itself regardless of any included chiral molecules (*15, 16*). The strong enantiomorph-distinguishing power originates mainly from the scattering of the chiral framework and is enhanced by chiral and achiral bound molecules. It is sufficient for determining the absolute structure of the resulting crystal, including the absolute configuration of the bound molecule, even when the occupancy of the latter is low.

The coordinative alignment has potential in being the method of choice for the determination of the absolute configuration of molecules because it could reduce the dependence on the absolute structure parameters of the inclusion crystal data. For example, when a single crystal with absolute structure **Λ** has been determined by SXRD and subsequently used in the inclusion, the absolute configuration of the incorporated molecule can be directly deduced from the pre-determined **Λ** structure. In this case, the correctness of the absolute configuration of incorporated molecules is highly dependent on the pre-determined absolute structure and the knowledge of the enantiopurity of the single crystal used for the inclusion. (*6*).

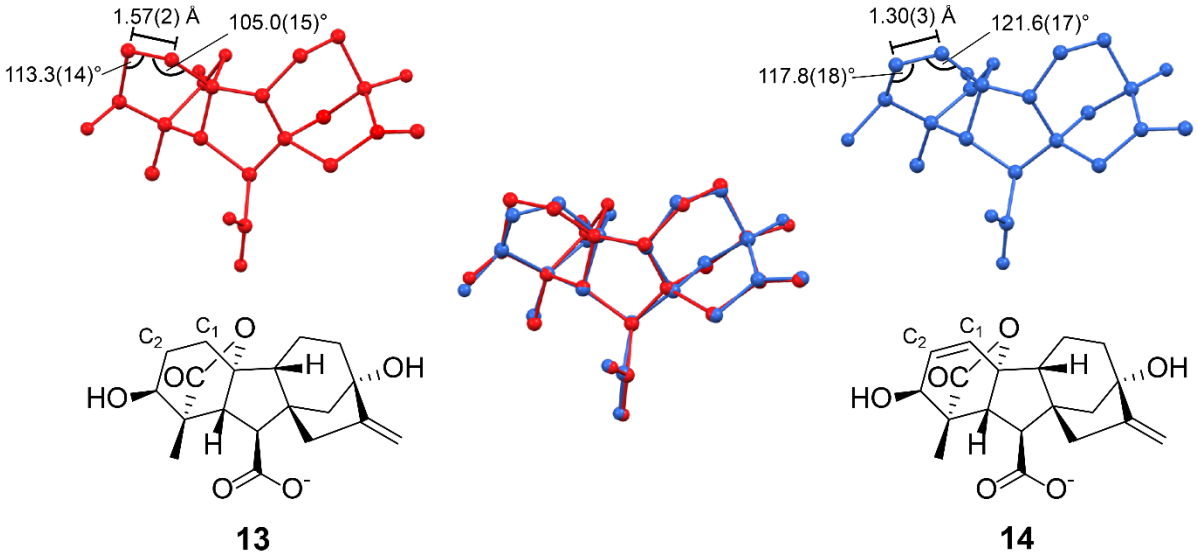

Fig. 4. Comparison of the molecular geometries of 13 and 14. Ball-and-stick models of the structures of **13** and **14** crystallized in **Λ**-MOF-520 are shown in red and blue, respectively. Their conformations are overlaid in the middle. The structural difference, a single bond between C_1 and C_2 for **13** and a double bond for **14**, can be distinguished from the distances and the angles indicated on the models. Only atoms C_1 and C_2 are labeled for clarity.

Finally, we demonstrate that the chirality of the binding sites of MOF-520 can separate enantiomers when one interacts more favorably with the binding site of one of the enantiomorphs of the MOF. We determined the absolute configuration of another plant hormone, jasmonic acid, for which a crystal structure has heretofore not been reported. A solution of a racemic mixture of (-)-jasmonic acid, **15**, and (+)-jasmonic acid, **16**, was reacted with a racemic conglomerate of

MOF-520, and SXRD data for two enantiomorphic crystals was collected after the reaction. The molecule **15** selectively attached to **Δ**-MOF-520 and **16** to **Λ**-MOF-520 (Fig. 3, O and P). The positions of the last three carbons were not clearly defined, presumably because of their conformational flexibility, the low occupancy of 33%, and the ensuing overlap with the electron density of residual disordered solvent. However, the atoms defining the stereocenters of **15** and their absolute configurations, *R* for C_3 and *R* for C_7, were observed unambiguously with a Flack parameter of 0.037(8). This result corresponds to that deduced from the absolute configurations of a derivative of **15**, (-)-methyl jasmonate, which were determined by a synthetic approach (*17*). The enantiomer **16** attached to **Λ**-MOF-520 showed the opposite absolute configuration as indicated by a refined Flack parameter of 0.040(8). We note that the enantiomerically pure molecules, **13** and **14,** had an occupancy that was sufficiently high for unambiguous structure and absolute configuration determination only in one of the two enantiomorphs. This can potentially be applied to the absolute configuration determination of samples, which contain a minor enantiomer, without the need of chiral HPLC separation before carrying out the inclusion procedure (*7*).

References and notes

1. A. Holden, P. Morrison, *Crystals and Crystal Growing*. (London, 1982).
2. J. L. Atwood, J. E. D. Davies, D. D. MacNicol, *Inclusion Compounds: Structural aspects of inclusion compounds formed by inorganic and organometallic host lattices*. (Academic Press, 1984).
3. Y.-M. Legrand, A. van der Lee, M. Barboiu, Single-Crystal X-ray Structure of 1,3-Dimethylcyclobutadiene by Confinement in a Crystalline Matrix. *Science* **329**, 299 (2010).
4. Y. Inokuma, S. Yoshioka, J. Ariyoshi, T. Arai, Y. Hitora, K. Takada, S. Matsunaga, K. Rissanen, M. Fujita, X-ray analysis on the nanogram to microgram scale using porous complexes. *Nature* **495**, 461 (2013).
5. H. Furukawa, K. E. Cordova, M. O'Keeffe, O. M. Yaghi, The Chemistry and Applications of Metal-Organic Frameworks. *Science* **341**, 974 (2013).
6. H. D. Flack, G. Bernardinelli, Absolute structure and absolute configuration. *Acta Crystallogr. A* **55**, 908 (1999).
7. S. Yoshioka, Y. Inokuma, M. Hoshino, T. Sato, M. Fujita, Absolute structure determination of compounds with axial and planar chirality using the crystalline sponge method. *Chem. Sci.* **6**, 3765 (2015).
8. E. Sanna, E. C. Escudero-Adan, A. Bauza, P. Ballester, A. Frontera, C. Rotger, A. Costa, A crystalline sponge based on dispersive forces suitable for X-ray structure determination of included molecular guests. *Chem. Sci.* **6**, 5466 (2015).
9. M. Hoshino, A. Khutia, H. Xing, Y. Inokuma, M. Fujita, The crystalline sponge method updated. *IUCrJ* **3**, 139 (2016).
10. F. Gándara, H. Furukawa, S. Lee, O. M. Yaghi, High Methane Storage Capacity in Aluminum Metal–Organic Frameworks. *J. Am. Chem. Soc.* **136**, 5271 (2014).
11. H. D. Flack, G. Bernardinelli, Reporting and evaluating absolute-structure and absolute-configuration determinations. *J. Appl. Crystallogr.* **33**, 1143 (2000).
12. Materials and methods are available as supplementary materials at the Science website.
13. T. R. Ramadhar, S.-L. Zheng, Y.-S. Chen, J. Clardy, Analysis of rapidly synthesized guest-filled porous complexes with synchrotron radiation: practical guidelines for the crystalline sponge method. *Acta Crystallogr. A* **71**, 46 (2015).
14. H. D. Flack, G. Bernardinelli, D. A. Clemente, A. Linden, A. L. Spek, Centrosymmetric and pseudo-centrosymmetric structures refined as non-centrosymmetric. *Acta Crystallogr. B* **62**, 695 (2006).
15. H. D. Flack, U. Shmueli, The mean-square Friedel intensity difference in P1 with a centrosymmetric substructure. *Acta Crystallogr. A* **63**, 257 (2007).

16. J. M. Bijvoet, A. F. Peerdeman, A. J. van Bommel, Determination of the Absolute Configuration of Optically Active Compounds by Means of X-Rays. *Nature* **168**, 271 (1951).

17. R. K. Hill, A. G. Edwards, The absolute configuration of methyl jasmonate. *Tetrahedron* **21**, 1501 (1965).

18. G. Sheldrick, A short history of SHELX. *Acta Crystallogr. A* **64**, 112 (2008).

19. O. V. Dolomanov, L. J. Bourhis, R. J. Gildea, J. A. K. Howard, H. Puschmann, OLEX2: a complete structure solution, refinement and analysis program. *J. Appl. Crystallogr.* **42**, 339 (2009).

20. C. F. Macrae, P. R. Edgington, P. McCabe, E. Pidcock, G. P. Shields, R. Taylor, M. Towler, J. van de Streek, Mercury: visualization and analysis of crystal structures. *J. Appl. Crystallogr.* **39**, 453 (2006).

21. B. Rees, L. Jenner, M. Yusupov, Bulk-solvent correction in large macromolecular structures. *Acta Crystallogr. D* **61**, 1299 (2005).

22. A. L. Spek, PLATON SQUEEZE: a tool for the calculation of the disordered solvent contribution to the calculated structure factors. *Acta Crystallogr. C* **71**, 9 (2015).

Acknowledgements: Support for the synthesis by BASF SE (Ludwigshafen, Germany) and the characterization of compounds by King Abdulaziz City for Science and Technology (Center of Excellence for Nanomaterials and Clean Energy Applications). We thank Dr. Simon Teat for the synchrotron X-ray diffraction data acquisition support at the beamline 11.3.1 (Advanced Light Source, Lawrence Berkeley National Laboratory); Dr. Kevin Gagnon for discussion of structure refinement; and Prof. Hans-Beat Bürgi for invaluable discussions of structure refinement and edition of this manuscript. NMR data was acquired at the Molecular Foundry (LBNL). Work performed at the Advanced Light Source and the Molecular Foundry is supported by the Director, Office of Science, Office of Basic Energy Sciences, of the U.S. Department of Energy under Contract No. DE-AC02–05CH11231 (ALS and Foundry). Use of CheXray facility at the College of Chemistry (UC-Berkeley) is supported by NIH Shared Instrumentation Grant S10-RR027172. Data reported in this paper are tabulated in the Supplementary Materials and archived at the following database, Cambridge Crystallographic Data Centre under the reference numbers CCDC 1488938 to 1488955.

Supplementary materials

Materials and Methods

Table of contents

Section S1. MOF-520 synthesis and characterization

Materials for the synthesis of the MOF

Aluminum nitrate nonahydrate, $Al(NO_3)_3 \cdot 9H_2O$, N,N-dimethylformamide (DMF) (purity ≥ 99.9 %) were purchased form Sigma Aldrich Co. 1,3,5-benzenetribenzoic acid (H_3BTB) was purchased from TCI America. Formic acid (99.8 %) was obtained from EMD Chemicals. Anhydrous acetone (purity ≥ 99.8 %, extra dry with AcroSeal) was purchased from Acros Organics. All chemicals obtained were used without further purification. Scintillation vials (20 mL) and polypropylene cabs with foil liner were purchased form Wheaton.

Instrumentation

Attenuated total reflectance (ATR) FTIR spectra of neat samples were performed on a Bruker ALPHA Platinum ATR-FTIR Spectrometer equipped with a single reflection diamond ATR module (Section S1.1). Carbon, hydrogen, nitrogen elemental microanalyses (EA) were performed in the Microanalytical Laboratory of the College of Chemistry at UC Berkeley, using a Perkin Elmer 2400 Series II CHNS elemental analyzer (Section S1.1). Single-crystal X-ray diffraction (SXRD) data was collected using synchrotron radiation in beamline 11.3.1 of the Advanced Light Source, Lawrence Berkeley National Laboratory (LBNL), a Bruker MicroSTAR-H APEX II diffractometer and a Bruker D-8-Venture diffractometer (Sections S1.2 and S2.2). Beamline 11.3.1. is equipped with a PHOTO100 CMOS detector operating in shutterless mode equipped, and the radiation is monochromated using silicon (111). The Bruker MicroSTAR-H APEX II diffractometer is equipped with a CCD area detector and a micro-focus rotating anode X-ray source with a Cu-target (λ = 1.54178 Å). The Bruker D8-Venture diffractometer is equipped with a PHOTON100 CMOS detector and a micro-focus X-ray tube with a Cu-target (λ = 1.54178 Å). Powder X-ray diffraction (PXRD) patterns were acquired with a Bruker D8 Advance diffractometer (Cu Kα radiation, λ = 1.54056 Å). (Section S1.3). N_2 adsorption isotherms were recorded on a Quantachrome Autosorb-1 volumetric gas adsorption analyzer (Section S1.4). Thermogrametric analysis (TGA) traces were collected on a TA Instruments Q-500 series thermal gravimetric analyzer (Section S1.5). Solution ^1H NMR spectra were acquired on a Bruker Advance-500 MHz NMR spectrometer in Molecular Foundry in LBNL (Section S1.6 and S2.1).

Section S1.1. Synthesis of MOF-520 single crystals

MOF-520, **$Al_8(OH)_8(HCOO)_4BTB_4$.** In a 20 mL scintillation vial, the mixture solution of $Al(NO_3)_3 \cdot 9H_2O$ (90.0 mg, 0.240 mmol), H_3BTB (75.0 mg, 0.170 mmol) in DMF (17 mL) was prepared. The solution was sonicated for 1 min and formic acid (1.40 mL, 0.0310 mol) was added to the solution. The vial was capped and placed in the preheated 140 °C oven. After 4 days, block shaped clear single crystals with size range 50 to 100 μm were obtained on the wall of the vial. Subtle temperature difference can affect the quality of the single crystals. It is recommended that several vials containing the solution be set together and placed in different locations in the oven. The vial with the best single crystals was chosen and the single crystals were used for the inclusion of the molecules. For the characterization of MOF-520, the rest of the crystals were further processed.

Solvent exchange and guest removal activation procedure: The single crystals were washed with DMF (10.0 mL) three times per day for three days to remove the unreacted reagents in the pores. DMF solvent in the pore was exchanged with anhydrous acetone by washing the crystals with anhydrous acetone (10.0 mL) three times per day for three days. For supercritical CO_2 drying (SCD) activation, the acetone was decanted and acetone in the crystals was thoroughly exchanged with liquid CO_2 in the chamber of a Tousimis Samdri PVT-3D critical point dryer. The sample was subsequently kept in a supercritical CO_2 atmosphere (typical conditions of 40 °C and 1200 psi) for 30 min and then the supercritical CO_2 was slowly vented over the course of 6 hours. To remove the residual molecules in the pores, the crystals were evacuated for 6 h at 120 °C under 30 mTorr. Yield: 16 % based on Al. ATR-FTIR (cm^{-1}): 3059 (w), 1613 (s), 1600 (s), 1565 (m), 1517 (w), 1456 (s), 1423 (s), 1293 (w), 1183 (m), 1153 (w), 1105 (w), 1018 (w), 977 (m), 858 (w), 819 (w), 787 (s), 712 (m), 678 (m), 640 (s), 589 (s), 548 (s), 498 (m), 446 (w). EA: Found (wt %): C: 59.20; H: 3.19; N: < 0.2. Calculated (wt %): C: 58.81; H: 3.14; N: 0.0.

Section S1.2. Single crystal X-ray diffraction analysis of MOF-520

Single-crystalline samples were mounted on MiTeGen® kapton loops in LV CryoOil® and placed in a 100(2) K nitrogen cold stream from Oxford Cryosystems Cryostream equipment. In all cases, the raw data were processed with the Bruker APEX2 software package. The data were first integrated using the SAINT procedure and then corrected for absorption with SADABS procedure. The structures were solved by direct methods (XS-2008) and the refinement was done by full-matrix least squares on F^2 (SHELXL-2014), using the Olex2 software package (*18, 19*). Mercury software was used for structure visualization (*20*).

Λ-MOF-520. A truncated octahedron-shaped crystal (80 x 60 x 60 μm^3) of as-synthesized **Λ**-MOF-520 was measured at beamline 11.3.1 at the ALS with radiation of λ = 1.0333 Å. According to intensity statistics table for the whole dataset (PRP file), the resolution was cut off to 0.83 Å. Solvent masking was applied during structure refinement. Before solvent masking instruction, structure was refined anisotropically and hydrogen atoms were placed into positions calculated geometrically. The connected asymmetric unit was defined inside the unit cell: MOVE command was applied to all atoms. The weighting scheme is refined as well as the extinction coefficient. The void volume is estimated to be 8963 $Å^3$ with 9196 electrons removed during masking. Some reflections were omitted due to non-ideal solvent masking, beam stop clipping and the minor presence of diffuse scattering. The threshold $(I_{obs}-I_{calc})/\sigma(W)>10$ was chosen for omitting these reflections. Omission of these reflections did not affect the refinement; the fraction of omitted reflections is less than 0.1% of the whole dataset.

Name	**Λ**-MOF-520
Chemical composition of MOF per asymmetric unit	$Al_2\ C_{28}\ H_{18}\ O_{10}$
Chemical formula of bound molecule	none
Bound molecule occupancy	0%
Formula mass	568.38
Crystal system	Tetragonal
Space group	$P4_22_12$
a, Å	18.5370(6)
c, Å	37.4217(15)
V, Å^3	12858.9(10)
d, g cm^{-3}	0.587
μ, mm^{-1}	0.210
Z	8
Measured reflections	75723
Independent reflections	11665
Observed reflections	10335
θ_{min} , º	2.248
θ_{max} , º	38.523
h	-22 to 18
k	-22 to 22
l	-33 to 43
R int	0.0550
R [$F^2>2\sigma(F^2)$]	0.0290
wR(F^2)	0.0800
S	0.991
Parameters	373
Geometrical restraints on the molecule	0
Occupational constraints on the molecule	0
Geometrical constraints on the molecule	0
Flack parameter	0.049(17)
$\Delta\rho_{max}$, e Å^{-3}	0.144
$\Delta\rho_{min}$, e Å^{-3}	-0.114
Crystal size, mm^3	0.080 x 0.060 x 0.060
Radiation, Å	1.0333
Temperature, K	100
CCDC number	1488951

Table S1. Crystal data, data collection, and structure refinement parameters for **Λ**-MOF-520.

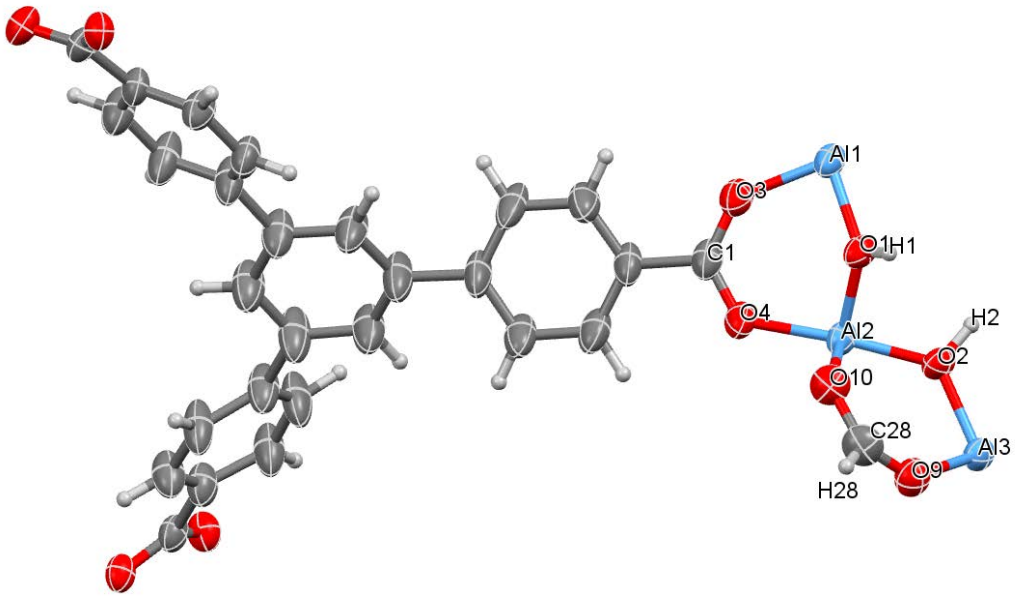

Fig. S1. Asymmetric unit in the single crystal structure of Λ-MOF-520. Thermal ellipsoids are drawn with 50% probability.

Name	**Δ**-MOF-520
Chemical composition of MOF per asymmetric unit	$Al_2\ C_{28}\ H_{18}\ O_{10}$
Chemical formula of bound molecule	none
Bound molecule occupancy	0%
Formula mass	568.38
Crystal system	Tetragonal
Space group	$P4_22_12$
a, Å	18.4753(4)
c, Å	37.4264(9)
V, Å^3	12775.0(6)
d, g cm^{-3}	0.662
μ, mm^{-1}	0.324
Z	8
Measured reflections	49798
Independent reflections	11725
Observed reflections	10446
θ_{min} , ^{o}	2.667
θ_{max} , ^{o}	68.374
h	-22 to 20
k	-21 to 15
l	-45 to 44
R int	0.0335
$R\ [F^2>2\sigma(F^2)]$	0.0339
$wR(F^2)$	0.0897
S	0.989
Parameters	373
Geometrical restraints on the molecule	0
Occupational constraints on the molecule	0
Geometrical constraints on the molecule	0
Flack parameter	0.031(11)
$\Delta\rho_{max}$, e Å^{-3}	0.403
$\Delta\rho_{min}$, e Å^{-3}	-0.165
Crystal size, mm^3	0.080 x 0.070 x 0.070
Radiation, Å	1.54178
Temperature, K	100
CCDC number	1488944

Table S2. Crystal data, data collection, and structure refinement parameters for Δ-MOF-520.

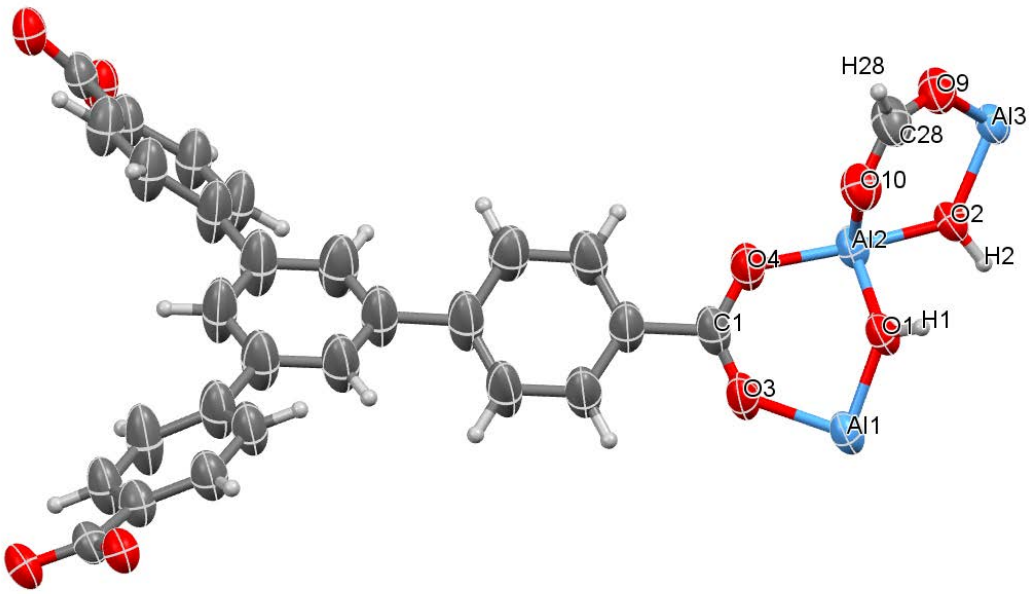

Fig. S2. Asymmetric unit in the single crystal structure of Δ-MOF-520. Thermal ellipsoids are drawn with 50% probability.

Form	*R* int	*R* [*I*>2σ(*I*)]	*S*	*Flack parameter, **x**(u)*
Δ (delta)	0.0415	0.0310	1.092	0.106(9)
Δ (delta)	0.0716	0.0411	0.950	-0.01(8)
Δ (delta)	0.0566	0.0333	0.890	0.01(2)
Δ (delta)	0.0820	0.0414	0.963	-0.01(7)
Δ (delta)	0.0490	0.0289	1.027	0.073(19)
Δ (delta)	0.0414	0.0286	1.053	0.077(11)
Δ (delta)	0.0409	0.0390	0.938	0.05(3)
Δ (delta)	0.0299	0.0378	0.928	0.08(4)
Δ (delta)	0.0307	0.0418	0.956	0.11(4)
Δ (delta)	0.0204	0.0343	1.119	0.15(4)
Δ (delta)	0.0391	0.0404	0.920	0.05(6)
Δ (delta)	0.0595	0.0498	1.055	0.08(6)
Δ (delta)	0.0430	0.0348	1.010	0.10(1)
Λ (lambda)	0.0356	0.0305	1.054	0.040(13)
Λ (lambda)	0.0479	0.0325	1.072	0.03(4)
Λ (lambda)	0.0650	0.0281	1.074	0.11(3)
Λ (lambda)	0.0892	0.0432	1.056	0.06(2)
Λ (lambda)	0.0661	0.0331	1.035	0.13(3)
Λ (lambda)	0.0596	0.0336	0.969	0.06(3)
Λ (lambda)	0.0497	0.0461	0.910	-0.12(5)
Λ (lambda)	0.0382	0.0289	1.103	0.07(1)

Table S3. The structure refinement parameters for MOF-520 from statistical experiment to estimate the racemic character for twenty one single-crystalline samples (thirteen Δ and eight Λ forms).

Section S1.3. Powder X-ray diffraction analysis

Guest free single crystals were used for PXRD experiment. Ground sample was placed on a quartz sample holder and was mounted on the diffractometer. The data was collected from 2 to 50 degrees by 0.02 step for total 60 minutes data collection time.

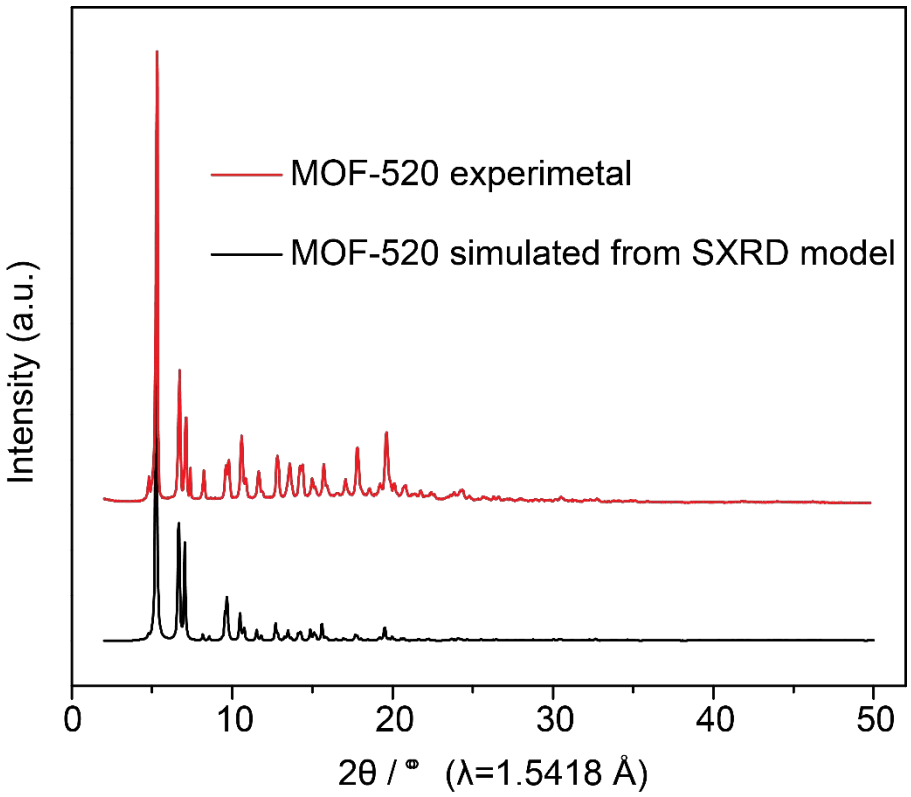

Fig. S3. PXRD pattern of MOF-520 and the simulated pattern of MOF-520 structure from SXRD data.

Section S1.4. N_2 isotherm

40 mg of guest free samples in 9 mm bulb gas cell was charged with Ar to avoid air contamination and the cell was mounted on the instrument. Liquid nitrogen bath was used for the measurements at 77 K. Helium was used for the estimation of dead space for gas adsorption measurements. Ultra-high-purity grade N_2 and He gases (Praxair, 99.999% purity) were used throughout the adsorption experiments. 46 adsorption and 16 desorption points were collected.

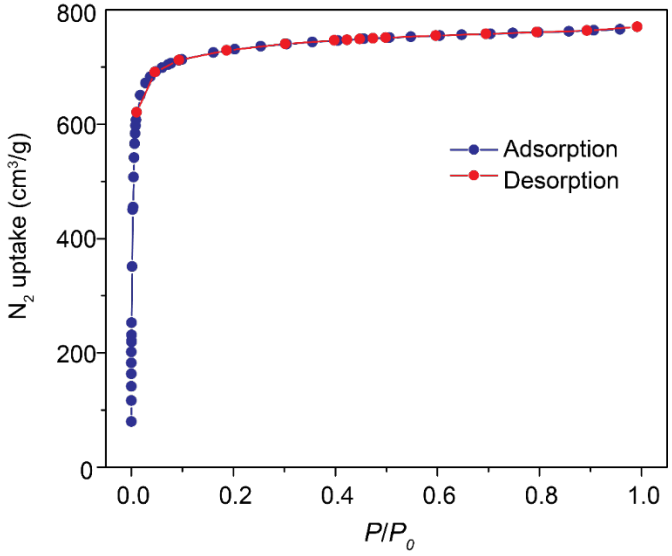

Fig. S4. N_2 isotherm of MOF-520 at 77K.

Section S1.5. Thermogravimetric analysis

The guest free sample was held in a platinum pan under nitrogen atmosphere with a flow rate of 40 mL/min. Temperature was controlled by the furnace heating from 25 °C up to 800 °C with a ramp rate of 5 °C/ min.

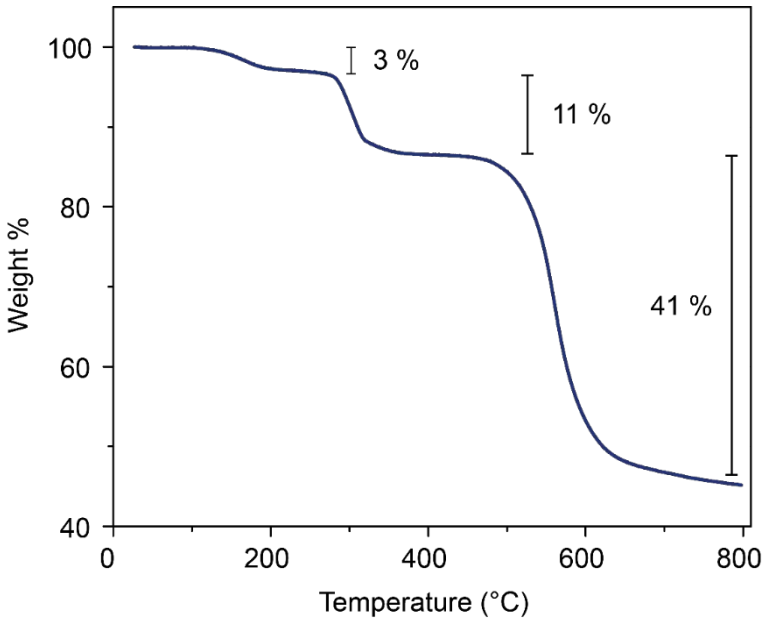

Fig. S5. TGA data of the guest free MOF-520.

Section S1.6. ^{1}H NMR

The guest free sample (1 mg) was transferred to a 4 mL vial. Deuterated dimethyl sulfoxide (d6-DMSO) (600 µL) was add to the vial followed by the addition of 20 µL of NaOH (1 M in D_2O). The solution was sonicated for 10 min to digest the crystals. The vial was capped and placed in a preheated 120 °C oven for 20 min to completely dissolve the crystals. The final clear solution was used for the 1H NMR experiment.

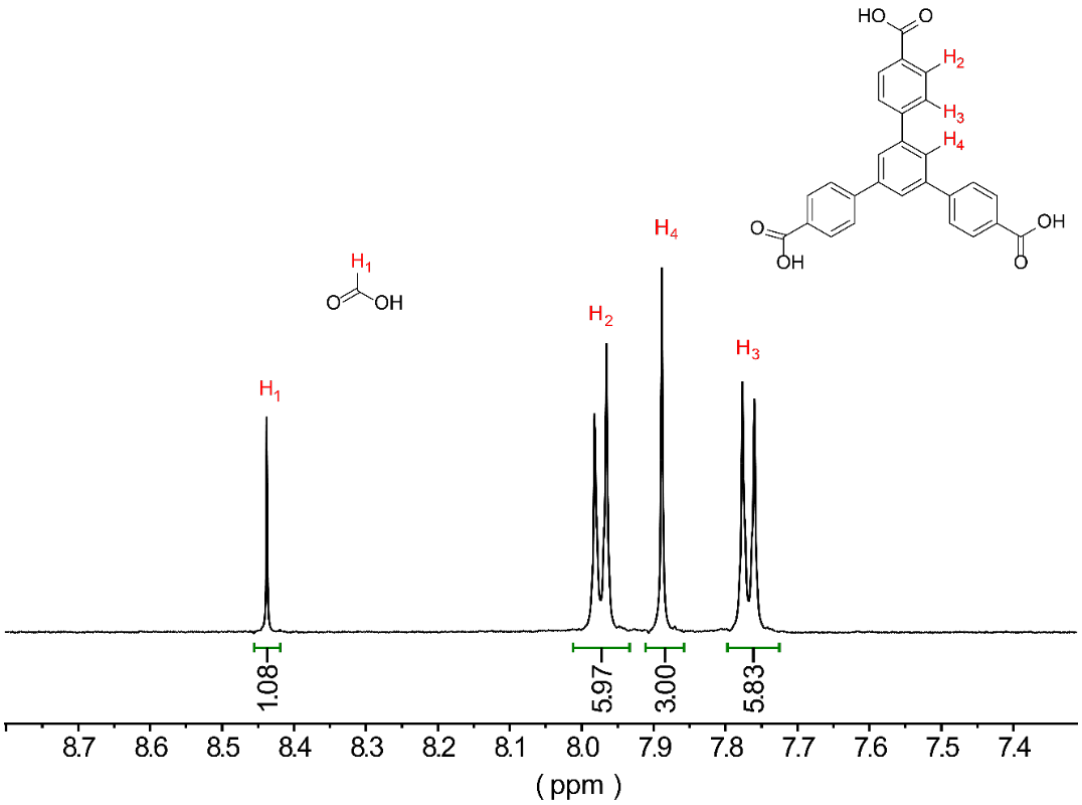

Fig. S6. ^{1}H NMR data of digested guest free MOF-520 in d_6-DMSO.

Section S2. Inclusion procedures and single crystal X-ray diffraction analyses

Section S2.1. Inclusion procedures

Diclofenac sodium salt, benzoic acid, heptanoic acid, anhydrous ethylene glycol (99.8 %), and anhydrous methanol (99.8 %) were purchased form Sigma Aldrich Co. 3-hydroxybenzoic acid, gibberellin A_3, genistein, (±)-jasmonic acid, 4-bromophenol, 1,3,5-benzentricarboxylic acid , 3-nitrophenol, and 3,5-diaminobenzoic acid were purchased from TCI America. Boc-(RS)-3-amino-1,2-propanediol was purchased from AnaSec Inc. Gibberellin A_1 was purchased from Santa Cruze Biotechnology, Inc. All chemicals obtained were used without further purification.

MOF-520 single crystal preparation. As-synthesized MOF-520 single crystals were washed with fresh DMF (10 mL), three times per day for three days to remove unreacted starting materials in the pore. Between each washing procedure, the crystals were kept in fresh DMF (18 mL in a 20 mL vial). Otherwise mentioned in the detail procedure, MOF-520 single crystals impregnated with DMF were used for the molecule showing better solubility in DMF. When the molecules dissolve better in acetone, MOF-520 single crystals impregnated with acetone were prepared by exchanging DMF in the pore with fresh acetone following the solvent exchange procedure in Section S1.1. Since the bulk sample is a racemic conglomerate, a mixture of both enantiomers was used for the inclusion.

General inclusion procedure. In general, the introduction of the molecules (15 to 50 mg scale) into MOF-520 was carried out by soaking MOF-520 single crystals impregnated with fresh DMF or acetone in a saturated solution of the molecule in DMF or acetone, respectively. The choice of the solvent of the solution was decided by the solubility of the molecules. The mixture of MOF-520 and the molecule solution was prepared in a scintillation vial. The vial was closed with a polypropylene cap having foil liner and placed in a preheated isothermal oven, 40 °C for acetone solution and 100 °C for DMF solution. After several days, SXRD data collection was carried out with the resulting single crystals. To confirm the incorporation of molecules along with SXRD data, ^{1}H NMR data was collected for MOF-520-**1** to -**5** following the procedure in Section S1.6**.** They represent the whole functionalities though which the molecules, **1** to **16**, bind to Al. Although the incorporation can be confirmed from the NMR data, some of the integration ratio, molecule to H_3BTB linker, show deviation from the occupancy in the refined structures (Section S2.2). This can be explained by that the molecule incorporation in a single crystal does not represent the whole batch of the sample.

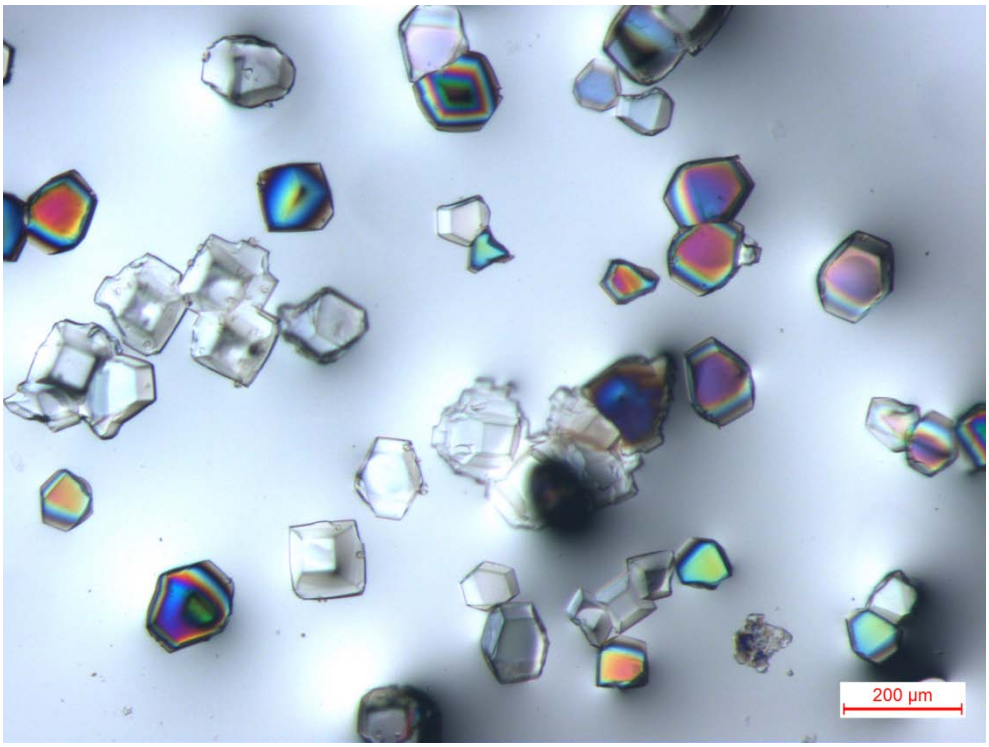

Fig. S7. As-synthesized MOF-520 single crystals image obtained from optical microscope under polarized light.

MOF-520-1 (**1** = benzoic acid). Benzoic acid solution was prepared by adding benzoic acid (40.0 mg, 0.326 mmol) to DMF (200.0 µL) in a 4 mL vial and the solution was sonicated for 10 min to dissolve the material. MOF-520 single crystals (1.0 mg) impregnated with DMF were added to the solution. The vial was closed and placed in the preheated 100 °C oven. After 12 hours, the vial was kept at room temperature to slowly cool down the solution. SXRD data was collected with a single crystal from the vial.

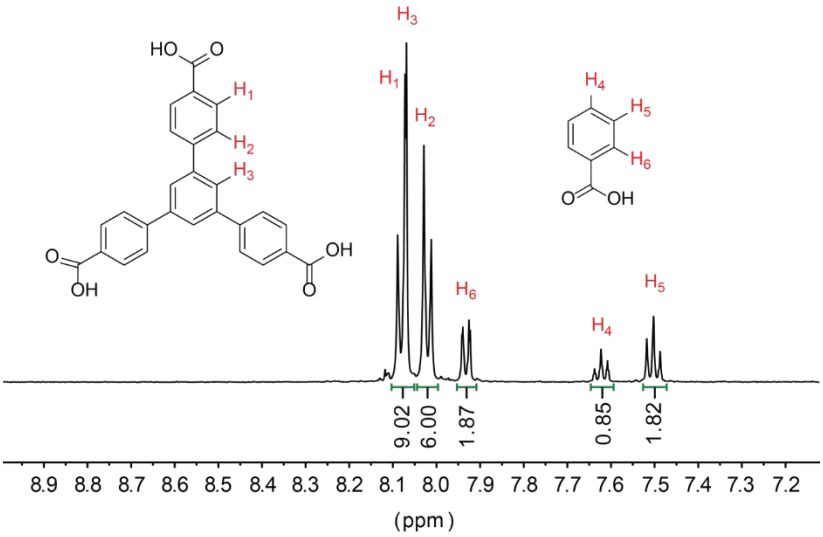

Fig. S8. ^{1}H NMR data of digested guest free MOF-520-**1** in d_6-DMSO.

MOF-520-2 (**2 =** methanol). The activated guest free single crystals of MOF-520 (50 mg) were soaked in anhydrous methanol (10 mL) in a 20 mL vial. The vial was kept in a preheated 40 °C oven for 15 days. After the reaction, the vial was cooled down at room temperature. One of the single crystals was used for SXRD analysis and rest of the crystals were activated to evacuate the pore. The same solvent exchange and activation procedure for MOF-520 was applied (Section S1.1)

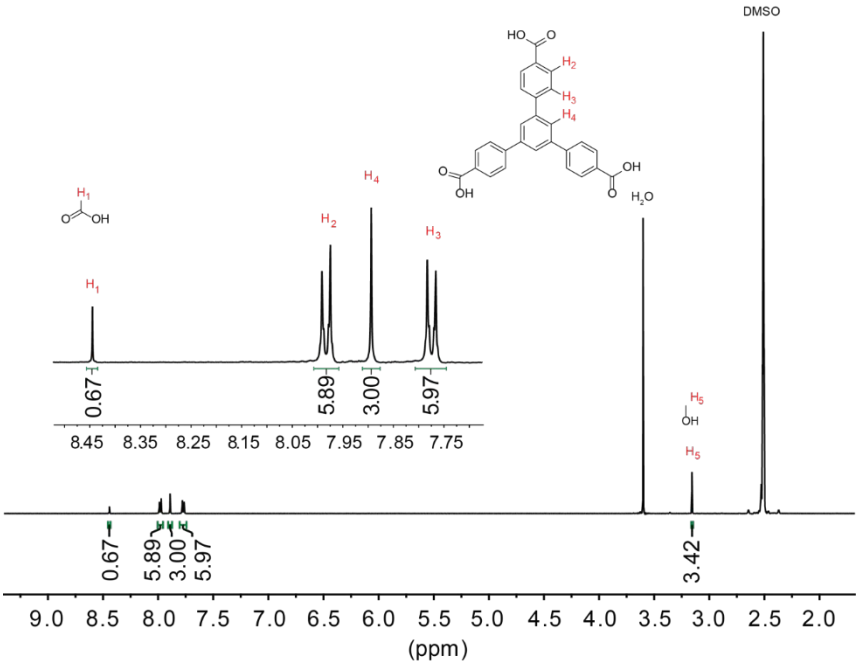

Fig. S9. ^{1}H NMR data of digested guest free MOF-520-**2** in d_6-DMSO.

MOF-520-3 (3 = ethylene glycol). The activated single crystals of MOF-520 (50 mg) were soaked in ethylene glycol (10 mL) in a 20 mL vial. The vial was kept in a preheated 100 °C oven for 5 days. After the reaction, one of the single crystals was used for SXRD analysis and rest of the crystals were activated to evacuate the pore. The same solvent exchange and activation procedure for MOF-520 was applied (Section S1.1).

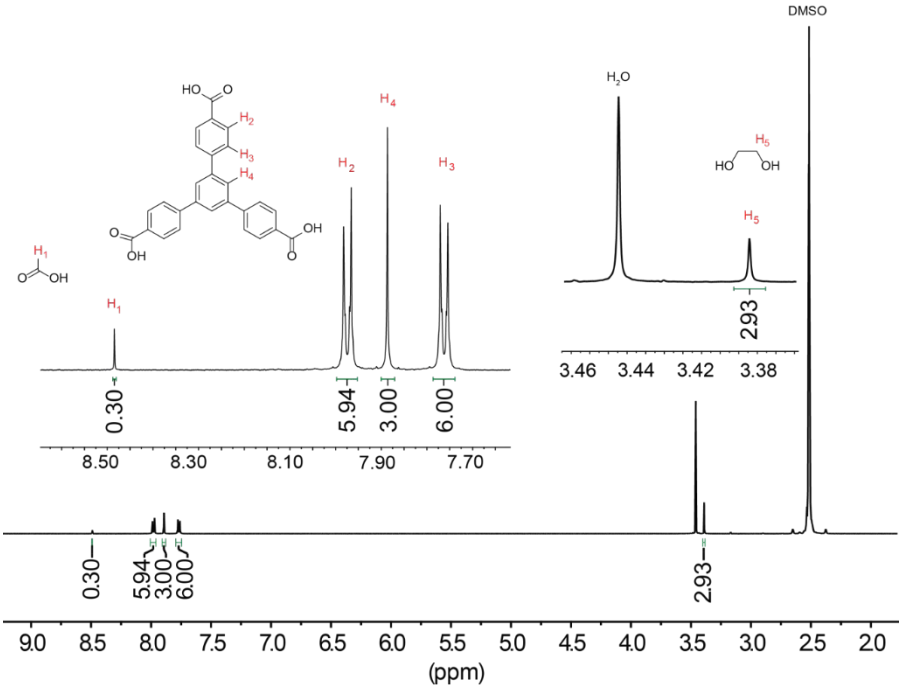

Fig. S10. ^{1}H NMR data of digested guest free MOF-520-**3** in d_6-DMSO.

MOF-520-4 (4 = 3-nitrophenol). 3-nitrophenol solution was prepared by adding 3-nitrophenol (60.0 mg, 0.432 mmol) to anhydrous acetone (200.0 µL) in a 4 mL vial followed by adding triethylamine (2.0 µL) into the solution. MOF-520 single crystals (1.0 mg) impregnated with acetone were added to the solution. The vial was capped and placed in the room temperature for 10 days. SXRD data was collected with a single crystal from the vial.

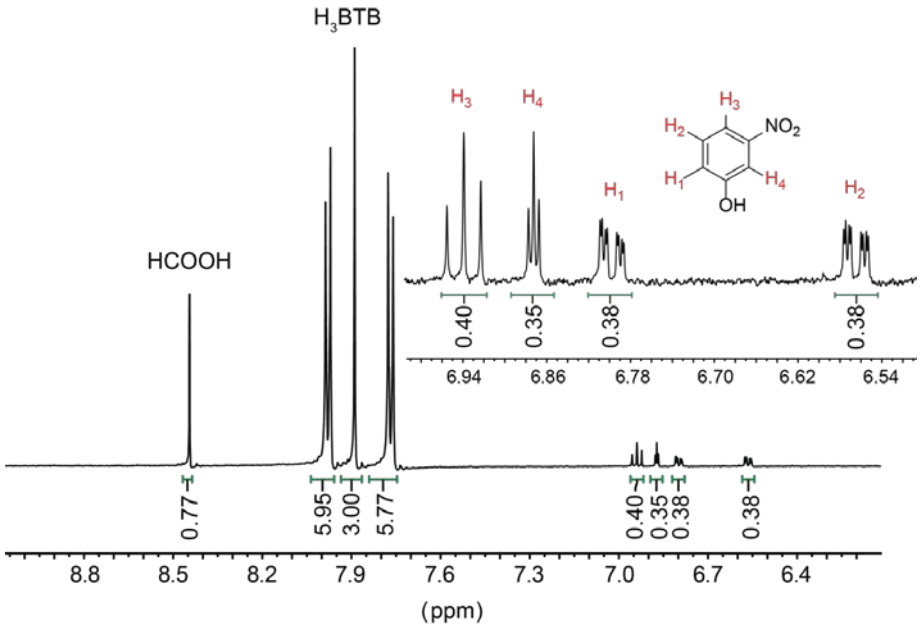

Fig. S11. ^{1}H NMR data of digested guest free MOF-520-**4** in d_6-DMSO.

MOF-520-5 (5= heptanoic acid). Heptanoic acid solution was prepared by adding heptanoic acid (60.0 µL, 0.424 mmol) to anhydrous DMF (200.0 µL) in a 4 mL vial. MOF-520 single crystals (1.0 mg) impregnated with DMF were added to the solution. The vial was closed and placed in the preheated 100 °C oven. After 2 days, SXRD data was collected with a single crystal from the vial.

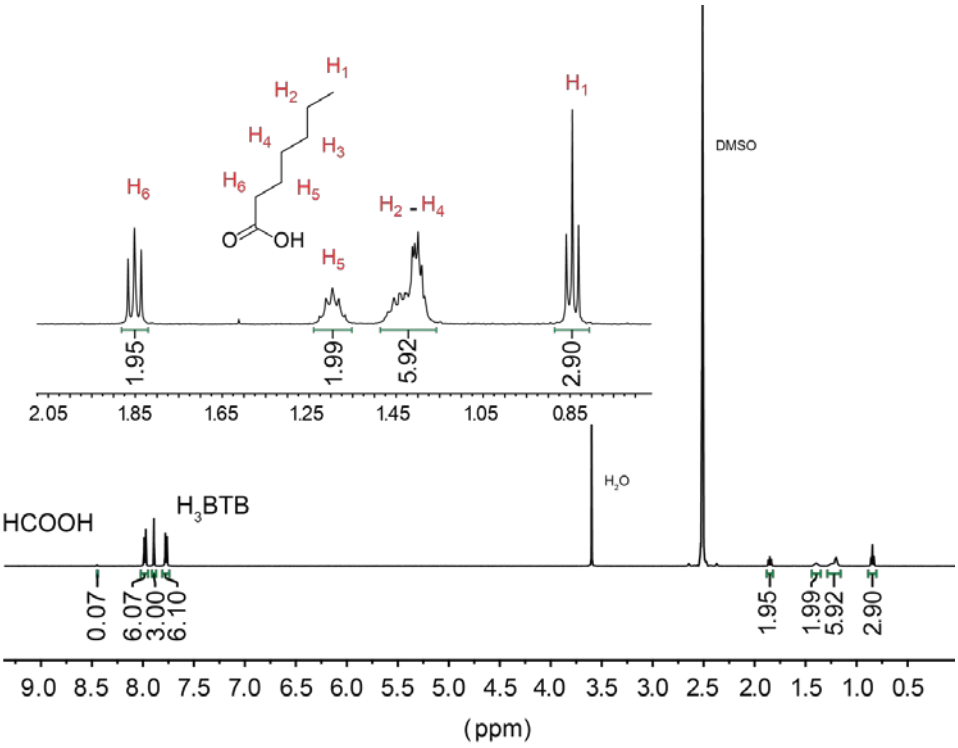

Fig. S12. ^{1}H NMR data of digested guest free MOF-520-**5** in d_6-DMSO.

MOF-520-6 (6 = 3-hydroxybenzoic acid). 3-hydroxybenzoic acid (60.0 mg, 0.434 mmol) was added to DMF (200.0 µL) in a 4 mL vial and the solution was sonicated for 10 min to dissolve the material. MOF-520 single crystals (1.0 mg) impregnated with DMF were added to the solution. The vial was capped and placed in preheated 100 °C oven for 24 hrs. SXRD data was collected with a single crystal from the vial.

MOF-520-7 (7 = 3,5-diaminobenzoic acid). 3-hydroxybenzoic acid (60.0 mg, 0.394 mmol) was added to anhydrous acetone (200.0 µL) in a 4 mL vial and the solution was sonicated for 10 min to dissolve the material. MOF-520 single crystals (1.0 mg) impregnated with acetone were added to the solution. The vial was capped and placed in preheated 40 °C oven for 2 days. SXRD data was collected with a single crystal from the vial.

MOF-520-8 (8 = Trimesic acid). Trimesic acid (50.0 mg, 0.238 mmol) was added to DMF (200.0 µL) in a 4 mL vial and the solution was sonicated for 10 min to dissolve the material. MOF-520 single crystals (1.0 mg) impregnated with DMF were added to the solution. The vial was capped and placed in preheated 100 °C oven for 24 hrs. SXRD data was collected with a single crystal from the vial.

MOF-520-9 (9 = 4-bromophenol). 4-bromophenol solution was prepared by adding 4-bromophenol (60.0 mg, 0.432 mmol) to anhydrous acetone (200.0 µL) in a 4 mL vial followed by adding triethylamine (2.0 µL) into the solution and the solution was sonicated for 10 min to dissolve the material. MOF-520 single crystals (1.0 mg) impregnated with acetone were added to the solution and the vial was placed in the preheated 40 °C oven for 10 days. SXRD data was collected with a single crystal from the vial.

MOF-520-10 (10 = diclofenac). Diclofenac solution was prepared by adding sodium diclofenac sodium salt (30.0 mg, 0.094 mmol) to anhydrous DMF (150.0 µL) in a Pyrex tube measuring 10 × 8 mm (o.d × i.d) and the solution was sonicated for 10 min to dissolve the material. MOF-520 single crystals (2.0 mg) impregnated with DMF were added to the solution. The tube was sealed by freeze-pump- thaw method (30 mTorr) and placed in the preheated 100 °C oven for 3 days. SXRD data was collected with a single crystal from the tube.

MOF-520-2-11 (11 = genistein). Genistein solution was prepared by adding genistein (10.0 mg, 0.0370 mmol) to anhydrous acetone (400.0 µL) in a 4 mL vial followed by adding triethylamine (10 µL), and the solution was sonicated for 10 min to dissolve the material. MOF-520-**2** single crystals (3.0 mg) impregnated with acetone were added to the solution. The vial was capped and placed in the preheated 45 °C oven for 5 days. SXRD data was collected with a single crystal from the vial.

MOF-520-12 (12 = Boc-(RS)-3-amino-1,2-propanediol). Boc-(RS)-3-amino-1,2-propanediol solution was prepared by adding Boc-(RS)-3-amino-1,2-propanediol (50.0 mg, 0.094 mmol) to DMF (300.0 µL) and the solution was sonicated for 10 min to dissolve the material. MOF-520 single crystals (1.0 mg) impregnated with DMF were added to the solution. The vial was capped and placed in preheated 100 °C oven for 3 days. SXRD data was collected with a single crystal from the vial.

MOF-520-3-13 (13 = gibberellin A_1). Gibberellin A_1 solutions was prepared by adding gibberellin A_1 (15.0 mg, 0.0433 mmol) to DMF (200.0 µL) in a 4 mL vial, and the solution was sonicated for 10 min to dissolve the material. MOF-520-**3** single crystals (5.0 mg) impregnated with DMF were added to the solution. The vial was capped and placed in the preheated 100 °C oven for 5 days. SXRD data was collected with a single crystal from the vial.

MOF-520-3-14 (14 = gibberellin A_3). Gibberellin A_3 solutions was prepared by adding gibberellin A_3 (15.0 mg, 0.0433 mmol) to DMF (200.0 µL) in 10 mm opening Pyrex tube, and the solution was sonicated for 10 min to dissolve the material. MOF-520-**3** single crystals (5.0 mg) impregnated with DMF were added to the solution. The tube was sealed by freeze-pump- thaw method (50 mTorr) and placed in the preheated 100 °C oven for 4 days. SXRD data was collected with a single crystal from the tube.

MOF-520-15 and -16 (15 = (-)-jasmonic acid, 16 = (+)-jasmonic acid). (±)-Jasmonic acid solution was prepared by adding (±)-jasmoic acid (100 µL) to anhydrous DMF (100.0 µL) in the Pyrex tube, and the solution was sonicated for 1 min to dissolve the material. MOF-520 single crystals (2.0 mg) impregnated with DMF were added to the solution. The tube was sealed by

freeze-pump- thaw method (30 mTorr) and placed in the preheated 100 °C oven for 4 days. SXRD data was collected with a single crystal from the tube.

Section S2.2. Single crystal X-ray analysis of inclusion crystals

After the inclusion of the molecules, several single crystals from each batch were mounted on the diffractometer and SXRD data was collected. In a typical experiment the single-crystalline sample was mounted on MiTeGen® kapton loops in LV CryoOil® and placed in a 100(2) K nitrogen cold stream from Oxford Cryosystems Cryostream equipment. All the resulting batches after the inclusion are also racemic conglomerate as pristine MOF-520. The best data in terms of the occupancy of the molecules incorporated was chosen and reported here. Since the chirality of a single crystal could not be distinguished by inspection of the shape of the crystal or by polarized light, the choice of the chirality of the inclusion crystal from the batch was not in control. The resolution obtained for all samples was limited due to inherent disorder in the crystals; in order to improve the refinement of the model, the resolution was cut off, according to intensity statistics table. In case of measurements with synchrotron radiation, i.e. the wavelength is not CuK_α, the DISP command was used to set the f′, f″, and μ values for atoms in the structures.

The refinement procedure can be divided into several parts: the anisotropic refinement of the MOF structure, the localization and assignment of the bound molecule, the anisotropic refinement of the bound molecule, and solvent masking procedure. First, the structure of MOF is refined anisotropically and all hydrogen atoms are placed into geometrically calculated positions. The connected asymmetric unit was defined inside the unit cell: MOVE command was applied to all atoms. The weighting scheme is refined as well as the extinction coefficient. After this step, we started to assign the electron density peaks, which are closest to the binding site, and can be interpreted as a part of the bound molecule. The assigned atoms are refined with $U^{iso} = 0.05$. Once assignment of large part of the molecule is done, the occupancy of the bound molecule is estimated with a free variable and isotropic displacement parameters were refined freely. Once the refinement has run to convergence, the resulting occupancy is fixed throughout the whole bound molecule. Typically, standard deviations of U^{iso}'s tend to increase with increasing distance from the binding site. The occupancy of binding carboxylate group or alcoholic or phenolic oxygen atoms are given unit value. Once the whole molecule is localized and fixed, a step-by-step anisotropic refinement is carried out: the closest atom to the binding site is refined first followed by the refinement of further atom. Once all non-hydrogen atoms are refined anisotropically, hydrogen atoms present at the target molecule are placed into geometrically calculated positions. The electron density due to the presence the highly disordered solvent molecule of DMF within the pore, is accounted for by a solvent masking procedure (*21*). Note that due to partial occupancy of the target molecule at the binding site of the SBU, the electron density of the target molecule is superimposed by some solvent density, which cannot be taken into account by the solvent masking procedure. In addition, it needs to be considered that obscuring of low-angle reflections significantly affects the amount of unassigned electron density, accounted by solvent masking procedure, but not the geometry of bound molecule. Before and after solvent masking, the Flack parameters are within the 3σ error range, i.e.

$$|x_{\text{before masking}} - x_{\text{after masking}}| < 3[(u_{\text{before masking}})^2 + (u_{\text{after masking}})^2]^{1/2},$$

where x is the absolute Flack parameter value and u is its estimated standard deviation (*22*).

All geometrical restraints and occupational constraints, applied to non-hydrogen atoms of bound molecules, are listed in the CIF files as well as on the corresponding table of each structure.

Structure	*MOF-bound molecule Al–O distance [a]/ Å*	*Types of non-covalent interactions [b]*	*R* [$I>2\sigma(I)$]	*S*	*Flack parameter, x(u)*
Δ-MOF-520-**1**	1.913(4) 1.994(4)	N/A	0.0508	0.965	0.076(15)
Λ-MOF-520-**2**	1.8648(12) 1.9008(12)	N/A	0.0334	0.982	0.059(14)
Δ-MOF-520-**3**	1.882(3) 1.941(3)	N/A	0.0385	0.916	0.10(3)
Λ-MOF-520-**4**	1.876(3) 1.944(3)	π–π (P) [c]	0.0560	1.051	0.07(4)
Λ-MOF-520-**5**	1.9084(16) 1.9268(16)	CH–π	0.0372	1.024	0.064(8)
Δ-MOF-520-**6**	1.904(3) 1.918(3)	N/A	0.0542	1.025	0.07(3)
Λ-MOF-520-**7**	1.8978(18) 1.8986(19)	NH–π	0.0418	1.002	0.06(4)
Λ-MOF-520-**8**	1.900(7) 1.966(8)	OH–π	0.0620	0.988	0.10(3)
Λ-MOF-520-**9**	1.889(3) 1.911(3)	π–π (P), π–π (T) [d]	0.0613	1.018	0.10(3)
Δ-MOF-520-**10**	1.907(6) 1.921(6)	π–π (T), NH–O	0.0532	1.050	0.13(2)
Δ-MOF-520-**2**-**11**	1.878(3)	π–π (P), π–π (T), OH- π	0.0516	1.081	0.144(16)
Λ -MOF-520-**12**	1.873(3) 1.922(3)	CH–π, NH–O	0.0523	1.024	0.040(15)
Λ -MOF-520-**3**-**13**	1.9106(18) 1.9238(17)	CH–π, OH–π	0.0568	1.082	0.063(9)
Λ -MOF-520-**3**-**14**	1.909(3) 1.918(3)	CH–π, OH–π	0.0580	0.942	0.05(2)
Δ-MOF-520-**15**	1.9025(18) 1.9299(17)	CH–π, CH–O	0.0474	1.040	0.037(8)
Λ -MOF-520-**16**	1.9099(16) 1.9255(15)	CH–π, CH–O	0.0460	1.082	0.040(8)

Table S4. The distances of covalent bonding and types of intramolecular interactions in all structures with their crystallographic refinement parameters. Superscript a: more than one covalent interactions are indicated by the range of the distances, b: the types of interactions are estimated considering the functional groups and the distance between them, c: parallel-displaced, d: T-shaped configuration.

Δ-MOF-520-1. A colorless truncated octahedron-shaped crystal (110 x 80 x 80 μm^3) of **Δ**-MOF-520-**1** was measured at a Bruker D-8-Venture diffractometer with radiation of λ = 1.54178 Å. According to intensity statistics table for the whole dataset (PRP file), the resolution was cut off to 1.00 Å. Solvent masking was applied during structure refinement. Before solvent masking instruction, structure was refined anisotropically and hydrogen atoms were placed into positions calculated geometrically. The molecule of benzoic acid was found to be positionally disordered (two parts with 0.5 occupancy). The connected asymmetric unit was defined inside the unit cell: MOVE command was applied to all atoms. The weighting scheme is refined as well as the extinction coefficient. The void volume is estimated to be 8312 $Å^3$ with 5692 electrons. Some reflections were omitted due to non-ideal solvent masking, beam stop clipping and the minor presence of diffuse scattering. The threshold $(I_{obs}-I_{calc})/\sigma(W)>10$ was chosen for omitting these reflections. Omission of these reflections did not affect the refinement; the fraction of omitted reflections is less than 0.1% of the whole dataset.

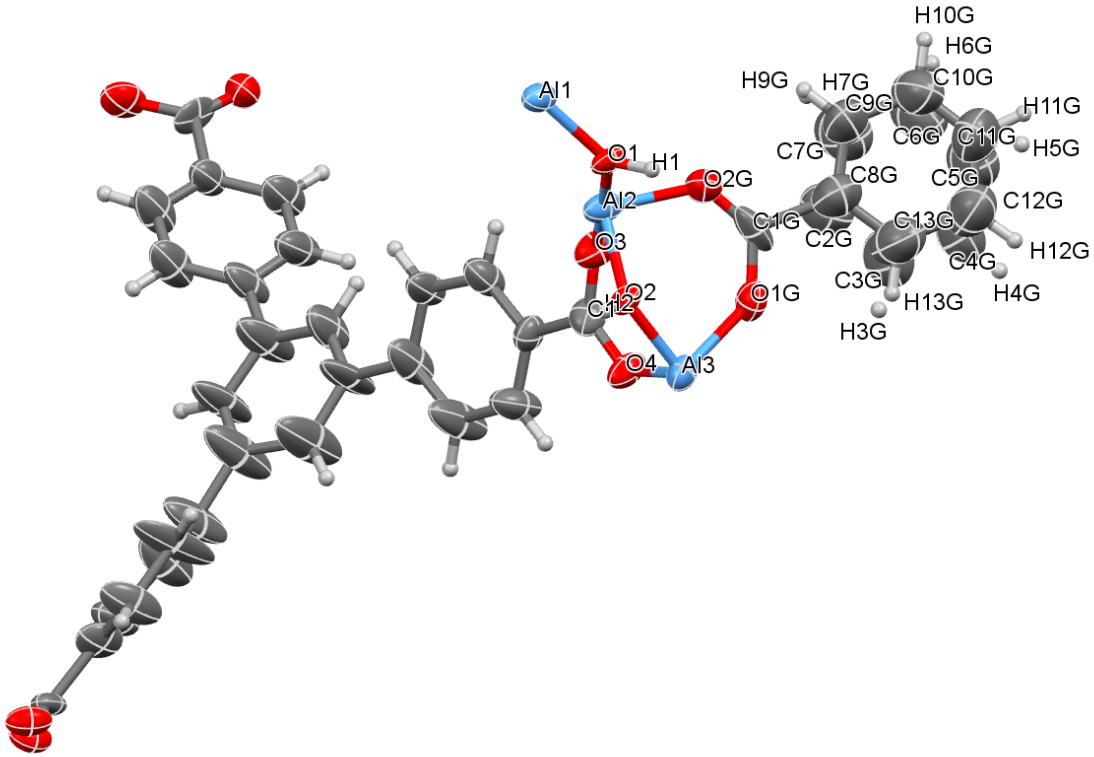

Fig. S13. Asymmetric unit in the single crystal structure of **Δ**-MOF-520-**1**. Thermal ellipsoids are drawn with 50% probability.

Λ-MOF-520-2. A colorless truncated octahedron-shaped crystal (60 x 40 x 40 μm^3) of **Λ**-MOF-520-**2** was measured at a beamline 11.3.1 at the ALS with radiation of λ = 1.0332 Å. According to intensity statistics table for the whole dataset (PRP file), the resolution was cut off to 0.84 Å. Solvent masking was applied during structure refinement. Before solvent masking instruction, structure was refined anisotropically and hydrogen atoms were placed into positions calculated geometrically. The connected asymmetric unit was defined inside the unit cell: MOVE command was applied to all atoms. The weighting scheme is refined as well as the extinction coefficient. The void volume is estimated to be 19048 Å^3 with 5013 electrons removed during masking. The occupancy for 2 bound molecules of methanol was constrained to 1. Some reflections were omitted due to non-ideal solvent masking, beam stop clipping and the minor presence of diffuse scattering. The threshold $(I_{obs}-I_{calc})/\sigma(W)>10$ was chosen for omitting these reflections. Omission of these reflections did not affect the refinement; the fraction of omitted reflections is less than 0.1% of the whole dataset.

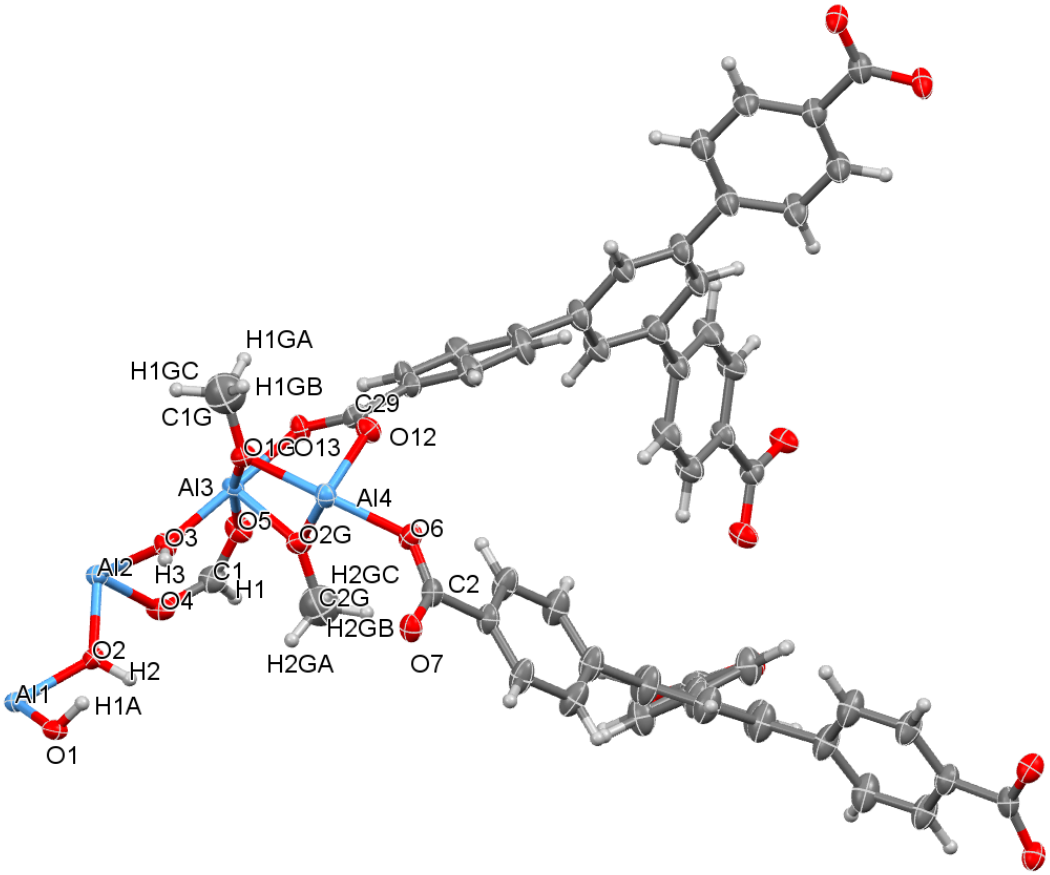

Fig. S14. Asymmetric unit in the single crystal structure of **Λ**-MOF-520-**2**. Thermal ellipsoids are drawn with 50% probability.

Δ-MOF-520-3. A colorless truncated octahedron-shaped crystal (100 x 85 x 85 μm^3) of **Δ**-MOF-520-**3** was measured at a beamline 11.3.1 at the ALS with radiation of λ = 1.23990 Å. According to intensity statistics table for the whole dataset (PRP file), the resolution was cut off to 0.97 Å. The occupancy of each ethylene glycol was found through adding a new variable and then constrained to 1.0. The occupancy of the dangling moiety of the formic acid was set to 0.4. Solvent masking was applied during structure refinement. Before solvent masking instruction, structure was refined anisotropically and hydrogen atoms were placed into positions calculated geometrically. The connected asymmetric unit was defined inside the unit cell: MOVE command was applied to all atoms. The weighting scheme is refined as well as the extinction coefficient. The void volume is estimated to be 17397 $Å^3$ with 18733 electrons removed during masking. Some reflections were omitted due to non-ideal solvent masking, beam stop clipping and the minor presence of diffuse scattering. The threshold $(I_{obs}-I_{calc})/\sigma(W)>10$ was chosen for omitting these reflections. Omission of these reflections did not affect the refinement; the fraction of omitted reflections is less than 0.1% of the whole dataset.

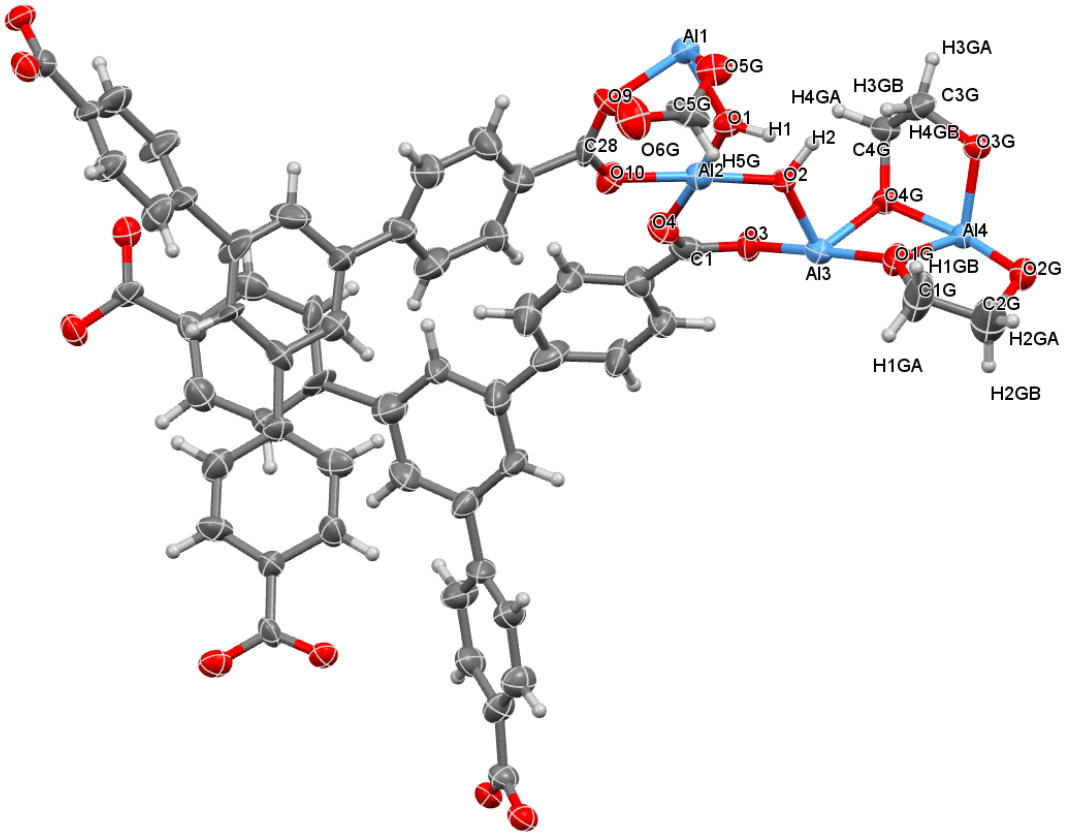

Fig. S15. Asymmetric unit in the single crystal structure of **Δ**-MOF-520-**3**. Thermal ellipsoids are drawn with 50% probability.

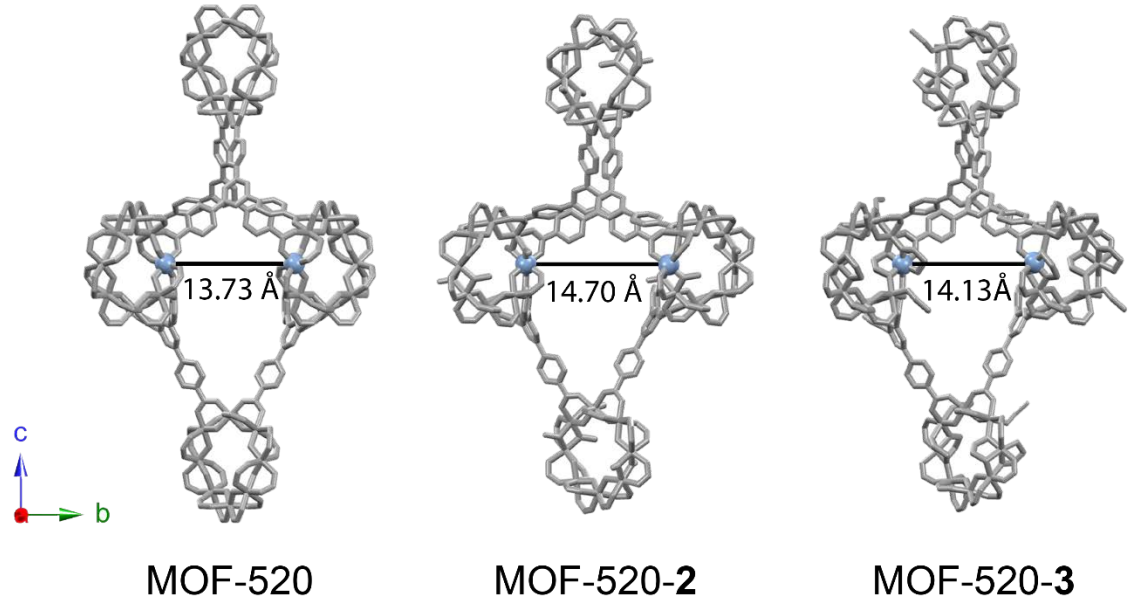

Fig. S16. Channel width comparison between MOF-520, MOF-520-**2**, and -**3.** The frameworks are indicated with gray stick models and the Al on adjacent SBUs are indicated with blue sphere. MOF-520 was used for the crystallization of incoming molecules **1** to **10**, **12**, **15**, and **16**; MOF-520-**2** for **11** (the molecule **11** is 12.68 Å along its longest dimension); MOF-520-**3** for **13** and **14 (**the molecules **13, 14** are 10.20 Å along their longest dimensions).

Λ-MOF-520-4. A colorless truncated octahedron-shaped crystal (80 x 60 x 60 μm^3) of **Λ**-MOF-520-**4** was measured at a beamline 11.3.1 at the ALS with radiation of λ = 0.88560 Å. According to intensity statistics table for the whole dataset (PRP file), the resolution was cut off to 1.00 Å. The occupancy of each 3-nitrophenol was found through adding a new variable and then constrained to 0.65, 0.35 and 0.5 values. The occupancy of the dangling moiety of the formic acid was set to 0.5. Solvent masking was applied during structure refinement. Before solvent masking instruction, structure was refined anisotropically and hydrogen atoms were placed into positions calculated geometrically. The connected asymmetric unit was defined inside the unit cell: MOVE command was applied to all atoms. The weighting scheme is refined as well as the extinction coefficient. Once solvent masking instruction was introduced, the weight scheme was refined to convergence. The void volume is estimated to be 15573 Å^3 with 3598 electrons removed during masking. Some reflections were omitted due to non-ideal solvent masking, beam stop clipping and the minor presence of diffuse scattering. The threshold $(I_{obs}-I_{calc})/\sigma(W)>10$ was chosen for omitting these reflections. Omission of these reflections did not affect the refinement; the fraction of omitted reflections is less than 0.1% of the whole dataset.

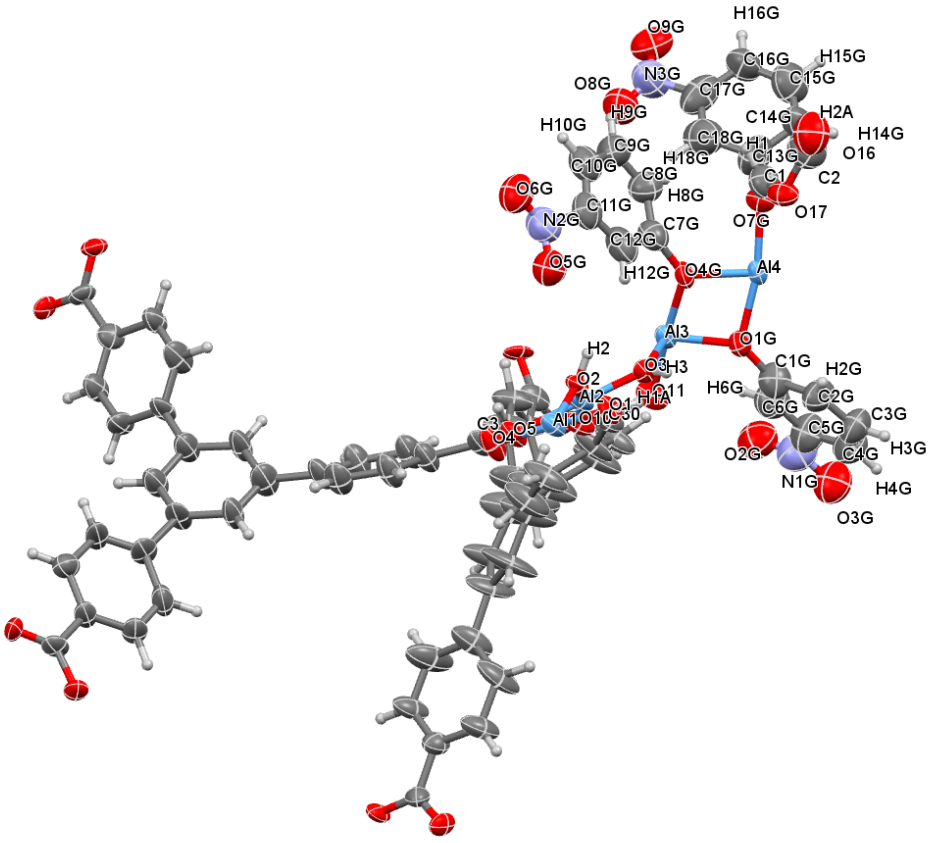

Fig. S17. Asymmetric unit in the single crystal structure of **Λ**-MOF-520-**4**. Thermal ellipsoids are drawn with 50% probability.

Λ-MOF-520-5. A colorless truncated octahedron-shaped crystal (90 x 60 x 60 μm^3) of **Λ**-MOF-520-**5** was measured at a beamline 11.3.1 at the ALS with radiation of λ = 1.23990 Å. According to intensity statistics table for the whole dataset (PRP file), the resolution was cut off to 0.80 Å. The occupancy of heptanoic acid was found to be 0.55 for the most of the structure and this occupancy value was set for the whole molecule. Solvent masking was applied during structure refinement. Before solvent masking instruction, structure was refined anisotropically and hydrogen atoms were placed into positions calculated geometrically. The connected asymmetric unit was defined inside the unit cell: MOVE command was applied to all atoms. The weighting scheme is refined as well as the extinction coefficient. Once solvent masking instruction was introduced, the weight scheme was refined to convergence. The C7G, C6G and C5G atoms are heavily overlapped with the solvent present in the crystal, so they were initially put into calculated positions using DFIX and DELU restraints. The void volume is estimated to be 8446 $Å^3$ with 5312 electrons removed during masking. Some reflections were omitted due to non-ideal solvent masking, beam stop clipping and the minor presence of diffuse scattering. The threshold (I_{obs}-I_{calc})/σ(W)>10 was chosen for omitting these reflections. Omission of these reflections did not affect the refinement; the fraction of omitted reflections is less than 0.1% of the whole dataset.

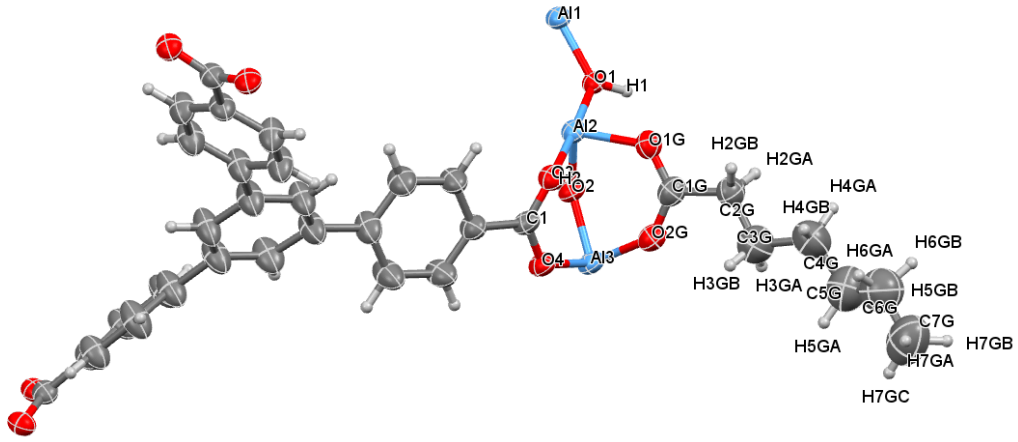

Fig. S18. Asymmetric unit in the single crystal structure of **Λ**-MOF-520-**5**. Thermal ellipsoids are drawn with 50% probability.

Δ-MOF-520-6. A colorless truncated octahedron-shaped crystal (100 x 80 x 80 μm^3) of **Δ**-MOF-520-**6** was measured at a beamline 11.3.1 at the ALS with radiation of λ = 0.77490 Å. According to intensity statistics table for the whole dataset (PRP file), the resolution was cut off to 0.83 Å. The overall occupancy of 3-hydroxybenzoic acid was constrained to 1. The molecule of 3,5-diaminobenzoic acid was found to be positionally disordered. The occupancy of each part of 3-hydroxybenzoic acid was found through adding a new variable: 0.58 and 0.42, respectively Solvent masking was applied during structure refinement. Before solvent masking instruction, structure was refined anisotropically and hydrogen atoms were placed into positions calculated geometrically. The connected asymmetric unit was defined inside the unit cell: MOVE command was applied to all atoms. The weighting scheme is refined as well as the extinction coefficient. Once solvent masking instruction was introduced, the weight scheme was refined to convergence. The void volume is estimated to be 7952 $Å^3$ with 1165 electrons removed during masking. Some reflections were omitted due to non-ideal solvent masking, beam stop clipping and the minor presence of diffuse scattering. The threshold $(I_{obs}-I_{calc})/\sigma(W)>10$ was chosen for omitting these reflections. Omission of these reflections did not affect the refinement; the fraction of omitted reflections is less than 0.1% of the whole dataset.

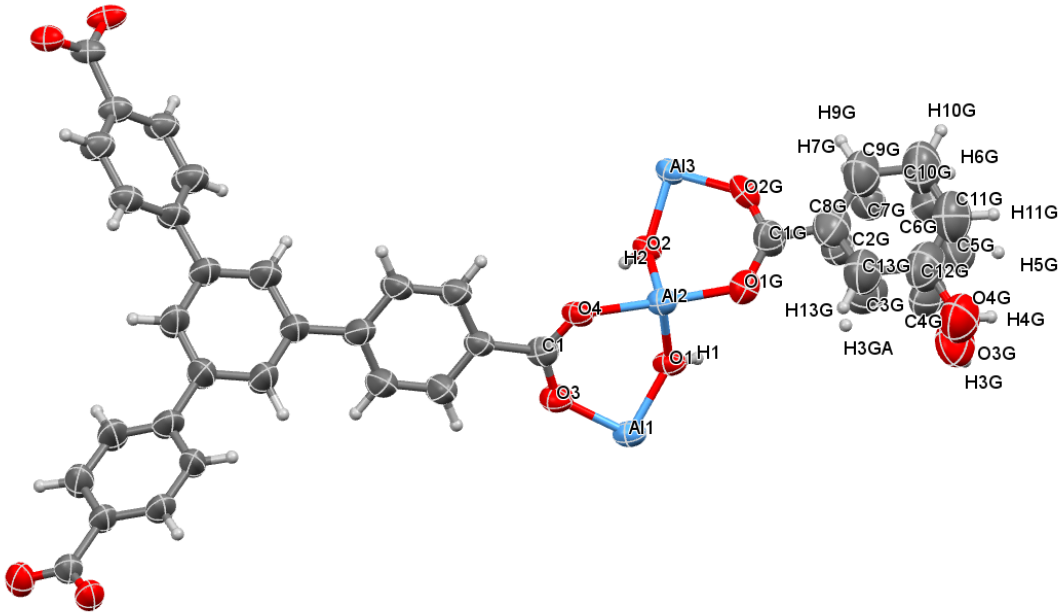

Fig. S19. Asymmetric unit in the single crystal structure of **Δ**-MOF-520-**6**. Thermal ellipsoids are drawn with 50% probability.

Λ-MOF-520-7. A colorless truncated octahedron-shaped crystal (80 x 50 x 50 μm^3) of **Λ**-MOF-520-**7** was measured at a beamline 11.3.1 at the ALS with radiation of λ = 0.77490 Å. According to intensity statistics table for the whole dataset (PRP file), the resolution was cut off to 0.83 Å. The molecule of 3,5-diaminobenzoic acid was found to be positionally disordered. The occupancy of each part of 3,5-diaminobenzoic acid was found through adding a new variable and then constrained to 0.5. Solvent masking was applied during structure refinement. Before solvent masking instruction, structure was refined anisotropically and hydrogen atoms were placed into positions calculated geometrically. The connected asymmetric unit was defined inside the unit cell: MOVE command was applied to all atoms. The weighting scheme is refined as well as the extinction coefficient. Once solvent masking instruction was introduced, the weight scheme was refined to convergence. The void volume is estimated to be 8064 $Å^3$ with 1078 electrons removed during masking. Some reflections were omitted due to non-ideal solvent masking, beam stop clipping and the minor presence of diffuse scattering. The threshold $(I_{obs}-I_{calc})/\sigma(W)>10$ was chosen for omitting these reflections. Omission of these reflections did not affect the refinement; the fraction of omitted reflections is less than 0.1% of the whole dataset.

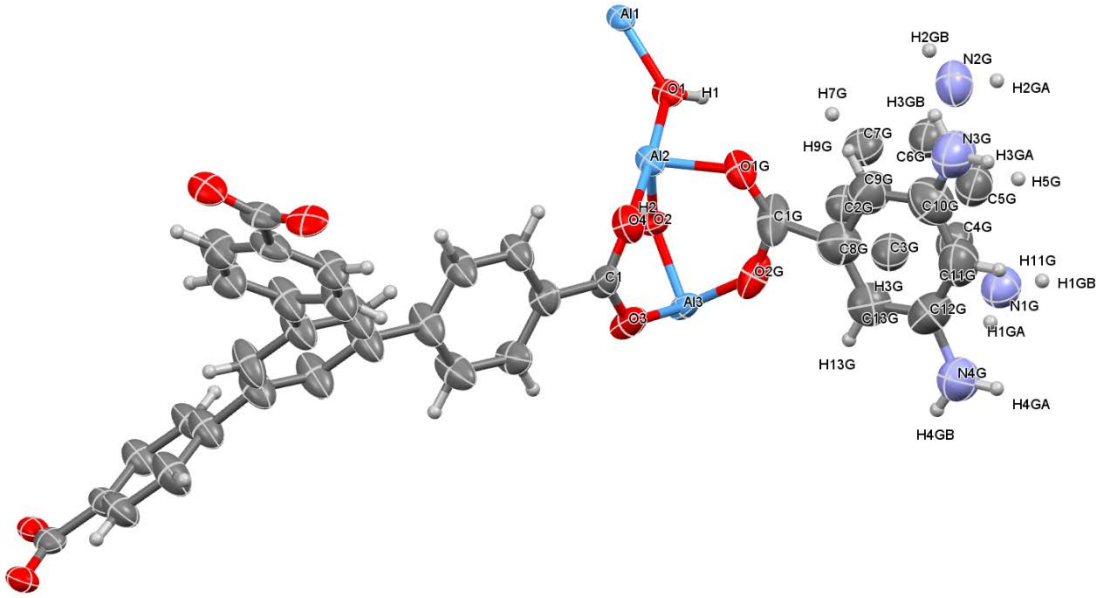

Fig. S20. Asymmetric unit in the single crystal structure of **Λ**-MOF-520-**7**. Thermal ellipsoids are drawn with 50% probability.

Λ-MOF-520-8. A colorless truncated octahedron-shaped crystal (110 x 90 x 90 μm^3) of **Λ**-MOF-520-**7** was measured at a Bruker D-8-Venture diffractometer with radiation of λ = 1.54178 Å. According to intensity statistics table for the whole dataset (PRP file), the resolution was cut off to 1.09 Å. The occupancy of trimesic acid was found through adding a new variable and then constrained to 0.75. Before solvent masking instruction, structure was refined anisotropically and hydrogen atoms were placed into positions calculated geometrically. The connected asymmetric unit was defined inside the unit cell: MOVE command was applied to all atoms. The weighting scheme is refined as well as the extinction coefficient. Once solvent masking instruction was introduced, the weight scheme was refined to convergence. The void volume is estimated to be 7995 $Å^3$ with 4902 electrons removed during masking. Some reflections were omitted due to non-ideal solvent masking, beam stop clipping and the minor presence of diffuse scattering. The threshold $(I_{obs}-I_{calc})/\sigma(W)>10$ was chosen for omitting these reflections. Omission of these reflections did not affect the refinement; the fraction of omitted reflections is less than 0.1% of the whole dataset.

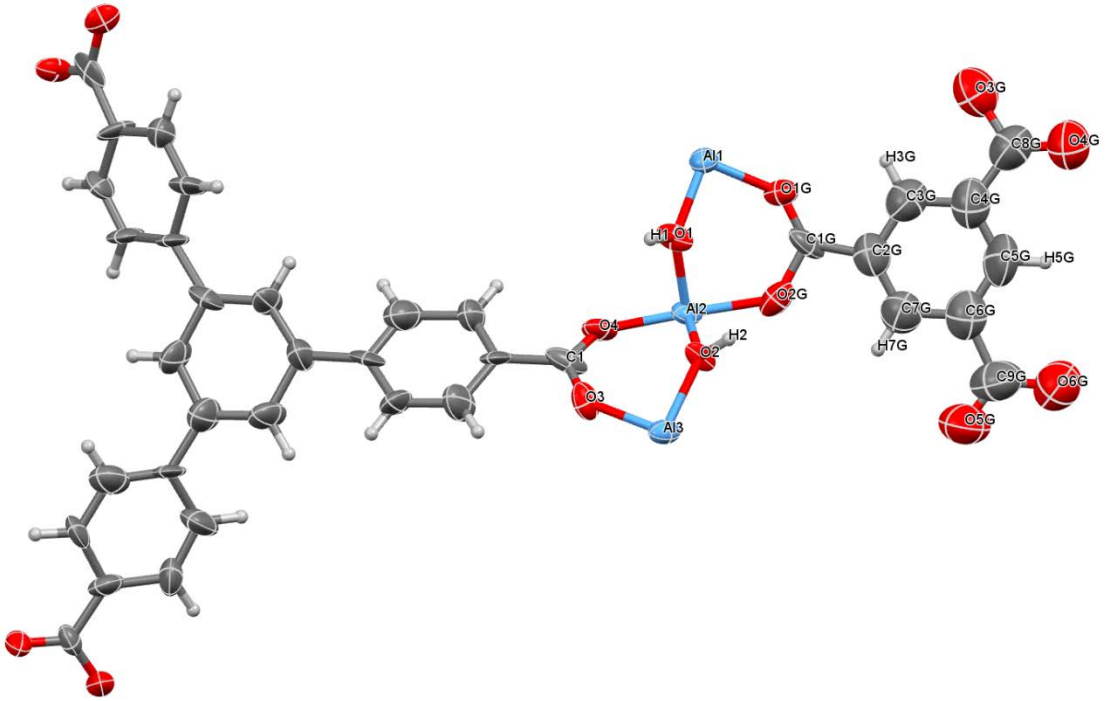

Fig. S21. Asymmetric unit in the single crystal structure of **Λ**-MOF-520-**8**. Thermal ellipsoids are drawn with 50% probability.

Λ-MOF-520-9. A colorless truncated octahedron-shaped crystal (100 x 80 x 80 μm^3) of **Λ**-MOF-520-**9** was measured at a beamline 11.3.1 at the ALS with radiation of λ = 0.95370 Å. According to intensity statistics table for the whole dataset (PRP file), the resolution was cut off to 0.83 Å. The occupancy of 4-bromophenol was found through adding a new variable and then constrained to 0.3 and 0.2. Before solvent masking instruction, structure was refined anisotropically and hydrogen atoms were placed into positions calculated geometrically. The connected asymmetric unit was defined inside the unit cell: MOVE command was applied to all atoms. The weighting scheme is refined as well as the extinction coefficient. Once solvent masking instruction was introduced, the weight scheme was refined to convergence. Since the amount of significant anomalous scatterers within the pore was not significant, the application of the solvent masking procedure was valid. The flack parameters for MOF-520-**9** before solvent masking and after was within 3σ error range: before, 0.010(2) and after, 0.010(3).The void volume is estimated to be 16409 Å^3 with 4945 electrons removed during masking. Some reflections were omitted due to non-ideal solvent masking, beam stop clipping and the minor presence of diffuse scattering. The threshold $(I_{obs}-I_{calc})/\sigma(W)>10$ was chosen for omitting these reflections. Omission of these reflections did not affect the refinement; the fraction of omitted reflections is less than 0.1% of the whole dataset.

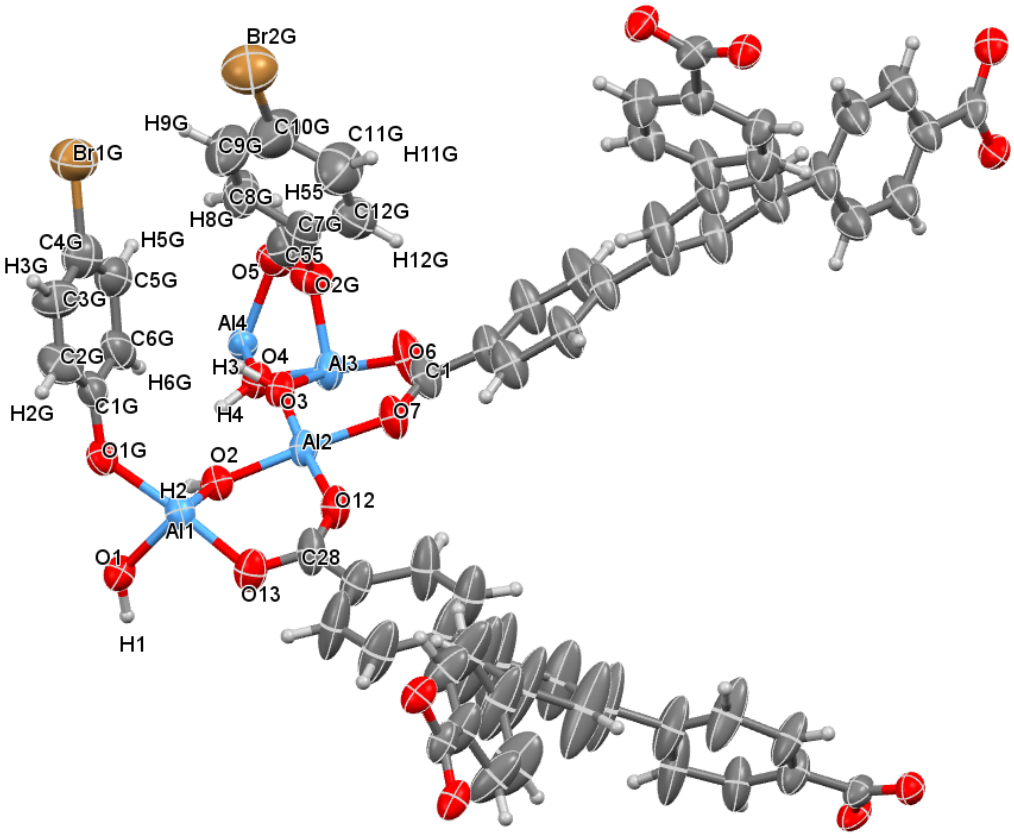

Fig. S22. Asymmetric unit in the single crystal structure of **Λ**-MOF-520-**9**. Thermal ellipsoids are drawn with 50% probability.

Δ-MOF-520-10. A colorless truncated octahedron-shaped crystal (70 x 55 x 55 μm^3) of **Δ**-MOF-520-**10** was measured at a beamline 11.3.1 at the ALS with radiation of λ = 1.0332 Å. According to intensity statistics table for the whole dataset (PRP file), the resolution was cut off to 0.83 Å. The occupancy of diclofenac was found through adding a new variable and then constrained to 0.35. Before solvent masking instruction, structure was refined anisotropically and hydrogen atoms were placed into positions calculated geometrically. The connected asymmetric unit was defined inside the unit cell: MOVE command was applied to all atoms. The weighting scheme is refined as well as the extinction coefficient. Once solvent masking instruction was introduced, the weight scheme was refined to convergence. Since the amount of significant anomalous scatterers within the pore was not significant, the application of the solvent masking procedure was valid. The flack parameters for MOF-520-**10** before solvent masking and after was within 3σ error range: before, 0.09(2) and after, 0.013(2). The void volume is estimated to be 16371 $Å^3$ with 13287 electrons removed during masking. The large value of unassigned electron density within the unit cell is due to missing of some low-angle observations. Some reflections were omitted due to non-ideal solvent masking, beam stop clipping and the minor presence of diffuse scattering. The threshold $(I_{obs}-I_{calc})/\sigma(W)>10$ was chosen for omitting these reflections. Omission of these reflections did not affect the refinement; the fraction of omitted reflections is less than 0.1% of the whole dataset.

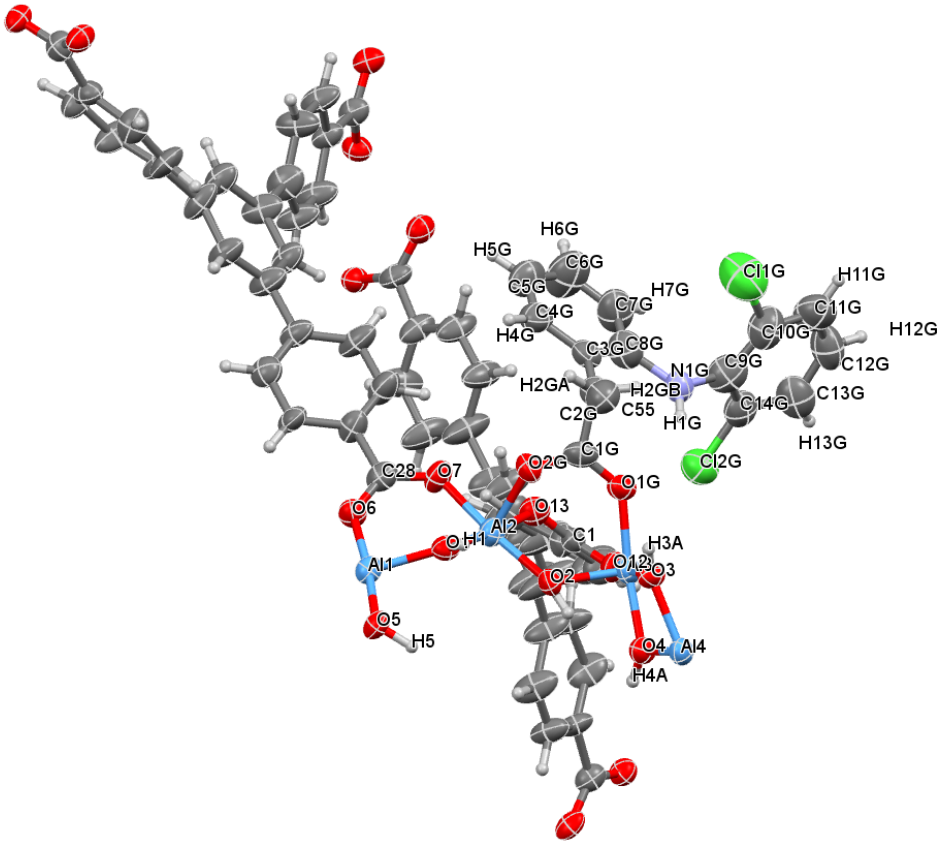

Fig. S23. Asymmetric unit in the single crystal structure of **Δ**-MOF-520-**10**. Thermal ellipsoids are drawn with 50% probability.

Δ-MOF-520-2-11. A colorless truncated octahedron-shaped crystal (85 x 55 x 55 μm^3) of **Δ**-MOF-520-**2-11** was measured at a beamline 11.3.1 at the ALS with radiation of λ = 1.2398 Å. According to intensity statistics table for the whole dataset (PRP file), the resolution was cut off to 0.89 Å. The occupancy of genistein was found through adding a new variable and then constrained to 0.40. The occupancy of 2 molecules of methanol was constrained to 0.50. The occupancy of dangling moiety was constrained to 0.40. Before solvent masking instruction, structure was refined anisotropically and hydrogen atoms were placed into positions calculated geometrically. After refining the framework anisotropically, **11** was found initially assigning C1G and C2G carbons in the electron density difference map. The connected asymmetric unit was defined inside the unit cell: MOVE command was applied to all atoms. The weighting scheme is refined as well as the extinction coefficient. Once solvent masking instruction was introduced, the weight scheme was refined to convergence. The FLAT command was used to set the planar geometry for part of the bound molecule. The void volume is estimated to be 16326 $Å^3$ with 12794 electrons removed during masking. The large value of unassigned electron density within the unit cell is due to missing of some low-angle observations. Some reflections were omitted due to non-ideal solvent masking, beam stop clipping and the minor presence of diffuse scattering. The threshold (I_{obs}-I_{calc})/σ(W)>10 was chosen for omitting these reflections. Omission of these reflections did not affect the refinement; the fraction of omitted reflections is less than 0.1% of the whole dataset.

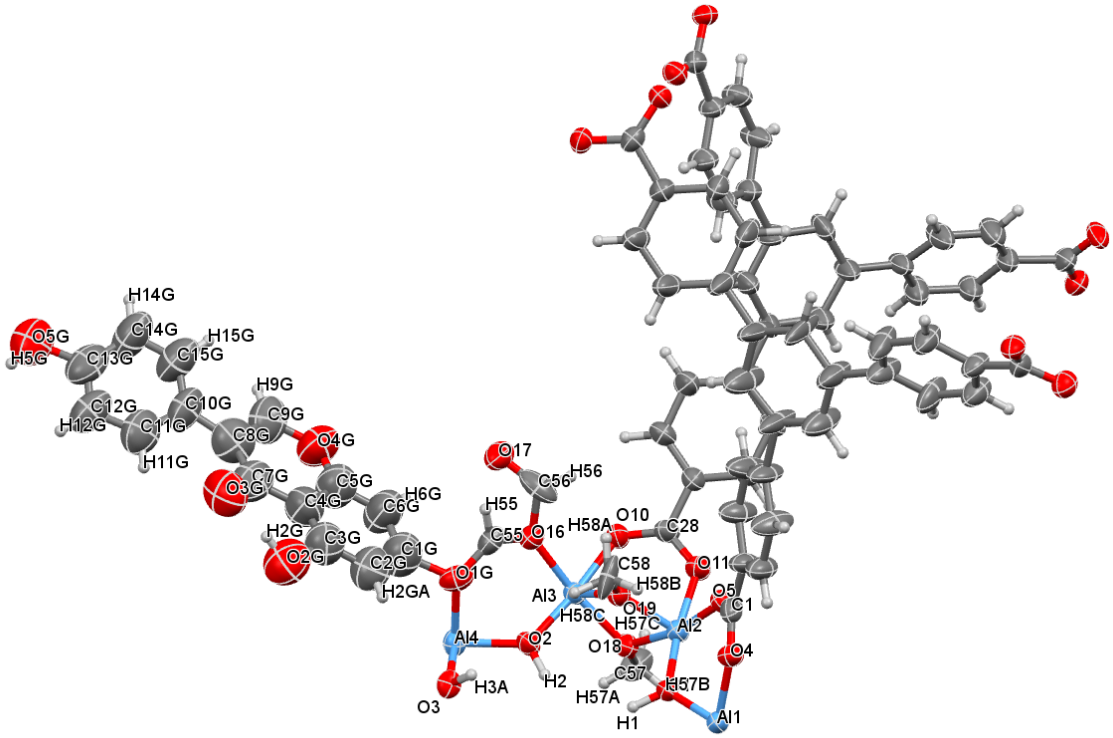

Fig. S24. Asymmetric unit in the single crystal structure of **Δ**-MOF-520-**2-11**. Thermal ellipsoids are drawn with 50% probability.

Λ-MOF-520-12. A colorless truncated octahedron-shaped crystal (90 x 60 x 60 μm^3) of **Λ**-MOF-520-**9** was measured at a beamline 11.3.1 at the ALS with radiation of λ = 1.2398 Å. According to intensity statistics table for the whole dataset (PRP file), the resolution was cut off to 1.00 Å. The occupancy of Boc-(RS)-3-amino-1,2-propanediol was found through adding a new variable and then constrained to 0.80. Before solvent masking instruction, structure was refined anisotropically and hydrogen atoms were placed into positions calculated geometrically. The connected asymmetric unit was defined inside the unit cell: MOVE command was applied to all atoms. The weighting scheme is refined as well as the extinction coefficient. Once solvent masking instruction was introduced, the weight scheme was refined to convergence. The tert-butyl part of the bound molecule was found to be disordered and overlapped with solvent, so DFIX command was used to fix the geometry this fragment. The void volume is estimated to be 7968 Å^3 with 3223. Some reflections were omitted due to non-ideal solvent masking, beam stop clipping and the minor presence of diffuse scattering. The threshold $(I_{obs}-I_{calc})/\sigma(W)>10$ was chosen for omitting these reflections. Omission of these reflections did not affect the refinement; the fraction of omitted reflections is less than 0.1% of the whole dataset.

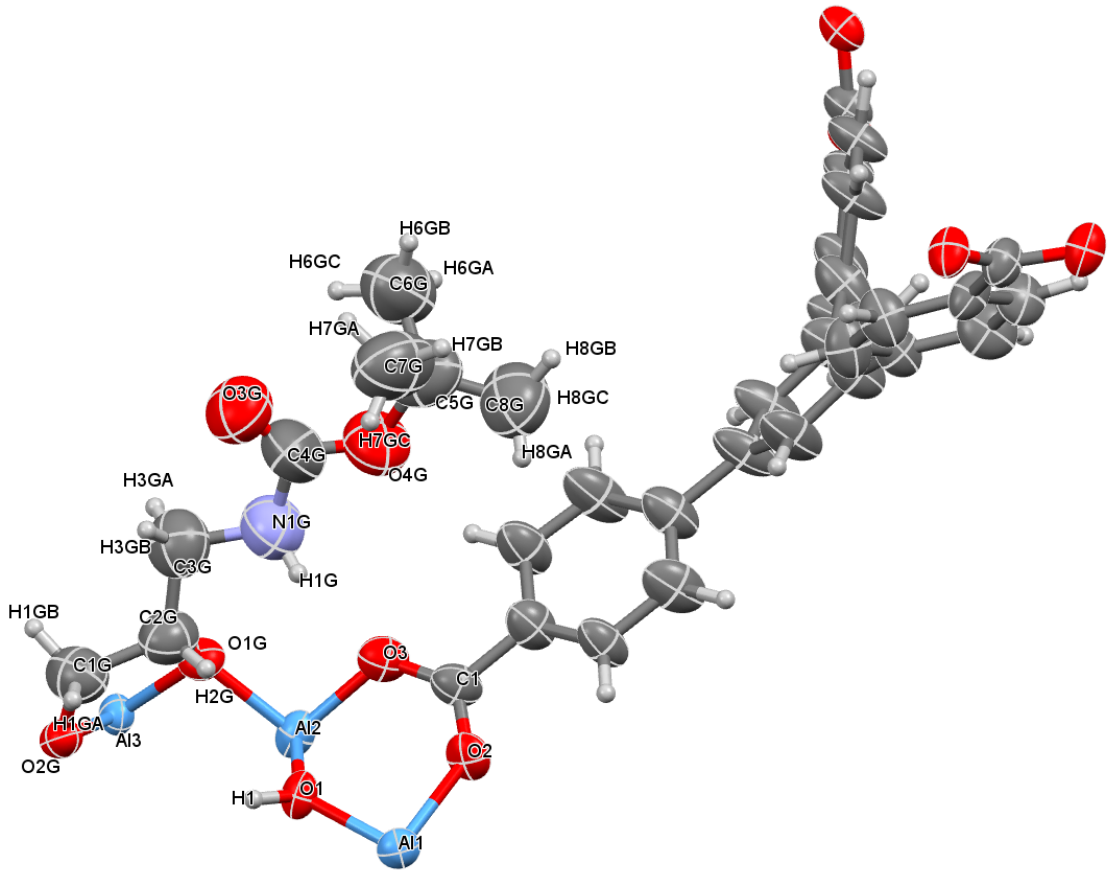

Fig. S25. Asymmetric unit in the single crystal structure of **Λ**-MOF-520-**12**. Thermal ellipsoids are drawn with 50% probability.

Λ-MOF-520-3-13. A colorless truncated octahedron-shaped crystal (80 x 55 x 55 μm^3) of **Λ**-MOF-520-**3-13** was measured at a beamline 11.3.1 at the ALS with radiation of λ = 1.03320 Å. According to intensity statistics table for the whole dataset (PRP file), the resolution was cut off to 0.70 Å. The occupancy of gibberellin A1 was found through adding a new variable and then constrained to 0.30. Before solvent masking instruction, structure was refined anisotropically and hydrogen atoms were placed into positions calculated geometrically. The connected asymmetric unit was defined inside the unit cell: MOVE command was applied to all atoms. The weighting scheme is refined as well as the extinction coefficient. Once solvent masking instruction was introduced, the weight scheme was refined to convergence. The FREE command was used to remove the connectivity due to partial overlap of two molecules within the asymmetric unit. The void volume is estimated to be 6432 $Å^3$ with 2832 electrons removed during masking. Some reflections were omitted due to non-ideal solvent masking, beam stop clipping and the minor presence of diffuse scattering. The threshold $(I_{obs}-I_{calc})/\sigma(W)>10$ was chosen for omitting these reflections. Omission of these reflections did not affect the refinement; the fraction of omitted reflections is less than 0.1% of the whole dataset.

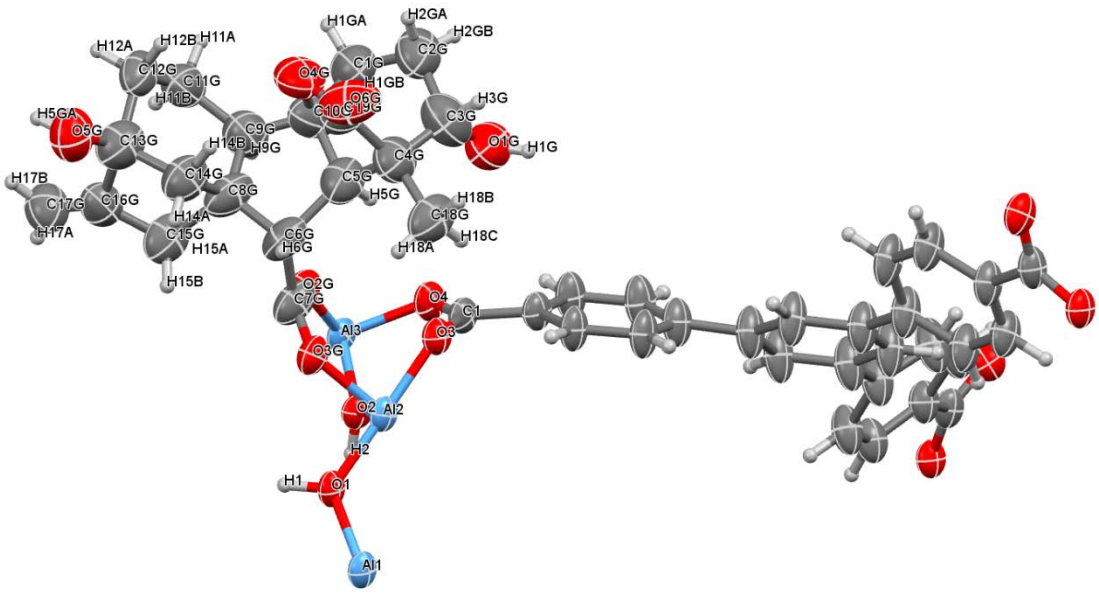

Fig. S26. Asymmetric unit in the single crystal structure of **Λ**-MOF-520-**3-13**. Thermal ellipsoids are drawn with 50% probability.

Λ-MOF-520-3-14. A colorless truncated octahedron-shaped crystal (80 x 65 x 65 μm^3) of **Λ**-MOF-520-**3-14** was measured at a beamline 11.3.1 at the ALS with radiation of $\lambda = 0.8856$ Å. According to intensity statistics table for the whole dataset (PRP file), the resolution was cut off to 0.76 Å. The occupancy of gibberellin A3 was found through adding a new variable and then constrained to 0.30. The occupancy of ethylene glycol molecule was set to 0.50. Before solvent masking instruction, structure was refined anisotropically and hydrogen atoms were placed into positions calculated geometrically. The connected asymmetric unit was defined inside the unit cell: MOVE command was applied to all atoms. The weighting scheme is refined as well as the extinction coefficient. Once solvent masking instruction was introduced, the weight scheme was refined to convergence. The FREE command was used to remove the connectivity due to partial overlap of two molecules within the asymmetric unit. The void volume is estimated to be 6633 $Å^3$ with 1488 electrons removed during masking. Some reflections were omitted due to non-ideal solvent masking, beam stop clipping and the minor presence of diffuse scattering. The threshold (I_{obs}-I_{calc})/σ(W)>10 was chosen for omitting these reflections. Omission of these reflections did not affect the refinement; the fraction of omitted reflections is less than 0.1% of the whole dataset.

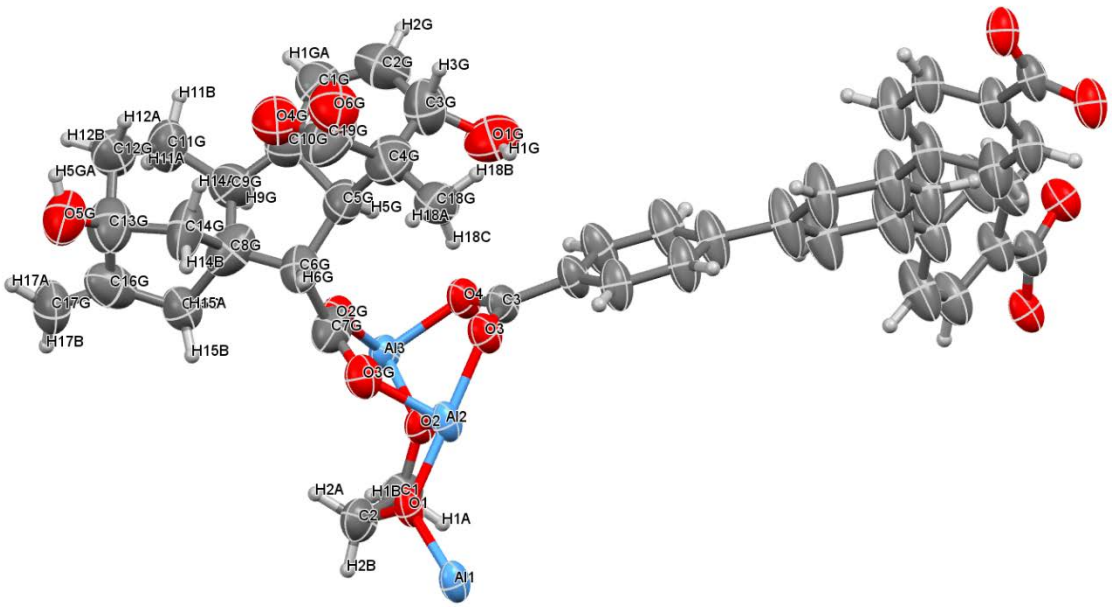

Fig. S27. Asymmetric unit in the single crystal structure of **Λ**-MOF-520-**3-14**. Thermal ellipsoids are drawn with 50% probability.

Δ-MOF-520-15. A colorless truncated octahedron-shaped crystal (60 x 40 x 40 μm^3) of **Δ**-MOF-520-**15**. was measured at a beamline 11.3.1 at the ALS with radiation of $\lambda = 1.03330$ Å. According to intensity statistics table for the whole dataset (PRP file), the resolution was cut off to 0.80 Å. The occupancy of (-)-jasmonic acid was found through adding a new variable and then constrained to 0.33. Before solvent masking instruction, structure was refined anisotropically and hydrogen atoms were placed into positions calculated geometrically. The connected asymmetric unit was defined inside the unit cell: MOVE command was applied to all atoms. The weighting scheme is refined as well as the extinction coefficient. Once solvent masking instruction was introduced, the weight scheme was refined to convergence. Last three carbon atoms of the bound molecule (C12G, C11G and C10G) are heavily overlapped with solvent molecule so they were placed initially into geometrically calculated positions. DFIX and DANG commands were used to set the geometry of this fragment. The void volume is estimated to be 7465 $Å^3$ with 3732 electrons removed during masking. Some reflections were omitted due to non-ideal solvent masking, beam stop clipping and the minor presence of diffuse scattering. The threshold $(I_{obs}-I_{calc})/\sigma(W)>10$ was chosen for omitting these reflections. Omission of these reflections did not affect the refinement; the fraction of omitted reflections is less than 0.1% of the whole dataset.

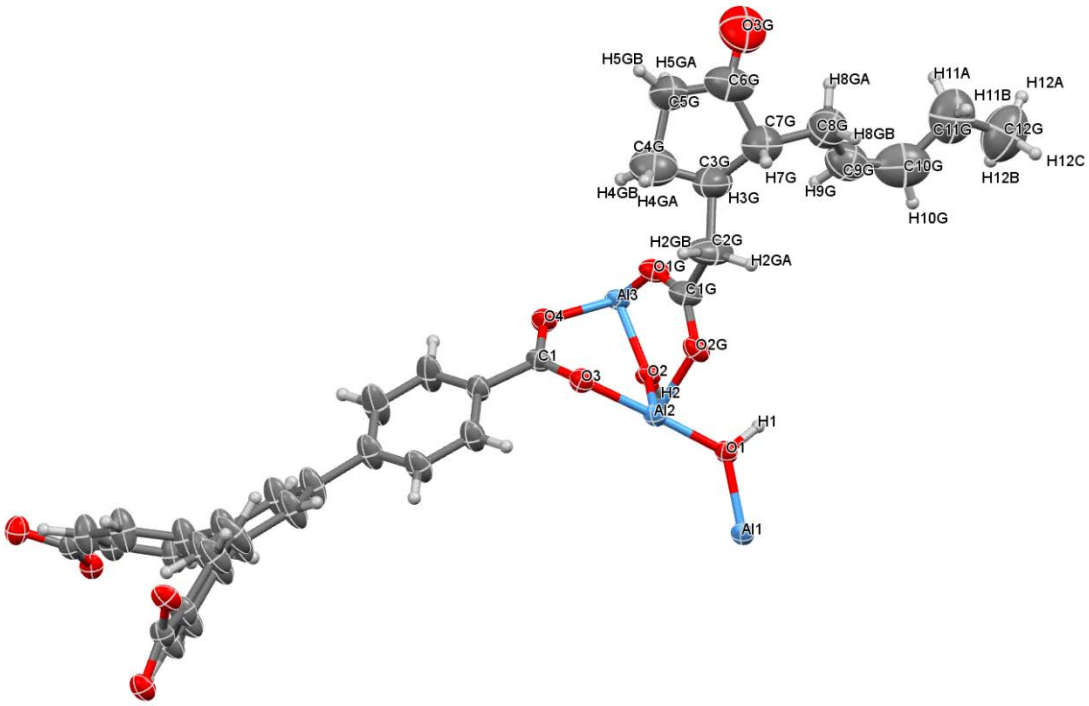

Fig. S28. Asymmetric unit in the single crystal structure of **Δ**-MOF-520-**15**. Thermal ellipsoids are drawn with 50% probability.

Λ-MOF-520-16. A colorless truncated octahedron-shaped crystal (60 x 40 x 40 μm^3) of **Λ**-MOF-520-**16** was measured at a beamline 11.3.1 at the ALS with radiation of λ = 1.03330 Å. According to intensity statistics table for the whole dataset (PRP file), the resolution was cut off to 0.80 Å. The occupancy of (+)-jasmonic acid was found through adding a new variable and then constrained to 0.33 Before solvent masking instruction, structure was refined anisotropically and hydrogen atoms were placed into positions calculated geometrically. The connected asymmetric unit was defined inside the unit cell: MOVE command was applied to all atoms. The weighting scheme is refined as well as the extinction coefficient. Once solvent masking instruction was introduced, the weight scheme was refined to convergence. Last three carbon atoms of the bound molecule (C12G, C11G and C10G) are heavily overlapped with solvent molecule so they were placed initially into geometrically calculated positions. DFIX and DANG commands were used to set the geometry of this fragment. ISOR command was used to restrain the thermal parameters of these carbon atoms. The void volume is estimated to be 7652Å^3 with 3862 electrons removed during masking. Some reflections were omitted due to non-ideal solvent masking, beam stop clipping and the minor presence of diffuse scattering. The threshold $(I_{obs}-I_{calc})/\sigma(W)>10$ was chosen for omitting these reflections. Omission of these reflections did not affect the refinement; the fraction of omitted reflections is less than 0.1% of the whole dataset.

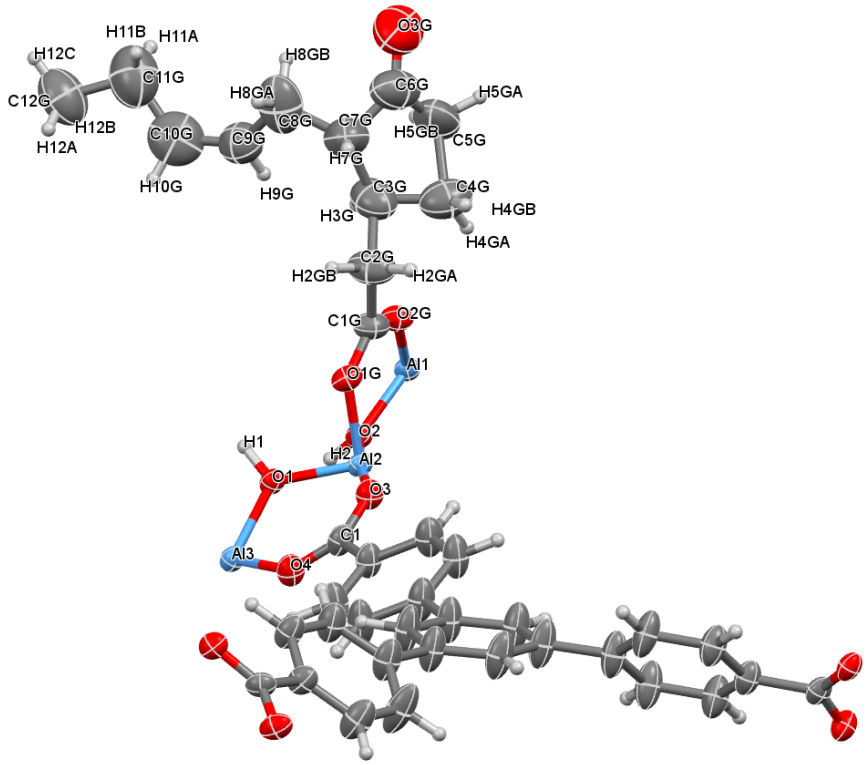

Fig. S29. Asymmetric unit in the single crystal structure of **Λ**-MOF-520-**16**. Thermal ellipsoids are drawn with 50% probability.

Chapter 3.

Effects of disordered guests on x-ray diffraction of UiO-66

Abstract

Single crystals of UiO-66, which is known for its high mechanical stability, charged with and without DMF were studied with SXRD technique. The effect of the disordered guest molecules on the internal structure and diffraction pattern was studied during temperature variations. The evacuated MOF showed multiple times higher mean I/σ values at the resolution limit, ~0.75 Å, than the MOF with the guests. The results of the data analysis suggest the disordered guest molecules interacting with the MOF make the framework also disordered, thus reducing x-ray scattering power of the framework at high angles.

Introduction

Metal-organic frameworks (MOFs), as a class of crystalline porous material, have various applications that depend on their internal structures (*1*). New MOFs with more sophisticated decoration of the pores allow CO_2 capture by cooperative binding with multiple functional groups and attachment of guest molecules to pore surfaces in controlled orientation thus allowing structure determination without the need of producing crystals of the guest molecules (*2-4*). MOFs with large pore sizes and appropriate shapes incorporate enzyme molecules (*5-7*). The determination of these structures, preferably at the atomic level and under the operating conditions of the materials, provide a starting point for understanding their properties.

MOFs containing condensed guests in their pores are composite materials. In general, the guests take up more space of the composite than the MOF itself and play an important role during and after the crystallization process supporting the porous structures and retaining the crystallinity. The guest molecules lack crystallographic orders and are, in general, heavily disordered in the pores of MOFs. This intrinsic property of the guest molecules poses special problems on determining their location and orientation accurately with the help of x-ray diffraction techniques. Although, their bulk property that induces phase transition and thermal expansion of MOFs has been well studied, we still do not know much about the effect of their disordered nature on the internal structure and diffraction property of MOFs (*8-10*).

In this chapter, I present x-ray diffraction property of UiO-66, $Zr_6(\mu_3\text{-}O)_4(\mu_3\text{-}OH)_4(BDC)_6$, (BDC:1,4-benzenedicarboxylate), which is well-known for its mechanical stability, affected by the disordered guest molecules (*11*,*12*). Specifically, data sets of a single crystal of UiO-66 with and without DMF were collected, and the effect of the disordered guests on the internal structure and diffraction intensity of the MOF was studied by analyzing Fourier synthesized electron density maps of the pore, the MOF structures refined, and diffraction intensity statistic. In theory, if the frameworks of the MOF with and without the guests are identical, the diffraction intensity of the MOF with the guests should be higher, since x-rays scattered by averaged electron density of the disordered guests would additionally contribute to the intensity of Bragg reflections, although it would be marginal (*13*). However, the result showed that the intensity of the MOF without the

guests is higher multiple folds at the resolution limit in a range, 0.80 to 0.75 Å, than that of the MOF with the guests. The data analysis shows that the internal structure of the MOF with the guests is more disordered, possibly, affected by the guests and thus lose x-ray scattering power at high angles (*14,15*).

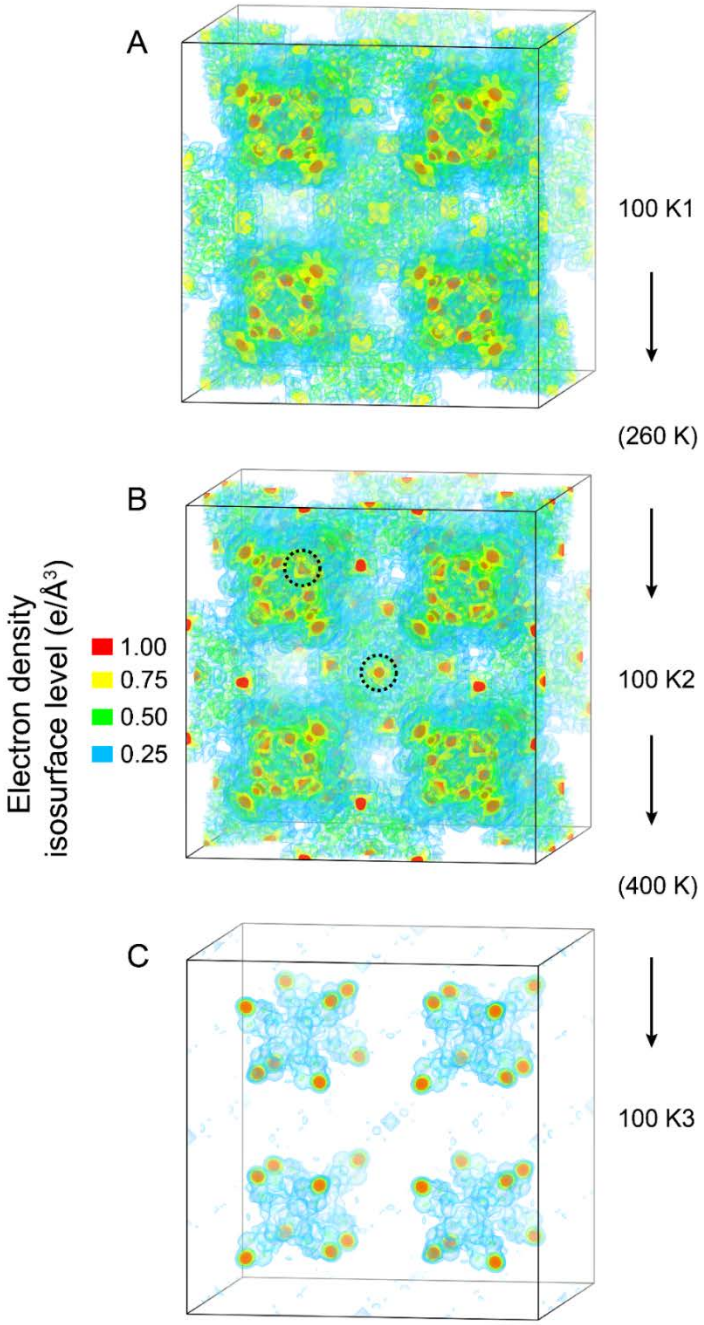

Fig. 1. Fourier synthesized electron density in the pores of UiO-66 through temperature swings. (**A** to **C**) The electron density maps of the guest molecules in the tetrahedral (¼, ¼, ¼) and the octahedral (½, ½, ½) pores of the unit cell are Fourier synthesized, where the framework is masked out. The levels of the electron density are indicated by red, yellow, green, and blue isosurfaces. All three data are collected at 100 K and the temperatures reached between the measurements are indicated in the parenthesis.

Results and discussion

The synthesis of UiO-66 in this work is described in Supplementary materials. The pore of the as-synthesized UiO-66 was evacuated following a general activation procedure using anhydrous acetone for the solvent exchange and super critical CO_2 drier to minimize pore collapse during solvent removal. The evacuated MOF was soaked in *N*,*N*'-dimethylformamide (DMF) for three days to charge the pores with guest molecules. A single crystalline UiO-66 (~100 μm) with DMF was mounted on a goniometer equipped with a liquid nitrogen cryostream whose temperature was preset to 100 K (synchrotron beamline, 11.3.1. at the Advanced Light Source), and data set 100 K1 was collected. The electron density map of the guests in the pores is shown in Fig. 1A, where the framework is masked out. Electron densities are found in two different types of pore of tetrahedral and octahedral shapes, the centers of which are located in ¼, ¼, ¼ and ½, ½, ½ of the unit cell, respectively. After the data collection, the temperature was increased to 260 K and cooled down to 100 K with a rate 0.1 Ks^{-1} to see if the arrangement of guest molecules is affected by the temperature swing. The electron density map of 100 K2 is shown in Fig. 1B. Although the two data sets were collected at the same temperature, noticeable changes are observed on the corners of the octahedral and tetrahedral pores where the localization of the electron density is observed compared to data set 100 K1. The localized area is emphasized in circles embedded in Fig. 1B. This result shows that the heavily disordered guests in the pores of the MOF become more ordered with the temperature swing. Even if there is doubt that the guests can be completely ordered by an optimized temperature swing, it might indeed be possible to improve the characterization of dangling functionalities or molecules bound to the backbone within the pores as in crystalline sponge and coordinative alignment methods.

Subsequently, the temperature was increased to 400 K and kept for an hour to evaporate the guest molecules. The crystal was cooled down to 100 K again, and data set 100 K3 was collected. The density map shows the guests are evaporated, and most of residual densities are observed in the tetrahedral pores (Fig 1C). The numbers of electrons found in the pores for 100 K1, K2, and K3 are 1459 (36 DMF), 1350 (34 DMF), and 384 (10 DMF), respectively (based on a theoretical calculation considering only the density of DMF in its crystalline form and the accessible pore volume of the MOF, maximum 48 DMF molecules can fit in the pore). The intensity statistics of the three data sets sorted by resolution are shown in Table 1. The statistic of data sets 100 K2 presents a slight improvement of a mean I/σ value compared to that of 100 K1 in a resolution limit, 0.80 to 0.75 Å, attributable to the guests organization induced by the temperature swing. Data set 100 K3 has a substantially improved mean I/σ value about three folds higher than that of 100 K2. The values found for 100 K1, K2, and K3 are 5.7, 6.2, and 20.2, respectively.

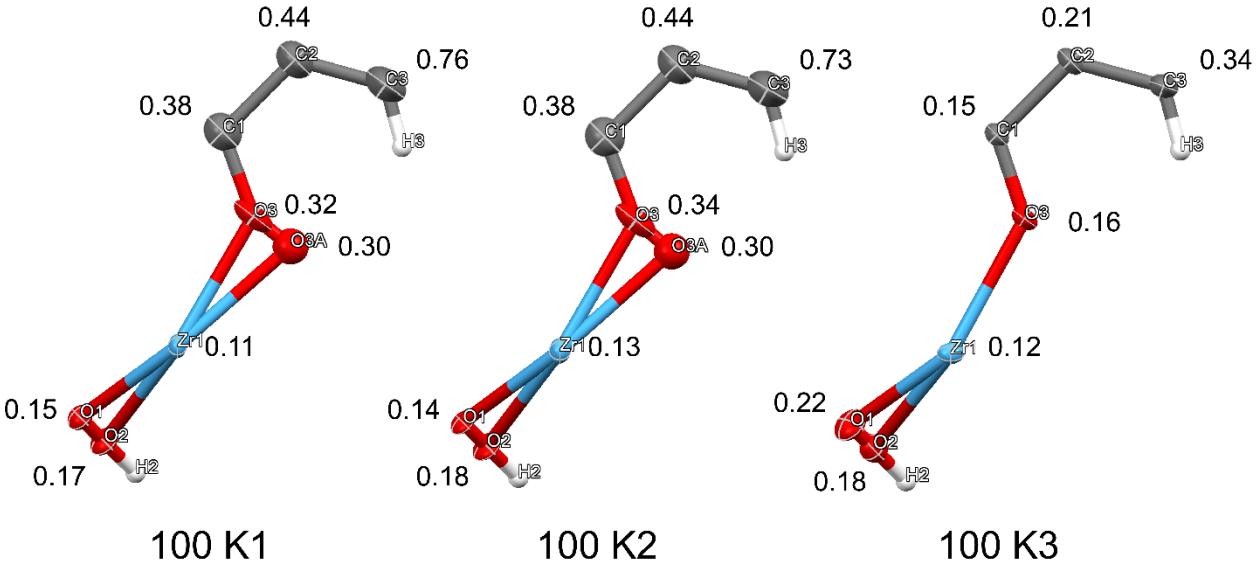

Fig 2. Asymmetric units of UiO-66 structures. The models are shown in 50 % probability ellipsoids. Isotropic ADP values are shown next to corresponding atoms.

The further spread out reflections of the evacuated MOF to higher resolution is reflected in the localized atomic positions of the internal structure (Fig. 2) (*16*). For example, the ADPs of the *ortho*-carbon on the phenyl ring, which is relatively far from the SBU and thus subject to interactions with the guests, are 0.76, 0.73, and 0.34 $Å^2$ for the refined structures of 100 K1, K2, and K3, respectively. A similar experiment was carried out with a single crystal of UiO-66 with a in-house diffractometer, where the mean I/σ values for UiO-66 with DMF and the evacuated UiO-66 are found as 5.5 and 9.0, respectively, in the resolution range of 0.81 to 0.75 Å (Table 2).

Conclusion

These results indicate that the internal structure of mechanically robust UiO-66 is affected by the disordered guest molecules and become more disordered compared to the evacuated MOF. The guests in the pores would contribute to the intensities of Bragg reflections in two different opposing ways. Their averaged electron density would increase the intensities of Bragg reflections. On the other hand, the disordered nature would make the frameworks also disordered, decreasing the intensities. The latter overwhelms the former in this work.

100 K1 (DMF)	Resolution			#Data	#Theory	%Complete	Redundancy	Mean I	Mean I/s	Rmerge	Rsigma
	Inf	-	4.23	9	9	100	10.22	188.46	28.6	0.0886	0.0729
	4.23	-	2.44	22	22	100	17.64	139.12	32.66	0.0924	0.0419
	2.44	-	1.81	31	31	100	23.9	124.35	29.79	0.0884	0.0398
	1.81	-	1.56	28	28	100	23.61	103.57	37.33	0.0929	0.0256
	1.56	-	1.4	31	31	100	27.71	64.91	33.05	0.1028	0.0274
	1.4	-	1.27	33	33	100	30.27	41.85	28.67	0.1158	0.0307
	1.27	-	1.19	28	28	100	30.54	28.67	23.3	0.1188	0.0287
	1.19	-	1.12	29	29	100	30.48	36.75	26.79	0.1116	0.0307
	1.12	-	1.06	30	30	100	34.03	38.88	30.8	0.1158	0.0252
	1.06	-	1.02	30	30	100	28.7	30.95	23.25	0.1268	0.0317
	1.02	-	0.97	36	36	100	32.11	33.59	25.51	0.1307	0.0292
	0.97	-	0.94	27	27	100	31.3	19.44	18.44	0.1745	0.0387
	0.94	-	0.91	32	32	100	26.38	26.06	21.46	0.1505	0.0379
	0.91	-	0.89	24	24	100	22.79	15.49	15.9	0.1883	0.0467
	0.89	-	0.86	35	35	100	18.26	22.81	15.95	0.1484	0.0473
	0.86	-	0.84	27	27	100	15.96	10.58	11.33	0.2005	0.0638
	0.84	-	0.82	31	31	100	15.97	16.96	12.91	0.1935	0.0541
	0.82	-	0.8	32	32	100	12.88	13.49	10.74	0.2002	0.066
	0.8	-	0.78	43	43	100	7.09	16.91	7.6	0.2388	0.122
	0.78	-	0.77	15	16	93.8	3.81	12.85	4.71	0.2373	0.2026
	0.77	-	0.75	35	43	81.4	3.44	10.92	3.68	0.2939	0.2395
100 K2 (DMF)	Resolution			#Data	#Theory	%Complete	Redundancy	Mean I	Mean I/s	Rmerge	Rsigma
	Inf	-	3.99	11	11	100	12.18	189.53	37.76	0.0654	0.0474
	3.99	-	2.44	20	20	100	20.75	150.61	41.06	0.0744	0.0345
	2.44	-	1.81	31	31	100	25.23	133.29	36.14	0.0695	0.0276
	1.81	-	1.55	31	31	100	27.23	102.95	46.88	0.0695	0.0199
	1.55	-	1.4	28	28	100	29.61	67.85	39.19	0.0758	0.0222
	1.4	-	1.27	31	31	100	32.03	44.62	33.85	0.095	0.0293
	1.27	-	1.19	29	29	100	31.76	22.49	26.34	0.1098	0.0272
	1.19	-	1.12	30	30	100	31.07	42.49	32.64	0.0937	0.0259
	1.12	-	1.06	30	30	100	35.37	38.96	36.86	0.0886	0.0212
	1.06	-	1.02	30	30	100	29.43	30.9	27.37	0.0965	0.0274
	1.02	-	0.97	36	36	100	33.17	33.53	29.86	0.1011	0.0244
	0.97	-	0.94	27	27	100	31.56	19.55	20.12	0.1359	0.0344
	0.94	-	0.91	30	30	100	30.33	27.19	26.34	0.1243	0.0305
	0.91	-	0.88	37	37	100	27.46	14.54	18.5	0.1655	0.0412
	0.88	-	0.86	24	24	100	25.12	26.79	20.01	0.122	0.0366
	0.86	-	0.84	27	27	100	23.15	10.03	12.28	0.1836	0.0554
	0.84	-	0.82	30	30	100	21.97	15.6	14.79	0.1816	0.0462
	0.82	-	0.8	33	33	100	18.61	13.71	11.93	0.1961	0.0564
	0.8	-	0.78	41	41	100	9.22	16.05	8.6	0.2236	0.0915
	0.78	-	0.77	17	18	94.4	6	11.33	6.17	0.2722	0.1444
	0.77	-	0.75	39	43	90.7	3.09	8.88	3.65	0.2231	0.2234
100 K3 (Evac.)	Resolution			#Data	#Theory	%Complete	Redundancy	Mean I	Mean I/s	Rmerge	Rsigma
	Inf	-	3.98	9	11	81.8	6.09	139.94	35.47	0.0625	0.0526
	3.98	-	2.39	21	22	95.5	12.09	188.86	37.8	0.0618	0.048
	2.39	-	1.8	31	31	100	18.71	152.1	39.98	0.0618	0.0364
	1.8	-	1.54	31	31	100	23.03	128.52	53.95	0.0612	0.0285
	1.54	-	1.37	32	32	100	27.5	100.02	59.31	0.0573	0.0224
	1.37	-	1.26	28	28	100	30.86	49.89	55.81	0.0598	0.0261
	1.26	-	1.18	31	31	100	33.03	36.7	50.95	0.0619	0.0159
	1.18	-	1.11	31	31	100	31.58	57.82	54.58	0.0553	0.0213
	1.11	-	1.05	31	31	100	33.32	67.33	63.97	0.0548	0.014
	1.05	-	1.01	32	32	100	33.06	37.89	51.95	0.0608	0.0164
	1.01	-	0.97	24	24	100	32.71	45.16	55.66	0.0605	0.0158
	0.97	-	0.94	30	30	100	33.17	29.47	44.96	0.0659	0.0187
	0.94	-	0.91	30	30	100	32.67	35.68	54.25	0.0638	0.0165
	0.91	-	0.88	35	35	100	29.54	22.84	42.25	0.0675	0.0181
	0.88	-	0.86	26	26	100	29.42	38.68	43.75	0.0628	0.0189
	0.86	-	0.83	44	44	100	27.45	18.07	34.96	0.0743	0.0192
	0.83	-	0.81	29	29	100	24.97	27.03	40.13	0.0718	0.0195
	0.81	-	0.8	16	16	100	22.69	12.9	25.48	0.0991	0.0245
	0.8	-	0.78	39	39	100	13.33	22.77	24.94	0.08	0.0366
	0.78	-	0.76	38	40	95	7.4	22.71	21.09	0.0742	0.0424
	0.76	-	0.75	21	24	87.5	3.71	9.66	9.72	0.0899	0.0749

Table 1. Intensity statistic comparisons of 100 K1, K2, and K3 data sets collected with a synchrotron radiation (wavelength: 0.7288 Å).

100 K1 (DMF)		Resolution		#Data	#Theory	%Complete	Redundancy	Mean I	Mean I/s	Rmerge	Rsigma
	Inf	-	3.67	10	12	83.3	8.08	97.6	88.32	0.0232	0.0114
	3.67	-	2.39	21	21	100	16.19	203.85	86.39	0.0198	0.0097
	2.39	-	1.8	31	31	100	19.26	131.93	75.33	0.0264	0.0091
	1.8	-	1.55	29	29	100	19.03	112.16	76.84	0.0302	0.0107
	1.55	-	1.37	34	34	100	17.68	77.28	56.6	0.0435	0.014
	1.37	-	1.27	27	27	100	17.59	43.47	31.67	0.0753	0.0223
	1.27	-	1.18	32	32	100	18.69	30.65	26.39	0.0863	0.0262
	1.18	-	1.12	28	28	100	18.46	44.27	32.2	0.0788	0.0238
	1.12	-	1.05	34	34	100	18.79	55.24	38.58	0.0765	0.0208
	1.05	-	1.01	32	32	100	19.09	30.27	25.06	0.1069	0.0345
	1.01	-	0.97	27	27	100	19.22	38.21	24.65	0.1112	0.0312
	0.97	-	0.94	30	30	100	20	22.76	17.72	0.1552	0.0456
	0.94	-	0.91	29	29	100	20.62	31.65	21.2	0.1501	0.0405
	0.91	-	0.88	37	37	100	19.35	17.7	13.14	0.2208	0.0651
	0.88	-	0.85	40	40	100	17.15	25.17	13.39	0.2038	0.0612
	0.85	-	0.84	14	14	100	16.14	10.57	7.55	0.3521	0.1301
	0.84	-	0.81	44	44	100	13.84	20.62	9.78	0.2399	0.0867
	0.81	-	0.79	38	38	100	10.5	18.94	7.02	0.3092	0.1269
	0.79	-	0.78	19	19	100	10.47	18.6	6.88	0.3138	0.1237
	0.78	-	0.77	19	19	100	9.47	11.74	4.41	0.4752	0.211
	0.77	-	0.75	40	40	100	7.05	12.68	3.83	0.3883	0.257

100 K2 (Evac.)		Resolution		#Data	#Theory	%Complete	Redundancy	Mean I	Mean I/s	Rmerge	Rsigma
	Inf	-	3.66	10	12	83.3	8.17	112.87	82.26	0.0237	0.0127
	3.66	-	2.39	21	21	100	16.38	182.61	85.43	0.0199	0.0114
	2.39	-	1.8	31	31	100	20.03	123.53	74.55	0.0236	0.01
	1.8	-	1.55	29	29	100	20.07	107.11	81.28	0.0294	0.0103
	1.55	-	1.37	34	34	100	17.62	74.94	64.2	0.0375	0.0125
	1.37	-	1.26	28	28	100	17.54	39.05	38.85	0.0658	0.0195
	1.26	-	1.18	31	31	100	18.84	30.22	33.01	0.0649	0.0206
	1.18	-	1.11	31	31	100	19.39	48.43	43.88	0.057	0.0176
	1.11	-	1.05	31	31	100	18.84	57.11	50.48	0.052	0.0156
	1.05	-	1.01	32	32	100	18.78	31.78	34.8	0.0719	0.0233
	1.01	-	0.97	27	27	100	19.44	37.24	33.32	0.0835	0.0227
	0.97	-	0.94	27	27	100	20.74	25.96	25.2	0.1115	0.0304
	0.94	-	0.91	30	30	100	21.4	31.37	30.46	0.1063	0.0297
	0.91	-	0.88	37	37	100	18.84	20.42	20.24	0.1521	0.0409
	0.88	-	0.86	24	24	100	17.54	37.19	24.7	0.1087	0.0313
	0.86	-	0.83	44	44	100	15.84	16.69	14.2	0.1745	0.0601
	0.83	-	0.81	29	29	100	13.48	25.19	16.84	0.1561	0.052
	0.81	-	0.8	17	17	100	12.82	11.74	7.52	0.302	0.1035
	0.8	-	0.78	40	41	97.6	10.88	22.87	11.96	0.1763	0.0735
	0.78	-	0.76	39	40	97.5	8.27	18.86	9.18	0.216	0.1021
	0.76	-	0.75	20	21	95.2	6.52	8.62	4.21	0.3466	0.2187

Table 2. Intensity statistic comparison between 100 K1, and K2 of UiO-66 data sets measured with one single crystal with an in-house diffractometer (MoKα). A single crystal of UiO-66 charged with DMF was mounted on the goniometer with a temperature preset at 100 K. 100 K1 data was collected. After the data collection, the temperature increased to 400 K with a rate 0.1 K/s and kept for an hour to evaporate the DMF molecules in the pores. Then the temperature was cooled down to 100 K. 100 K2 data set was collected.

References and notes

1. H. Furukawa, K. E. Cordova, M. O'Keeffe, O. M. Yaghi, The Chemistry and Applications of Metal-Organic Frameworks. *Science* **341,** 974 (2013).

2. T. M. McDonald et al., Cooperative insertion of CO_2 in diamine-appended metal-organic frameworks. *Nature* **519**, 303 (2015).

3. Y. Inokuma et al., X-ray analysis on the nanogram to microgram scale using porous complexes. *Nature* **495**, 461 (2013).

4. S. Lee, E. A. Kapustin, O. M. Yaghi, Coordinative alignment of molecules in chiral metal-organic frameworks. *Science* **353**, 808 (2016).

5. H. Deng et al., Large-Pore Apertures in a Series of Metal-Organic Frameworks. *Science* **336**, 1018 (2012).

6. D. Feng et al., Stable Metal-Organic Frameworks Containing Single-Molecule Traps for Enzyme Encapsulation. *Nat. Commun*. **6**, 5979 (2015).

7. P. Li et al., Encapsulation of a Nerve Agent Detoxifying Enzyme by a Mesoporous Zirconium Metal-Organic Framework Engenders Thermal and Long-Term Stability. *J. Am. Chem. Soc.* **138**, 8052 (2016).

8. J.-P. Zhang, P.-Q. Liao, H.-L. Zhou, R.-B. Lin, X.-M. Chen, Single-crystal X-ray diffraction studies on structural transformations of porous coordination polymers. *Chem. Soc. Rev.* **43**, 5789 (2014).

9. A. Schneemann *et al.*, Flexible metal-organic frameworks. *Chem. Soc. Rev.* **43**, 6062 (2014).

10. T. D. Bennett, A. H. Fuchs, A. K. Cheetham, F.-X. Coudert, Flexibility and disorder in metal-organic frameworks. *Dalton Trans.* **45**, 4058 (2016).

11. J. H. Cavka et al., A New Zirconium Inorganic Building Brick Forming Metal Organic Frameworks with Exceptional Stability. *J. Am. Chem. Soc.***130**, 13850 (2008).

12. L. Valenzano et al., Disclosing the Complex Structure of UiO-66 Metal Organic Framework: A Synergic Combination of Experiment and Theory. *Chem. Mater.* **23**, 1700 (2011).

13. C. Giacovazzo, *Fundamentals of Crystallography*. (Oxford University Press, 2002).

14. P. Debye, Interferenz von Röntgenstrahlen und Wärmebewegung. *Annalen der Physik* **348**, 49 (1913).

15. I. Waller, Zur Frage der Einwirkung der Wärmebewegung auf die Interferenz von Röntgenstrahlen. *Zeitschrift für Physik* **17**, 398 (1923).

16. J. D. Dunitz, V. Schomaker, K. N. Trueblood, Interpretation of atomic displacement parameters from diffraction studies of crystals. *J. Phys. Chem.* **92**, 856 (1988).

17. G. Sheldrick, A short history of SHELX. *Acta Crystallogr. A* **64**, 112 (2008).

18. O. V. Dolomanov, L. J. Bourhis, R. J. Gildea, J. A. K. Howard, H. Puschmann, OLEX2: a complete structure solution, refinement and analysis program. *J. Appl. Crystallogr.* **42**, 339 (2009).

19. A. L. Spek, PLATON SQUEEZE: a tool for the calculation of the disordered solvent contribution to the calculated structure factors. *Acta Crystallogr. C* **71**, 9 (2015).

20. K. Momma, F. Izumi, VESTA 3 for three-dimensional visualization of crystal, volumetric and morphology data. *J. Appl. Crystallogr.* **44**, 1272 (2011).

21. C. F. Macrae, P. R. Edgington, P. McCabe, E. Pidcock, G. P. Shields, R. Taylor, M. Towler, J. van de Streek, Mercury: visualization and analysis of crystal structures. *J. Appl. Crystallogr.* **39**, 453 (2006).

Acknowledgements: Support for the synthesis by BASF SE (Ludwigshafen, Germany) and the characterization of compounds by King Abdulaziz City for Science and Technology (Center of Excellence for Nanomaterials and Clean Energy Applications). We thank Dr. Simon J. Teat and Dr. Laura J. McCormick for the synchrotron x-ray diffraction data acquisition support at the beamlines 11.3.1 and later 12.2.1 (Advanced Light Source, Lawrence Berkeley National Laboratory). This research used resources of the Advanced Light Source, which is a DOE Office of Science User Facility under contract no. DE-AC02-05CH11231.

Supplementary materials

Materials and Methods

Section S1. Materials

Section S1.1. Synthesis of UiO-66 single crystals

UiO-66, $Zr_6(O)_4(OH)_4(BDC)_6$: In a 20 mL scintillation vial, a mixture solution of $ZrOCl_2 \cdot 8H_2O$ (12.0 mg, 0.068 mmol) and H_2BDC (5.0 mg, 0.030 mmol) in DMF (2 mL) was prepared. The solution was sonicated for 1 min, and formic acid (3 mL, 0.080 mol) was added to the solution as an additive. The vial was capped and placed in the preheated 140 °C oven. After 1 days, homogeneous octahedron shape single crystals with size range from 30 to 150 μm were obtained on the wall of the vial.

Solvent exchange and guest removal procedure of UiO-66: The crystals in the vial were washed with DMF (10.0 mL) three times per day for three days to remove the unreacted reagents in the pores. DMF solvent in the pore was exchanged with anhydrous acetone by washing the crystals with acetone (10.0 mL) three times per day for three days. To remove the acetone in the pores, the crystals were evacuated for 10 h at 120 °C under 30 mTorr.

Section S2. Methods

Section S2.1. SXRD instrumentation

Single-crystal x-ray diffraction (SXRD) data was collected using synchrotron radiation in beamline 11.3.1 of the Advanced Light Source, Lawrence Berkeley National Laboratory (LBNL). Beamline 11.3.1 is equipped with Bruker laboratory diffractometer coupled with PHOTON 100 CMOS detector operating in shutterless mode. In the beamline, the x-rays are focused with a toroidal mirror (beam size: 200 μm^2), and A channel-cut Si(111) monochromator with an energy range of 6-17 keV is used as a monochromator. The temperature was controlled by cryostream 700 series, oxford cryosystems. For crystal mounting, MiTeGen loops were used with mineral oil.

Section S2.2. Data processing and refinement

Data processing, structure solution, and refinement: The Integrations were carried out with APEX3 Suite Bruker software, and scaling and absorption correction were done using multi-scan method implemented in SADABS. Space group determinations and .ins file generations were done using XPREP software with .hkl files generated from SADABS, and inspecting reconstruction

images of the data frames. Initial models for refinements were generated by direct method implemented in SHELXS and refined with SHELXL using Olex 2 as a graphical user interface (*17,18*). Non-hydrogen atomic positions were assigned first. Metals in the structures were refined anisotropically followed by carbon and oxygen atoms. Hydrogen atoms were attached to the model by riding models. Residual electron densities in pores were assigned with carbon and oxygen, and refined to improve the framework models. When there is no meaningful improvement observed, the carbon and oxygen atoms in pores were removed, and the improved framework models were used for PLATON SQUEEZE (*19*). The SQUEEZEd models were further refined with SHELXL until the parameters were converged.

Fourier synthesis of electron density map and visualization of the ellipsoidal model: .fab file was generated after the SQUEEZE instruction. Electron density map in pores were Fourier synthesized using VESTA software (*20*) with the .fab files. The number of elections for the synthesis was obtained from the SQUEEZE result. The ellipsoidal model was visualized using Mercury software (*21*).

Chapter 4

Phase transition and twinning of MOF-5 induced by guests during temperature control

Abstract

Diffraction pattern and internal structure of MOF-5 filled with guests were studied during a temperature control within a range between 290 and 110 K. The data analysis showed that the condensed guests induce a phase transition and twinning of the original crystal in *Fm*-3*m* symmetry, and lower the symmetry to *Pa*-3 upon cooling. The two-fold symmetry lost during the transition was indirectly conserved as the twin matrix for the domains. The transition and twinning were reversible, thus the original structure was recovered when the crystal was heated to 290 K. This phenomena was not observed with the evacuated MOF, where only the *Fm*-3*m* symmetry was observed during the temperature control.

Introduction

In the previous chapter, the importance of the disordered interaction between the disordered guests and mechanically robust MOF, UiO-66 was discussed. Here, I show how ordered interactions between the guests and framework induce a phase transition of a flexible MOF. Internal structure and diffraction pattern of MOF-5, $Zn_4(O)(BDC)_3$ (BDC: 1,4-dicarboxylic acid), which is relatively flexible compared to UiO-66, was studied with and without DMF guests, during temperature variations (*1*). It has been reported that an isoreticular version of MOF-5, IRMOF-10, $Zn_4(O)(BPDC)_3$ (BPDC: [1,1'-Biphenyl]-4,4'-dicarboxylate) showed a phase transition from $P4_2/ncm$ to a structure that was not able to be characterized upon cooling with DMF guest molecules (*2*,*3*). In my experiment, MOF-5 with DMF also showed a phase transition upon cooling. The diffraction patterns indicate a symmetry reduction from *Fm*-3*m* to a primitive unit cell and a twinning (*4*). The internal symmetry of the primitive unit cell was investigated with various space groups. The space group *Pa*-3 was chosen as the space group of the structure solution, and two-fold rotational matrix was adopted as the twin law by inspecting the diffraction patterns. A controlled experiment, where the guest molecules were evacuated before the measurement, showed no phase transition during the same temperature control, indicating the phase transition is possibly induced by the guest-framework interaction. This result also emphasizes the importance of guest-framework interactions under x-ray diffraction experiments.

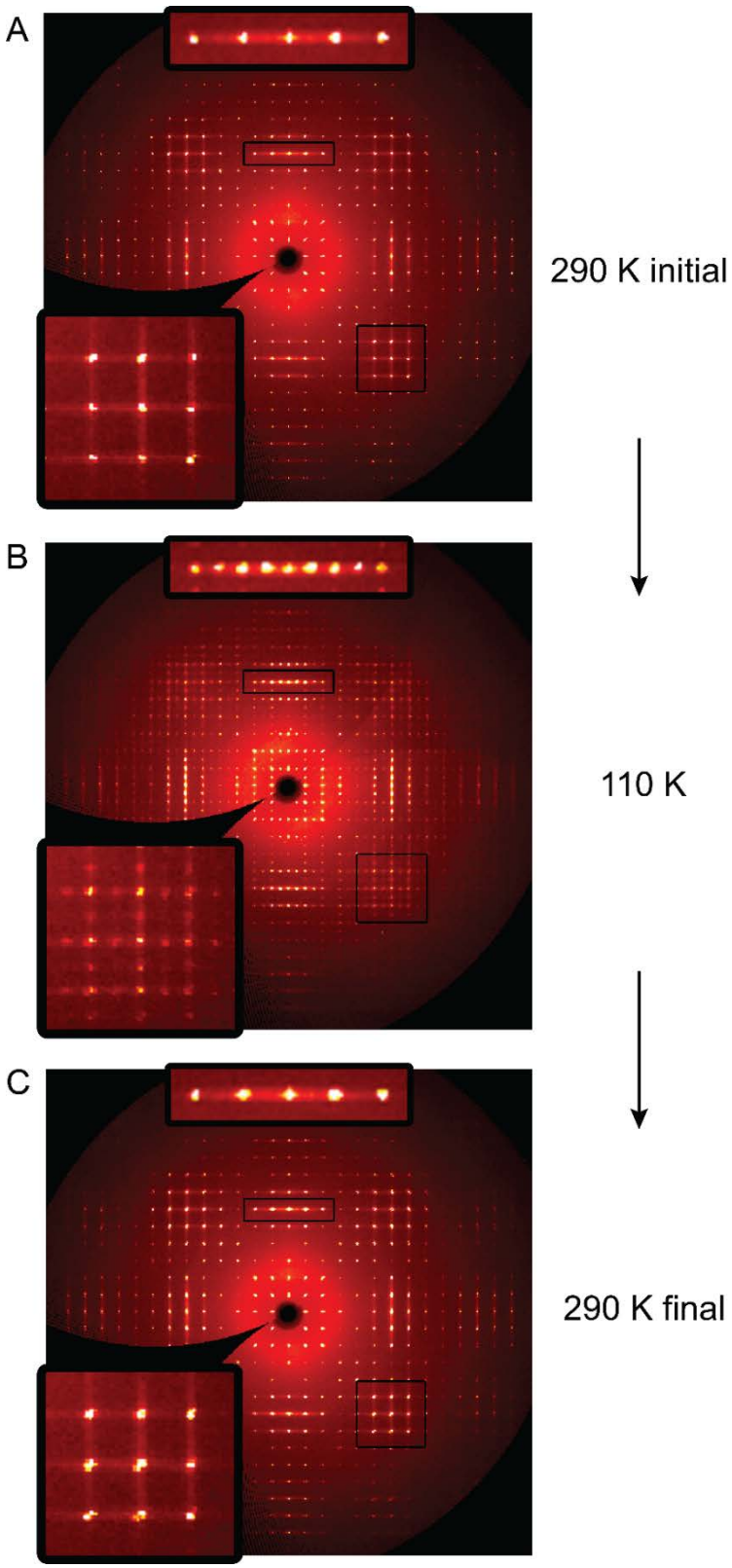

Fig 1. Temperature dependent diffraction analysis of MOF-5 charged with DMF. (**A** to **C**) The reconstruction images of (*hk*0) of the data collected at 290, 110, and 290 K, respectively.

Results and discussion

The synthesis of MOF-5 single crystals is described in Supplementary materials. The pore of the as-synthesized MOF-5 was evacuated following a general activation procedure using chloroform for the solvent exchange and super critical CO_2 drier to minimize pore collapse during solvent removal. The evacuated MOF-5 was soaked in *N*,*N*'-dimethylformamide (DMF) for three days to charge the pores with the guest molecules. A single crystalline MOF-5 (~100 μm) with DMF was mounted on a goniometer equipped with a liquid nitrogen cryostream whose temperature was preset to 290 K (synchrotron beamline, 11.3.1. at the Advanced Light Source). Full sets of data were collected in ~4 minutes with wavelength 0.7749 Å starting at 290 K. Between data collections, the shutter was kept closed to minimize beam damage and the temperature was reduced by 30 K at a rate of 0.1 K s^{-1}. The same experimental conditions were applied for data collections during temperature increase.

MOF-5 with the face-centered space group, *Fm*-3*m* was tested with the temperature control experiment. The (*hk*0) reconstruction images of the data sets collected at 290, 110, and 290 K are shown in Fig. 1A to C, respectively. In the images of the initial and final data sets measured at 290 K, reflections with Miller indices all even, as required by the space group symmetry, are seen. At 110 K, the density of reflections is doubled indicating a primitive lattice; however, the systematic absences are now *h* and *k*, both odd, incompatible with any of the 230 space groups (Fig. 1B) (*5*). The unusual diffraction pattern can be explained in terms of two twin domains, each with *Pa*-3 symmetry. The two domains are related to each other by a rotation of 180 degrees along [110] axis.

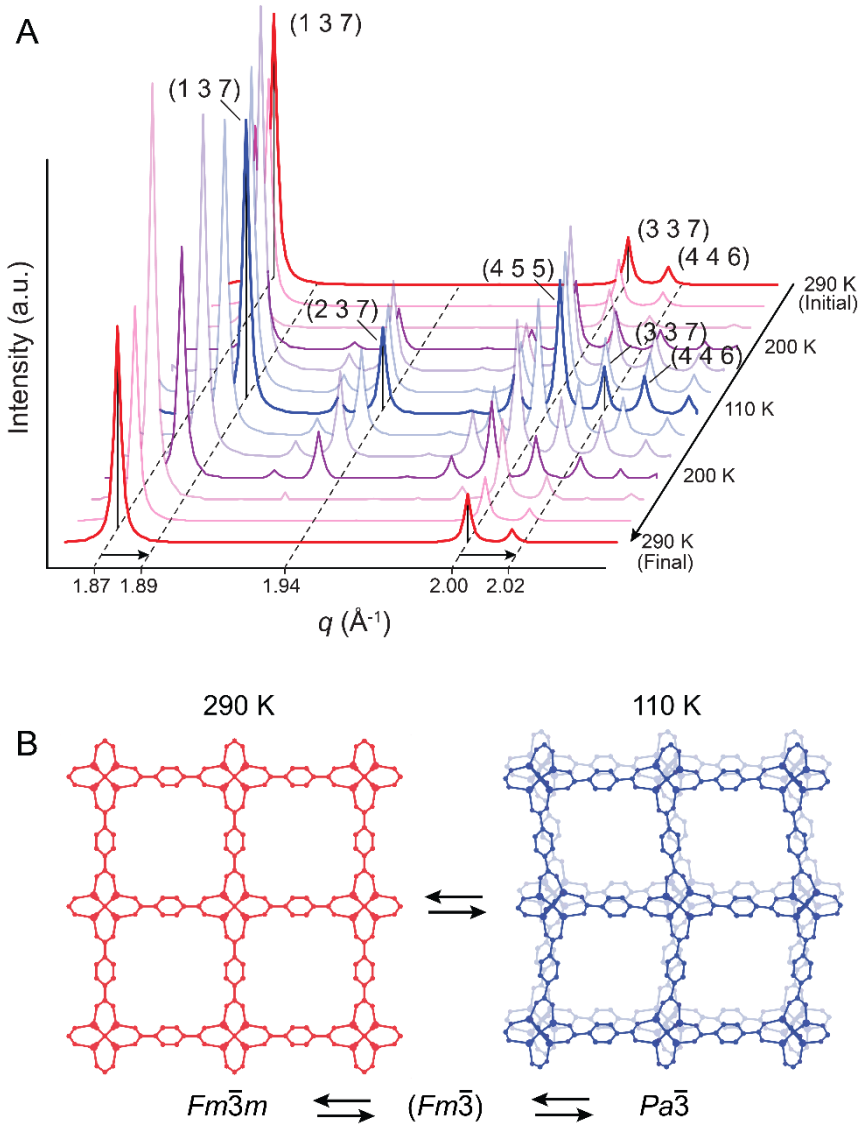

Fig 2. Temperature dependent diffraction analysis of MOF-5 charged with DMF and refined structures. (**A**) Calculated powder x-ray diffraction patterns from the SXRD raw files. (**B**) Projection images, along [100], of the refined structures of MOF-5 collected at 290 and 110 K

A comparison of the powder diffraction patterns simulated with the raw reflection files illustrates the intensity changes during the temperature variation (Fig. 2A). At about 230 K the systematic absences required for the space group *Fm*-3*m* start to be violated. For example, the intensity of the even-odd-odd reflection (237) shows a noticeable intensity which increases until 170 K and stays more or less constant upon further cooling to 100 K. When warming, a decrease in intensity was observed after reaching 170 K. The contraction and expansion of the unit cell is reflected by shifts in the peak positions. I assumed that there is no abrupt breaking and formation of bonds during the transition, so the symmetry reduction should follow the group and subgroup symmetry relationships between space groups according to group theory (*6*). The space group *Pa*-3 is the maximal *klassengleiche* subgroup of *Fm*-3 which is the maximal *translationengleiche* subgroup of *Fm*-3*m*. The lost two-fold symmetry along [110] was used as the twin matrix for

structure refinement (Section S3).The refined structure is shown in Fig 2B (and Fig. S1). The reduced symmetries were recovered to *Fm*-3*m* when the temperature was increased to the original setting. A controlled experiment with an evacuated MOF-5 showed no symmetry change throughout the temperature variation (Fig. S2).

Conclusion

In this experiment, guest induced phase transition and twinning of MOF-5 were studied. Although there are many examples about single crystal to single crystal phase transitions induced by guests, the result of this experiment still emphasizes the importance of understanding properties of MOFs charged with guest molecules considering the structure at 110 K showed quite significant changes on the internal structure and diffraction pattern.

References

1. H. Li, M. Eddaoudi, M. O'Keeffe, O. M. Yaghi, Design and synthesis of an exceptionally stable and highly porous metal-organic framework. *Nature* **402**, 276 (1999).

2. M. Eddaoudi *et al.*, Systematic Design of Pore Size and Functionality in Isoreticular MOFs and Their Application in Methane Storage. *Science* **295**, 469 (2002).

3. M. Ranocchiari, J. A. van Bokhoven, Synthesis and Reactivity of Zn-Biphenyl Metal-Organic Frameworks, Introducing a Diphenylphosphino Functional Group. *CHIMIA Journal* **67**, 397 (2013)

4. S. Parsons, Introduction to twinning. *Acta Crystallogr. D* **59**, 1995 (2003).

5. T. Hahn, *International Tables for Crystallography, Volume A: Space Group Symmetry*. (Springer Netherlands, 2005).

6. H. Wondratschek, U. Müller, *International Tables for Crystallography,Volume A1: Symmetry Relations Between Space Groups*. (Springer Netherlands, 2010).

7. A. Spek, Structure validation in chemical crystallography. *Acta Crystallogr. D* **65**, 148 (2009).

8. G. Sheldrick, A short history of SHELX. *Acta Crystallogr. A* **64**, 112 (2008).

9. O. V. Dolomanov, L. J. Bourhis, R. J. Gildea, J. A. K. Howard, H. Puschmann, OLEX2: a complete structure solution, refinement and analysis program. *J. Appl. Crystallogr.* **42**, 339 (2009).

10. A. L. Spek, PLATON SQUEEZE: a tool for the calculation of the disordered solvent contribution to the calculated structure factors. *Acta Crystallogr. C* **71**, 9 (2015).

11. C. F. Macrae, P. R. Edgington, P. McCabe, E. Pidcock, G. P. Shields, R. Taylor, M. Towler, J. van de Streek, Mercury: visualization and analysis of crystal structures. *J. Appl. Crystallogr.* **39**, 453 (2006).

Acknowledgements: Support for the synthesis by BASF SE (Ludwigshafen, Germany) and the characterization of compounds by King Abdulaziz City for Science and Technology (Center of Excellence for Nanomaterials and Clean Energy Applications). We thank Dr. Simon J. Teat and Dr. Laura J. McCormick for the synchrotron x-ray diffraction data acquisition support at the beamlines 11.3.1 and later 12.2.1 (Advanced Light Source, Lawrence Berkeley National Laboratory). This research used resources of the Advanced Light Source, which is a DOE Office of Science User Facility under contract no. DE-AC02-05CH11231.

Supplementary materials

Materials and Methods

Section S1. Materials

Section S1.1. Synthesis of MOF-5 single crystals

MOF-5, $Zn_4O(BDC)_3$: : In a 20 mL scintillation vial, a mixture solution of $Zn(NO_3)_2 \cdot 4H_2O$ (78 mg, 0.30 mmol) and H_2BDC (25 mg, 0.15 mmol) in DEF (1 mL) was prepared. The solution was sonicated for 1 min. The vial was capped and placed in the preheated 120 °C oven. After 3 days, homogeneous cube shape single crystals with size range from 50 to 100 μm were obtained on the wall of the vial.

Solvent exchange and guest removal procedure of MOF-5: The crystals in the vial were washed with DMF (10.0 mL) three times per day for three days to remove the unreacted reagents in the pores. DMF solvent in the pore was exchanged with chloroform by washing the crystals with chloroform (10.0 mL) three times per day for three days. For supercritical CO_2 drying (SCD) activation, chloroform in the crystals was thoroughly exchanged with liquid CO_2 in the chamber of Tousimis Samdri PVT-3D critical point dryer. The sample was subsequently kept in a supercritical CO_2 atmosphere (typical conditions of 40 °C and 1200 psi) for 30 min and then the supercritical CO_2 was slowly vented over the course of 6 hours. To remove the residual molecules in the pores, the crystals were evacuated for 10 h at 60 °C under 30 mTorr.

Section S2. Methods

Section S2.1. SXRD instrumentation

Single-crystal x-ray diffraction (SXRD) data was collected using synchrotron radiation in beamline 11.3.1 of the Advanced Light Source, Lawrence Berkeley National Laboratory (LBNL). Beamline 11.3.1 is equipped with Bruker laboratory diffractometer coupled with PHOTON 100 CMOS detector operating in shutterless mode. In the beamline, the x-rays are focused with a toroidal mirror (beam size: 200 μm^2), and A channel-cut Si(111) monochromator with an energy range of 6-17 keV is used as a monochromator. The temperature was controlled by cryostream 700 series, oxford cryosystems. For crystal mounting, MiTeGen loops were used with mineral oil.

Section S2.2. Single crystal x-ray diffraction experimental condition

The evacuated samples are soaked in anhydrous DMF for 3 day to charge the pores with the guest molecules. A single crystalline MOFs with and without the guests were mounted on the goniometer, with a distance, 0.5 mm from the cryostream head, where the temperature is calibrated, using a MiTeGen loop and mineral oil. A data collection was carried out including a phi fast scan data to replace saturated peaks in the main data sets. Between the data collections, the shutter was closed to minimize the beam damage and the temperature was reduced by 30 K with a rate, 0.1 K

s^{-1}. The same experimental condition was applied for the data collections during the reverse temperature increase procedure.

Section S3. Data processing and refinement

Calculated PXRD generation: The integrations of all collected reflections were carried out with the primitive unit cell matrix. The raw reflection file was used without further data processing to generate the PXRD patterns with PLATON (*7*).

Refinement of the twinned MOF-5 structure measured at 100 K: The reflections corresponding to the primitive unit cell were integrated and the raw data was scaled and absorption corrected by using m-3m point symmetry of the diffraction patterns. The space group determination by XPREP suggested $P2_13$ space group. However, I chose *P*a-3 as the space group, considering systematic absences from the glide plane on the reconstruction images and the twined pattern. A twin law (-100,001,010), the 2-fold rotation along [110] was used for the refinement with SHELXL (8). Considering the symmetry relations, (*Pa*-3 is the maximal *klassengleiche* subgroup of *Fm*-3 which is the maximal *translationengleiche* subgroup of *Fm*-3*m*), the 2-fold symmetry reduction from *Fm*-3*m* to *Pa*-3 can be an indication of the twin law (*6*). Also the twin law was suggested by twin matrix calculations by PLATON and Olex2 software (*9*). The structure was refined applying DELU, SIMU, and ISOR restraints on the carbon atoms of the phenyl ring and an EADP constraint on C7 and C8 for the anisotropic ADP refinement (Fig. S1). No geometrical restraints and constraints are applied. The residual electron density in the pore was SQUEEZED (*10*). Although the R_1 ($I/\sigma > 4$) was relatively high, 16.52 %, the refinement was converged to a chemically reasonable model. I also tested *Pbca* space group which is the maximal *translationengleiche* subgroup of *Pa*-3 with the six twin laws, the 2-fold multiplied by the 3-fold rotation along [111] matrixes. The refined structure showed slightly better in R_1 (14.32 %). However, the Zn atomic positions were still retaining the 3-fold symmetry along [111]. I have also looked at the LST file of the *Pa*-3 refinement to check the most disagreeable reflections. The first 30 reflections were either all even or all odds. From this, I speculate that there might be domains with Fm-3m symmetry. I tried to model the Fm-3m structure in addition to *Pa*-3 structure. However, the refinement was not stable.

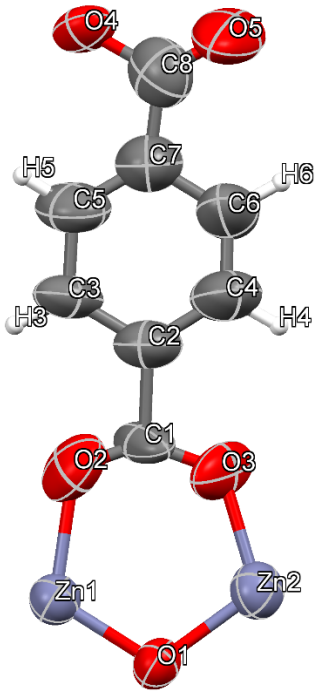

Fig. S1. The asymmetric unit of the twinned MOF-5 structure refined in *Pa*-3 space group. The ellipsoidal model is visualized with Mercury software (*11*).

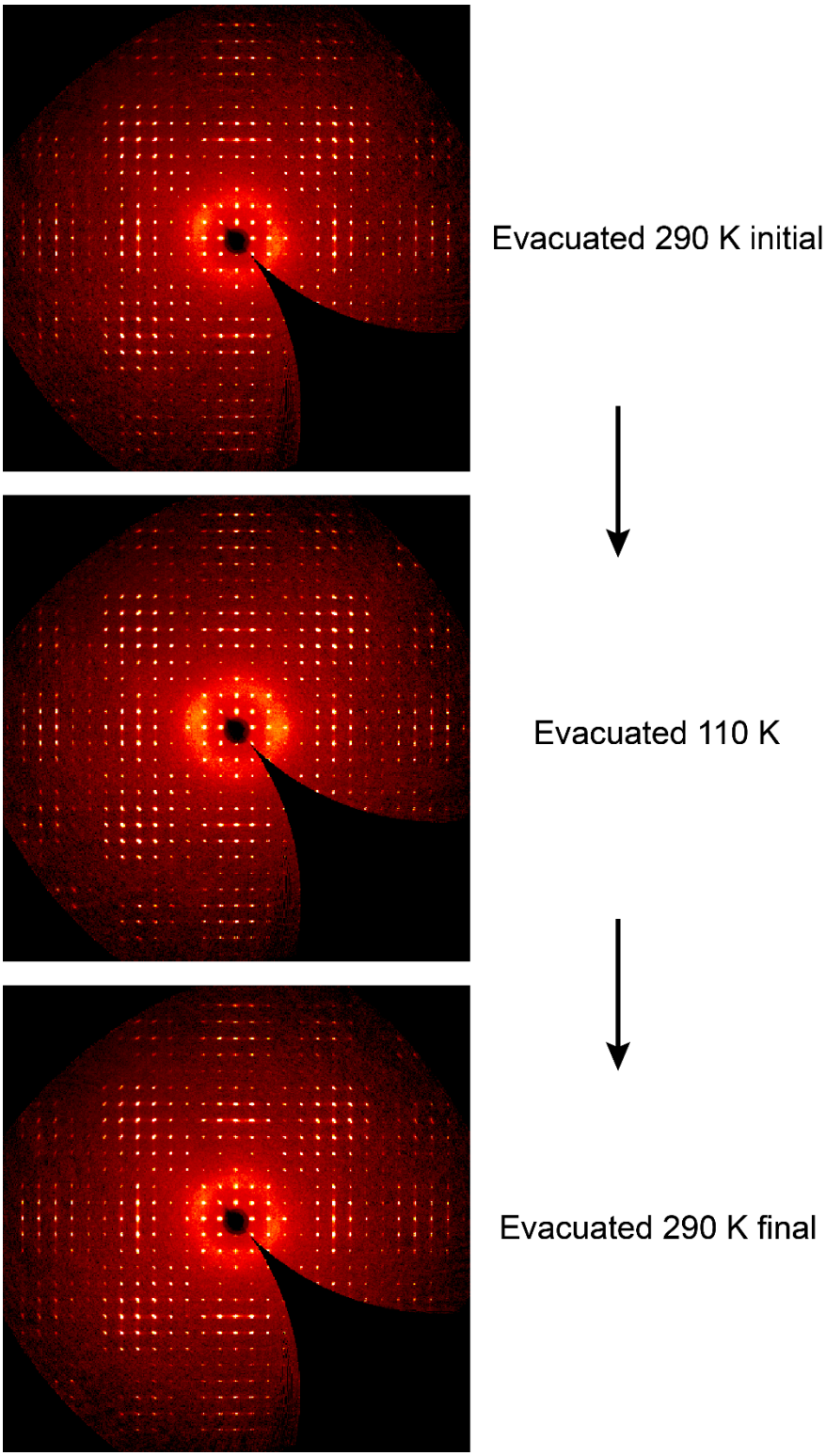

Fig. S2. Reconstruction images, (*hk*0), of the data sets of the evacuated MOF-5 collected at 290, 110, and 290 K.

Chapter 5 Perspective

Coordinative alignment of molecules in chiral metal-organic frameworks

Coordinative alignment method suggests more active controls of the guest organization, exploiting chemical functionalities of the guests, compared to the previous methods where multiple weak interactions were used (*1*-*3*). The key was the strong interactions to increase occupancies of the guests and reduce wiggling. Focusing on strong interactions, the method has potentials to be extended more. Other choices of strong bonds can be neutral coordinative bonding and covalent bonding by organic reactions. I don't think there is one approach to crystallize all types of molecules. Different strategies depending on nature of the guests should be adopted, where role of chemists is important.

After the project was finished, I have got frequently asked two questions in common from colleagues. One is about a technical issue and the other is about limitations of the method. In coordinative alignment method, absolute structure of a crystal is determined by examining anomalous scattering effect from the entire crystal where contribution from the frameworks overwhelms that from the guests. The question was about possibility of wrong assignment of the absolute configurations of the guests since the anomalous scattering from the guests is considered marginal. The question can be simplified to how precisely the method can distinguish diastereomorphs because the relationship between the correct and wrong structures is a diastereomorph. Distinguishing diastereomorphs is nothing to do with anomalous scattering. The wrong structure is excluded by assignments of relative atomic positions during the structure refinement, precision of which depends on quality and resolution of data. After the refinement, there are two choices left which are enantiomorphs. Actually, anomalously scattered x-ray do not tell which part is the guest or framework. The anomalous scattering reflects the entire crystal structure and is used for Flack parameter refinements to distinguish the enantiomorphs at the end of the refinement, where precision of the determination is related to standard uncertainty of the parameter (*4*,*5*). Another question is about a limitation of the method that the conformation of the guest incorporated would be different from natural forms of the molecules. Here, the natural conformations can be interpreted as the conformations of the molecules when they are bound with proteins or not bound free conformations in solutions. Crystalline sponge and coordinative alignment methods do not provide information of such conformations. The methods can only provide atomic connectivity and absolute configurations of the guests. I assume that if the conformations of bound guests in MOFs deviate from their favorable conformations in solutions, the occupancies would be low because of less favorable confirmations. This is not a limitation of the methods. This is a limitation of crystallography where molecules must have interactions with neighbors to be crystalline. Even in molecular crystals, if conformations of molecules has thermodynamically high energy, the crystals would not be crystallized or heavily disordered.

However, there are more limitations and potentials that this method should address and achieve. In addition to enhancing the interactions and precision of absolute configuration determinations, the scope of molecules that the method covers should be broadened. There are two directions in broadening the scope that are also related to each other. One is expanding size of guest molecules. Ultimately, if the method can crystallize proteins, there are potentials not only to solve structures of the proteins, which is already powerful, but to study conformations of substrates

bound in the proteins. This is possible since channels and pores of MOFs provide spaces through which the substrates can diffuse. There are many challenges to achieve the goal. Sizes of the pores and their opening should be large enough to accommodate proteins. In addition, the MOFs should be synthesized as large enough single crystals. So far, there is no MOF meeting the conditions. However, I think MOFs with these conditions are achievable in near future. I speculate that if proteins are incorporated in the pores, their locations and orientations will be mainly governed by shapes of pore where multiple weak interactions and steric hindrances would play important roles. The other direction is crystallizing various shapes of molecules. Fundamentally, the narrow scope of the method originates from specificity of shapes of pore and molecules. Ideally, the specificity need to be similar to that of enzyme-substrate, lock and key model. For this reason, it is obvious that one MOF cannot determine structures of all molecules. To address the problem, there should be a library of structure information of MOFs and case reports of structure determination of guests. The library will eventually be used to suggest MOFs for specific target molecules and predict success of the experiments. This is not a project one or several research groups can achieve.

In future, the method might not become a general method to solve structure of molecules because of the limitations explained above. However, if the method solves structures of several important molecules which have broad impacts in science. That would also be important.

Effects of guests on x-ray diffraction of metal-organic frameworks

It is shown that heavily disordered guest molecules in the pores have significant effects on internal structures of MOFs, thus their diffraction patterns. I believe this research will affect data collection strategies of porous crystalline materials, which is also related to crystalline sponge method. I hope this research will broaden understanding of the interactions between the frameworks and guests. It has been well-known that the interaction cause phase transitions of certain MOFs, where the transitions are ordered to some extent across unit cells of MOFs. However, the disordered interaction has been out of the center of the discussions, although it exists and affect significantly the diffraction of MOFs.

In this perspective, I want to think about the guests and framework relation in the opposite way, which deviates from the main idea of the researches in the dissertation, though. The question is how frameworks would affect properties of the guests. I have noticed that there are researches about confinement effects of guest molecules in the pores of mesoporous silica, which showed different physical properties of solvents in the pores from those of free bulk solvents (*6*). I think this is an important topic in porous materials since there are many chemical reactions happening in the pores. MOFs have several advantages for studying the confinement effects. The size and functionality of the pore can be tuned in an atomic level and also the highly crystalline nature of MOFs provides precise characterization and visualization of the guests by SXRD. Imagine a 4 to 5 nm diameter pore of a MOF and guest molecules such as ethanol packed in it. I'm wondering the way the molecules is packed and their relative orientations on average. They would not have the same properties of the free bulk solvent outside of the pores because of their restricted motions and orientation, which depend on the size, shape, and functionality of the pores. As the size of the pore gets larger, it would be more difficult to predict and characterize them by SXRD. At some points, the property would be similar to that of the free bulk solvent. We do not know much about

these disordered molecules in the pores of MOFs for the reasons mentioned in the introduction. I guess the size and shape of the first layer of the guests and the orientation of the guest molecules in the layer would mainly affect properties of the domain. If there are tools developed for the characterization, we might see unexpected relative orientations of guests which are not favored in the bulk solution or unexpected physical properties of the domains which can be tuned exploiting the structural diversity and flexibility of designing MOF structures.

References

1. M. Hoshino, A. Khutia, H. Xing, Y. Inokuma, M. Fujita, The crystalline sponge method updated. *IUCrJ* **3**, 139 (2016).

2. N. Zigon, M. Hoshino, S. Yoshioka, Y. Inokuma, M. Fujita, Where is the Oxygen? Structural Analysis of α-Humulene Oxidation Products by the Crystalline Sponge Method. *Angew. Chem. Int. Ed.* **54**, 9033 (2015).

3. Y. Inokuma *et al.*, X-ray analysis on the nanogram to microgram scale using porous complexes. *Nature* **495**, 461 (2013).

4. H. D. Flack, G. Bernardinelli, Absolute structure and absolute configuration. *Acta Crystallogr. A* **55**, 908 (1999).

5. H. D. Flack, U. Shmueli, The mean-square Friedel intensity difference in P1 with a centrosymmetric substructure. *Acta Crystallogr. A* **63**, 257 (2007).

6. G. Buntkowsky *et al.*, Structural and dynamical properties of guest molecules confined in mesoporous silica materials revealed by NMR. *Phys. Chem. Chem. Phys.* **9**, 4843 (2007).